

UC San Diego

UC San Diego Electronic Theses and Dissertations

Title

Heterogeneity of excitatory synapses in parvalbumin interneurons

Permalink

<https://escholarship.org/uc/item/4pq5n63p>

Author

Sancho, Laura

Publication Date

2018

Peer reviewed|Thesis/dissertation

UNIVERSITY OF CALIFORNIA SAN DIEGO

Heterogeneity of excitatory synapses in parvalbumin interneurons

A dissertation submitted in partial satisfaction of the requirements for the degree Doctor of

Philosophy

in

Neurosciences

by

Laura Sancho

Committee in charge:

Professor Brenda Bloodgood, Chair
Professor Edward Callaway
Professor Thomas Hnasko
Professor Jeffrey Isaacson
Professor Gentry Patrick

2018

©

Laura Sancho, 2018

All rights reserved.

The Dissertation of Laura Sancho is approved, and it is acceptable in quality and form for publication on microfilm and electronically:

Chair

University of California San Diego

2018

DEDICATION

A mi familia

TABLE OF CONTENTS

SIGNATURE PAGE	iii
DEDICATION	iv
TABLE OF CONTENTS	v
LIST OF ABBREVIATIONS	vii
LIST OF FIGURES.....	viii
ACKNOWLEDGEMENTS.....	ix
VITA.....	x
ABSTRACT OF THE DISSERTATION	xi
Chapter 1. Introduction.....	1
Ionotropic glutamate receptors.....	2
Function and physiology of dendritic spines.....	3
Ca signaling by glutamate receptors.....	5
Spines in interneurons	7
Parvalbumin-positive interneurons: properties and characteristics.....	8
NMDARs and CP-AMPA in PV INs.....	9
Differential engagement of NMDARs and CP-AMPA.....	10
References	13
Chapter 2. Functional distinctions between dendritic and spines synapses made onto parvalbumin-positive interneurons in mouse visual cortex.....	23
PV INs in layer II/III of V1 are sparsely spiny	23
Spines on PV INs enclose functional glutamatergic synapses	24
Two-photon glutamate uncaging and Ca imaging reveals NMDARs are enriched at spine synapses.....	26
CP-AMPA- mediated Ca influx and depolarization are similar in dendrites and spines	28
The rectification of CP-AMPA is similar in dendrites and spines	29
Ca signaling through glutamate receptors on dendrites, but not spines, is bi-directionally modulated by back-propagating action potentials.....	30
Spine synapses are sensitive to the co-activation of neighboring dendritic synapses	34
Discussion	35
Figures and legends	41
Methods.....	67

References	75
Chapter 3. What is next?	80
Figures and legends	91
References	101

LIST OF ABBREVIATIONS

PV	Parvalbumin
IN	Interneuron
PV IN	Parvalbumin positive interneuron
V1	Primary visual cortex
Ca	Calcium
NMDAR	N-methyl-D-aspartate receptor
AMPA	α -amino-3-hydroxy-5-methyl-4-isoazolepropionic acid receptor
CP-AMPA	calcium-permeable AMPA
CI-AMPA	calcium-impermeable AMPA
EC	Extracellular
AP	Action potential
bAP	back-propagating action potential
EPSC	excitatory postsynaptic current
uEPSC	uncaging-evoked EPSC
mEPSC	miniature EPSC
uEPSP	uncaging-evoked excitatory postsynaptic potential
Magnesium	Mg
TARP	transmembrane regulatory protein
NI	non-linearity index
VGCC	voltage-gated Ca channel

LIST OF FIGURES

Figure 2.1. PV INs are sparsely spiny	41
Figure 2.2. Spines on PV INs enclose functional glutamatergic synapses	43
Figure 2.3. Variability in receptor composition	45
Figure 2.4. Spines are enriched for NMDARs.....	47
Figure 2.5. Standardization of uncaging power.....	49
Figure 2.6. CP-AMPAR- mediated Ca influx and depolarization are similar in dendrites and spines	51
Figure 2.7. bAP-mediated Ca influx.....	53
Figure 2.8. Ca signaling through glutamate receptors on dendrites is bi-directionally modulated by back-propagating action potentials.....	55
Figure 2.9. Modulation of dendritic Ca signals by bAPs.....	57
Figure 2.10. Spine CP-AMPARs and NMDARs do not exhibit modulation by somatic activity	59
Figure 2.11. bAPs do not modulate spine Ca signals	61
Figure 2.12. Spines on PV INs produce NMDAR-dependent supra-linear Ca signals in response to local dendritic activity.....	63
Figure 2.13. Spine Ca signals are modulated by local dendritic activity	65
Figure 3.1. NR2A-containing NMDARs are biased towards spines synapses.....	91
Figure 3.2. Confocal imaging of PV INs.....	93
Figure 3.3. bAPs trigger Ca influx through VGCCs.....	95
Figure 3.4. Comparing Ca influx in voltage- clamp vs. current- clamp	97
Figure 3.5. Other conductances in PV IN spines	99

ACKNOWLEDGEMENTS

Firstly, I'd like to thank my family, especially my parents, for always encouraging me to pursue my passions. From an early age, they have been nothing but supportive of my goals and intellectual curiosity. I'd also like to acknowledge my grandmother, for showing me what true resilience looks like.

I'd also like to thank my supervisor and scientific mentor and *sensei*, Brenda Bloodgood. In the early days, the lab was mainly boxes and we were building a two-photon basically from scratch, an experience for which I will always be eternally grateful. Under her mentorship, I can undoubtedly say that my presentation and scientific writing skills have improved, as well as my attention to detail.

I'd like to thank the members of the Bloodgood Lab, especially Dr. Andrea Hartzell-Brigidi. We joined the lab more or less at the time, and she is my scientific fraternal twin. I can't imagine grad school without having gone through it side-by-side.

Lastly, I'd like to thank my cohort, my fellow grad students. Thank you for all your support over the years and all the laughs. You made it tolerable ☺

Chapter 2 is material currently being re-submitted for publication. Sancho, L., & Bloodgood, B.L. (2018). Functional distinctions between spine and dendritic synapses in parvalbumin positive interneurons of mouse cortex. The dissertation author was the primary investigator and author of this material.

Chapter 3 contains experiments done during the course of this PhD, but not submitted for publication.

VITA

- 2012 Bachelor of Arts in Neuroscience and Psychology
Boston University, Boston, MA
- 2018 Doctor of Philosophy in Neurosciences
University of California San Diego, La Jolla, CA

PUBLICATIONS

Goo, M.S., **Sancho, L.**, Slepak, N., Doassa, D., Deerinck, T.J., Ellisman, M.H., Bloodgood, B.L., Patrick, G.N. 2017. Activity-dependent trafficking of lysosomes in dendrites and dendritic spines. *Journal of Cell Biology*, 21(8), pp. 2499-2513.

Sancho, L. & Bloodgood, B.L. Functional distinctions between spine and dendritic synapses made onto parvalbumin-positive interneurons in mouse cortex. *Cell Reports* (*in press*).

FIELD OF STUDY

Major Field: Neurosciences

Studies in Cellular Neurobiology
Professor Brenda L. Bloodgood

ABSTRACT OF THE DISSERTATION

Heterogeneity of excitatory synapses in parvalbumin interneurons

by

Laura Sancho

Doctor of Philosophy in Neurosciences

University of California San Diego, 2018

Professor Brenda Bloodgood, Chair

Glutamatergic excitatory synapses are one of the main currencies of the mammalian central nervous system. Excitatory synapses have been most well-characterized in terms of dendritic spines, which are small membranous protrusions. Dendritic spines influence synapse function by boosting synaptic potentials and sequestering synaptically-generated second messengers. Spines have been extensively studied in densely spiny principal neurons, but little is known about how they expand the information-gathering capabilities of sparsely spiny interneurons (INs). We find in the mouse primary visual cortex, parvalbumin-positive INs have a low density of spines that enclose functional glutamatergic synapses. Both spine and dendritic synapses contain calcium-permeable AMPA and NMDA receptors (CP-AMPA, NMDARs), but NMDARs are enriched at spine synapses. Despite these similarities, spine synapses are imbued with distinct sensitivities to the ongoing activity of the neuron. Glutamate receptor-mediated

calcium (Ca) influx at proximal dendritic sites is bi-directionally modulated by the timing of action potentials (APs). Surprisingly, spine synapses are largely insensitive to APs but coincident activity originating in the adjacent dendrite strongly influences spine NMDAR-mediated Ca influx. Thus, while glutamate receptors on spines and dendrites are modulated by the activity of the neuron, they are distinctive in the type of coincident activity detected

Chapter 1. Introduction

Excitatory synapses in the mammalian central nervous system (CNS) account for a large portion of the synapses (Meldrum, 2000). While the overall balance of excitation to inhibition is important for proper function (Vogels et al. 2011; Yizhar et al. 2011; Haider 2006; Ridding et al. 1995; Dani et al. 2005), excitatory transmission is still the primary currency of the nervous system, as depolarizations at excitatory synapses increase the probability that a neuron will fire an action potential, the main output of a neuron (CITATIONS), by bringing the membrane potential closer to threshold (Fatt & Katz 1952; Fatt & Katz 1951; del Castillo & Katz 1954). Many neurological and psychiatric diseases and disorders, such as epilepsy, Alzheimer's Disease and schizophrenia, involve a dysfunction in excitatory transmission (Ting et al. 2007; Sutula & Dudek 2007; Howes et al. 2015).

At chemical synapses in the CNS, the predominant excitatory neurotransmitter is glutamate, an amino acid that is synthesized by glutaminase (Curthoys, 1995). Glutamate concentration in the extracellular space is maintained at very low levels, as high levels of glutamate can lead to excitotoxicity (Choi 1994, Doble 1999). The glutamate transporter EAAT (excitatory amino acid transporter) removes glutamate from the synaptic cleft (Kim et al., 2011), while VGLUT (vesicular glutamate transporter) moves glutamate from the neuronal cytosol into presynaptic synaptic vesicles (Juge, Yoshida, Yatsushiro, Omote, & Moriyama, 2006).

On the postsynaptic side, once released into the synaptic cleft, glutamate binds a variety of glutamate receptors. Some receptors are metabotropic, triggering an array of intracellular signal transduction pathways (Blacker, Lewis, Frye, & Veldic, 2017) that can lead to a variety of downstream changes in the neuron, including protein synthesis, and

regulation of other ion channels (Pin & Duvoisin, 1995; H. Wang et al., 2016). Others are ionotropic, in that they are ion channels that open in response to binding glutamate (S. Zhu & Gouaux, 2017). The ionotropic glutamate receptors are NMDA (N-methyl-d-aspartate) receptors, AMPA (α -amino-3-hydroxy-5-methyl-4-isoazolepropionic acid) receptors, and kainate receptors. NMDA receptors (NMDARs) and AMPA receptors (AMPA receptors) are both heterotetrameric and have been the most extensively studied for their role in regulating synaptic plasticity and long-term changes in neural connectivity. They are the primary focus of this dissertation.

Ionotropic glutamate receptors

NMDARs open in response to binding glutamate and glycine. Glycine is regularly present in the extracellular space between cells, but glutamate is released by the fusion of synaptic vesicles (Kirischuk, Héja, Kardos, & Billups, 2016). NMDARs are permeable to calcium (Ca), sodium (Na), and potassium (K), to a lesser extent. Additionally, the pore is blocked by extracellular magnesium (Mg) and zinc (Zn), when neurons are hyperpolarized (Nowak, Bregestovski, Ascher, Herbet, & Prochiantz, 1984). Postsynaptic depolarization, which expels the Mg/Zn block, in conjunction with presynaptic glutamate release allows current flow through NMDARs (Nowak et al. 1984). NMDARs are heteromeres that contain at least one obligatory NR1 subunit, which can occur as one of eight isoforms. There are also four distinct NR2 subunits (A, B, C, and D), as well as two NR3 subunits (A and B; Sugihara et al. 1992; Moriyoshi et al. 1991). Furthermore, the time course of the current generated by NMDARs is largely dependent on the NR2 subunit that is expressed; for example, NMDARs containing the NR2A subunit deactivate much faster and consequently produce currents with faster decay kinetics (Cull-Candy et al. 2001; Vicini et al. 1998).

The second major type of ionotropic glutamate receptor, the AMPAR, is also heterotetrameric, with four types of subunits, GluR1-4 (Dingledine, Borges, Bowie, & Traynelis, 1999). The cationic permeability of AMPARs is regulated by the presence of the post-transcriptionally modified GluA2 subunit. AMPARs lacking the GluA2 subunit entirely or the modified form are permeable to Ca (Greger, Ziff, & Penn, 2007). Additionally, GluA2-lacking CP-AMPARs are intracellularly blocked by polyamines, such as spermine or spermidine when the postsynaptic cells are depolarized; thus, currents mediated through GluA2-lacking (or CP-AMPARs)- AMPARs are said to be inwardly rectifying (Bowie & Mayer 1995; Washburn et al. 1997 Szabo et al. 2012). Thus, the presence of Ca-permeable AMPARs in addition to NMDARs at synapses has profound implications for how excitatory synapses produce and modulate Ca signals, as well as depolarization.

Function and physiology of dendritic spines

Synaptic ionotropic glutamate receptors on many types of principal neurons that contain high densities of dendritic spines have been extensively characterized. Dendritic spines are small, membranous protrusions that typically enclose excitatory synapses (Gulyá et al. 1999; Harris & Weinberg 2012; Sheng & Hoogenraad 2007). Dendritic spines serve to biochemically and electrically compartmentalize the any signals generated by transmission onto excitatory synapses (Nimchinsky et al. 2002; (Gulledge, Carnevale, & Stuart, 2012). For example, a synapse that is enclosed within a spine head and separated from the dendrite by a high resistance spine neck can produce a local synaptic potential that is tens of millivolts in amplitude (Yuste 2013; Beaulieu-Laroche & Harnett 2017; Jayant et al. 2017; Kwon et al. 2017), while a similar current originating from a dendritic shaft

synapse may be an order of magnitude smaller (Gulledge et al. 2012; Kawato & Tsukahara 1984; Araya, Jiang, et al. 2006; Araya, Eiselthal, et al. 2006).

The large synaptic potentials produced at spine synapses are capable of engaging an array of local voltage-dependent receptors and channels such as NMDARs and AMPARs, as well as a host of voltage-gated Ca and K channels (Bloodgood et al. 2009; Svoboda & Sabatini 2000; Sobczyk et al. 2005; Bloodgood & Sabatini 2007; Yuste & Denk 1995; Griffith et al. 2016; Losonczy et al. 2008; Wang et al. 2014; Branco & Häusser 2011), which shape the amplitude and kinetics of synaptic calcium (Ca) signals. Synaptically-evoked Ca influx through NMDARs has been extensively studied in excitatory neurons, such as pyramidal cells, and is highly modulated by a function of membrane voltage. For instance, a 20 mV depolarization in the postsynaptic membrane reduces the affinity of the NMDAR for Mg by 10- fold, resulting in a larger NMDAR-mediated Ca influx despite a reduction in the driving force (Burnashev et al. 1995; Jahr & Stevens 1990; Bloodgood & Sabatini 2009). Furthermore, Ca influx through NMDARs can lead to activation of SK channels, which are Ca-activated K channels that serve to repolarize the postsynaptic membrane (Faber, Delaney, & Sah, 2005; Ngo-Anh et al., 2005). These channels have also been demonstrated to be localized to dendritic spines, where they are activated by CaV_{2.3} voltage-sensitive Ca channels (VSCCs), which are in turn activated by synaptic depolarization due to activation of NMDARs as well as AMPARs (Bloodgood & Sabatini, 2007). Furthermore, the morphology of dendritic spines can lead to biphasic synaptic Ca influx. In pyramidal neuron, co-localized and co-activated AMPARs and NMDARs interact to produce two distinct phases of Ca influx, regulated in part by the opening of SK channels and the intrinsic NMDAR kinetics (Bloodgood et al., 2009).

In addition to electrical and Ca signaling, dendritic spines can also regulate biochemical compartmentalization of downstream effector molecules. After the induction of

long-term plasticity in a single spine head, CAMKII has been shown to be activated in a spatially restricted manner to the stimulated spine (Lee, Escobedo-Lozoya, Szatmari, & Yasuda, 2009). Moreover, induction of long-term plasticity activates small GTPases, one of which (GTP-bound Cdc42) is confined to the activated spine head (Murakoshi, Wang, & Yasuda, 2011). These small molecules are involved in several downstream signaling cascades that can produce long-lasting changes in the neuron, including structural plasticity, initiation of transcriptional programs, regulation of intracellular transport, and regulation of dendritic organelles.

Ca signaling by glutamate receptors

As NMDARs are modulated by membrane voltage, they are poised to generate non-linear synaptic Ca signals. Ca is an important second messenger that is capable of engaging multiple signal transduction pathways that lead to long-term plasticity and changes in connectivity (Griffith & Budnik 2006; Ghosh & Greenberg 1995; Pchitskaya et al. 2017). For instance, NMDARs can generate supra-linear Ca influx in response to the depolarization from somatic back-propagating action potentials invading dendritic spines (Yuste & Denk 1995a; Nevian & Sakmann 2006; Evans et al. 2012), as well as local dendritic depolarization or the co-activation of neighboring synapses (Harnett et al. 2012; Gambino et al. 2014; Weber et al. 2016).

The generation of non-linear Ca events, most thoroughly described in spines, can engage multiple down-stream cellular pathways. Long-term potentiation (LTP) as described can be engaged in a synapse-specific manner. LTP was first described in the hippocampus (Bliss & Lømo, 1973) and was thought to require Ca influx through postsynaptic NMDARs (Lüscher & Malenka, 2012). To this day, many forms of LTP have been described in many

brain regions and across many different synapse types. The most extensively described is the canonical LTP pathway in hippocampal neurons, which involves Ca/calmodulin-dependent protein kinase II (CaMKII; Lisman, Schulman, & Cline, 2002; Lisman, Yasuda, & Raghavachari, 2012). Furthermore, the activation of CaMKII has been shown to be directly involved in plasticity and memory formation (Giese, Fedorov, Filipkowski, & Silva, 1998; Zhou et al., 2007; Barria & Malinow, 2005). For example, CaMKII is capable of phosphorylating the AMPAR auxiliary protein stargazing to drive insertion of AMPARs into the postsynaptic density (Tomita, Stein, Stocker, Nicoll, & Bredt, 2005; Opazo et al., 2010). CaMKII can also stimulate the RAS-ERK pathway, driving the exocytosis of AMPARs (J. J. Zhu, Qin, Zhao, Van Aelst, & Malinow, 2002). Another set of molecules downstream of NMDARs is the Rho GTPase family, which is involved in structural plasticity and modifying the actin cytoskeleton, resulting in the enlargement of dendritic spines (Murakoshi et al., 2011a; O'Kane, Stone, & Morris, 2003; Segal, 2005; Tada & Sheng, 2006). In optic tectal cells of tadpoles, visual activity drives dendritic growth through NMDAR activation and consequent decreased RhoA and increased Rac and Cdc42 activity (Sin, Haas, Ruthazer, & Cline, 2002).

CP-AMPARs have also been shown to generate non-linearities in Ca signals, as well as long-term synaptic plasticity. For example, supra-linear Ca signals generated in hippocampal fast-spiking interneurons by increasing stimulation of their dendrites are dependent on CP-AMPARs; specifically, Ca influx through these receptors triggers the release of Ca from the endoplasmic reticulum leading to a supra-linear Ca signal (ER; Camiré & Topolnik 2014). Furthermore, some interneurons can generate non-NMDAR-mediated LTP, which is instead dependent on Ca influx through CP-AMPARs (Lamsa et al. 2007; Szabo et al. 2012; Nissen et al. 2010; Oren et al. 2009). While the cellular mechanisms downstream of NMDAR activation have been extensively characterized,

relatively little is known about the effector molecules downstream of CP-AMPARs. Some studies have shown that CP-AMPARs are required for the activation of the Rac/PAK/LIMK pathway that promotes F-actin polymerization in spines, leading to their enlargement (Fortin et al. 2010; Meng et al. 2002). Other research identified the role of CP-AMPARs in activating the Ras/Erk kinase cascade and the cAMP-response element-binding protein (CREB) transcription factor in mature mice (Tian & Feig, 2006). CREB has been shown to be involved in long-term forms for memory, and is a transcription factor that binds to promoter cAMP responsive element (CRE) sites (Silva, Kogan, Frankland, & Kida, 1998).

Thus, the downstream effector molecules of CP-AMPAR-mediated LTP seems to be independent of the extensively characterized CAMKII-dependent LTP, which is a main component of the downstream signaling cascade induced by NMDAR activation. Typically these receptors are not co-localized in the same neuron type, with a few notable exceptions to be discussed later. Thus, in a neuron that contains both NMDARs and CP-AMPARs, the presence of distinct downstream signaling cascades has important implications for the long-term changes that Ca influx through different receptors could engage.

Spines in interneurons

The consequences of housing a synapse within a spine have been extensively explored in densely spiny principle neurons where the overwhelming majority of excitatory synapses are made onto spines. However, many inhibitory interneurons (INs) are sparsely spiny with a wide range of spine densities that vary based on IN subtype (Peters & Regidor 1981; Kawaguchi et al. 2006; Azouz et al. 1997). In INs where spines have been studied, these spines contain functional synapses and undergo experience-driven structural plasticity (Keck et al. 2011; Guirado et al. 2014; Pérez-Rando et al. 2017; Gilabert-Juan et

al. 2011) as has been observed for spines on principal neurons. Nonetheless, in INs, spine synapses are interspersed among and often outnumbered by those formed directly onto the dendrites, raising the question of how spine synapses expand the information gathering capabilities of sparsely spiny interneurons.

Parvalbumin-positive interneurons: properties and characteristics

Parvalbumin-positive (PV) INs are a compelling cell type in which to study the operations performed by spine versus dendritic synapses. First, the dendrites of PV INs are densely innervated, receiving up to three excitatory synaptic inputs per micron (Gulyá et al., 1999). While this cell type is often described as having smooth dendrites, spines have been observed on the dendrites of PV INs in many brain regions, at various developmental stages, and in several species (Kawaguchi et al. 2006; Gulyá et al. 1999; Kubota et al. 2011; Kawaguchi 1993). However, whether spines on PV INs enclose functional synapses has not been established, let alone if they are functionally distinct from synapses made onto the dendrites.

Understanding excitatory transmission in PV INs is critical for understanding their larger network functions. For example, PV INs have been implicated in the regulation of cortical oscillations (Cardin et al. 2009; Sohal 2012), the amplitude of the response of principal neurons in primary sensory areas to specific stimuli (Atallah, Bruns, Carandini, & Scanziani, 2012), and the shape of hippocampal place fields (Royer et al., 2012). These neurons have a set of unique intrinsic properties that endow them with the ability to reliably modulate larger network activity. For example, they are fast spiking, display little to no spike frequency accommodation (McCormick, Connors, Lighthall, & Prince, 1985), have EPSPs with fast kinetics (Geiger et al. 1997). Moreover, they synapse at or near the soma of principal neurons (Freund & Buzsáki, 1998), are electrically coupled to each other

(Galarreta & Hestrin, 1999), and a single PV IN can inhibit multiple principal neurons (Bezaire & Soltesz, 2013). Consequently, their ability to regulate network activity requires us to further examine how excitatory transmission is regulated on these neurons.

NMDARs and CP-AMPARs in PV INs

Further adding to the complexity of understanding excitatory synaptic processing in PV INs, these interneurons express both NMDARs and CP-AMPARs at postsynaptic sites (Goldberg et al. 2003; Geiger et al. 1997; J. H Goldberg et al. 2003; Matta et al. 2013). Previous examination of fast-spiking INs indicates that synaptic Ca signals produced in dendritic shafts are generated by a combination of NMDARs and CP-AMPARs (Jesse H. Goldberg et al. 2003; J. H Goldberg et al. 2003). While the Ca signaling and plasticity consequences of both NMDARs and CP-AMPARs have been described, generally these receptors are not found in the same cell type, with the notable exceptions of PV INs and medium spiny interneurons (MSNs) of the striatum.

IN PV INs, CP-AMPARs are partly responsible for the fast kinetics of their EPSPs (excitatory postsynaptic potentials; Geiger et al. 1997) and mediate the majority of their AMPA current (J. R.P. Geiger et al., 1995). Additionally, in somatosensory cortex, synapses made by thalamocortical afferents onto PV INs produce significant NMDAR-mediated Ca transients (Bagnall, Hull, Bushong, Ellisman, & Scanziani, 2011). However, the analogous synapses in primary visual cortex (V1) lack NMDAR-mediated currents altogether (Kloc & Maffei, 2014). These studies collectively suggest that synaptic glutamate receptor composition in PV INs is heterogeneous, and many synapses have the capacity to produce both CP-AMPA and NMDAR-mediated Ca signals.

While both CP-AMPA and NMDAR-mediated currents are observed in whole-cell recordings in response to extracellular stimulation, NMDAR-mediated currents are notably small in PV INs (Matta et al. 2013; Hull et al. 2009). Yet, PV IN-specific knockout of NMDARs is associated with abnormal gamma oscillations (Cardin et al. 2009; Carlén et al. 2011; Korotkova et al. 2010), disrupted place fields, memory impairments (Carlén et al. 2011; Korotkova et al. 2010), and a host of behavioral abnormalities akin to those observed in mouse models of schizophrenia (Carlén et al. 2011; Korotkova et al. 2010). How NMDARs affect the cellular and network properties of PV INs is unclear. Thus, these receptors are crucial for several network level functions attributed to PV INs.

Differential engagement of NMDARs and CP-AMPARs

In hippocampal PV INs, activation of both CP-AMPARs and NMDARs can induce excitatory synapse plasticity (Lamsa et al., 2007; Le Roux, Cabezas, Böhm, & Poncer, 2013). However, the receptor type that is engaged is dependent on both the location of the synapses and the postsynaptic membrane potential. Le Roux et al. (2013) showed that NMDAR-dependent long-term potentiation (LTP) can be induced at feedback synapses originating from CA1 pyramidal neurons when the postsynaptic cells are depolarized, while CP-AMPA-dependent LTP can be induced at both feedback and feedforward (originating from Schaffer collaterals) synapses when the postsynaptic cells are hyperpolarized. While intriguing, these studies did not examine whether individual synapses on PV INs can switch between CP-AMPA and NMDAR-mediated Ca signaling.

Excitatory synapses on other cell types can differentially engage CP-AMPA and NMDAR-mediated signaling in response to distinct activity patterns or postsynaptic states. In the lateral amygdala, memory retrieval triggers the insertion of CP-AMPARs into

synapses already containing NMDARs, making fear memories more labile (Clem & Huganir, 2010; Hong et al., 2013). In medium spiny interneurons (MSNs) in the striatum, state transitions to a depolarized “upstate” change the predominant Ca signaling method from CP-AMPARs to NMDARs, facilitating NMDAR-dependent signaling non-linearities and LTP (Carter & Sabatini, 2004).

Since PV INs contain both CP-AMPARs and NMDARs, we need to understand the utility of having two different Ca permeable ionotropic glutamate receptors. The presence of two types of Ca permeable glutamate receptors endows excitatory synapses on PV INs with the capacity to generate a broad repertoire of membrane potential-dependent synaptic Ca signals that may engage divergent Ca-dependent biochemical pathways. Yet, this also presents a unique challenge: how and when do synapses switch between CP-AMPAR and NMDAR-mediated Ca signaling? The small NMDAR-mediated currents suggest that there may be either few NMDARs at each synapse or a few synapses with high numbers of NMDARs.

We find that in layer II/III of mouse primary visual cortex (V1), spines on PV INs enclose functional glutamatergic synapses and these synapses contain both CP-AMPARs and NMDARs much like dendritic shaft synapses. Despite these similarities, spine synapses are imbued with distinct sensitivities to the ongoing activity of the neuron. Using two-photon glutamate uncaging in combination with electrophysiology, Ca imaging, and pharmacology, we find that CP-AMPAR-mediated Ca signals are similar in spines and dendrites. NMDAR-mediated Ca influx, while present at synapses in both locations, is proportionally larger in spines. Ca influx through dendritic glutamate receptors is bi-directionally modulated as a function of the timing of coincident action potentials (APs), with sub-linearities relying on CP-AMPARs and supra-linearities relying on NMDARs. Unexpectedly, spine synapses are less sensitive to APs but are highly influenced by

EPSPs originating in the adjacent dendritic shaft. When individual spine synapses are co-active with those on the dendrite, they produce NMDAR-dependent supra-linear Ca signals that scale with the magnitude of the depolarization. Thus, we propose that spine synapses on PV INs may be preferentially engaged in monitoring ongoing local synaptic activity and respond by enhancing NMDAR Ca influx. Proximal dendritic synapses, in contrast, use both glutamate receptor types to read out the global activity of the neuron.

REFERENCES:

- Araya, R., Eiselthal, K. B., & Yuste, R. (2006). Dendritic spines linearize the summation of excitatory potentials. *Proceedings of the National Academy of Sciences*, *103*(49), 18799–18804. <http://doi.org/10.1073/pnas.0609225103>
- Araya, R., Jiang, J., Eiselthal, K. B., & Yuste, R. (2006). The spine neck filters membrane potentials. *Proceedings of the National Academy of Sciences*, *103*(47), 17961–17966. <http://doi.org/10.1073/pnas.0608755103>
- Atallah, B. V., Bruns, W., Carandini, M., & Scanziani, M. (2012). Parvalbumin-Expressing Interneurons Linearly Transform Cortical Responses to Visual Stimuli. *Neuron*, *73*(1), 159–170. <http://doi.org/10.1016/j.neuron.2011.12.013>
- Azouz, R., Gray, C. M., Nowak, L. G., & McCormick, D. A. (1997). Physiological properties of inhibitory interneurons in cat striate cortex. *Cerebral Cortex*, *7*(6), 534–545. <http://doi.org/10.1093/cercor/7.6.534>
- Bagnall, M. W., Hull, C., Bushong, E. A., Ellisman, M. H., & Scanziani, M. (2011). Multiple Clusters of Release Sites Formed by Individual Thalamic Afferents onto Cortical Interneurons Ensure Reliable Transmission. *Neuron*, *71*(1), 180–194. <http://doi.org/10.1016/j.neuron.2011.05.032>
- Barria, A., & Malinow, R. (2005). NMDA receptor subunit composition controls synaptic plasticity by regulating binding to CaMKII. *Neuron*, *48*(2), 289–301. <http://doi.org/10.1016/j.neuron.2005.08.034>
- Beaulieu-Laroche, & Harnett, M. T. (2017). Dendritic Spines Prevent Synaptic Voltage Clamp. *Neuron*, *97*, 75–82.
- Bezaire, M. J., & Soltesz, I. (2013). Quantitative assessment of CA1 local circuits: Knowledge base for interneuron-pyramidal cell connectivity. *Hippocampus*, *23*(9), 751–785. <http://doi.org/10.1002/hipo.22141>
- Blackner, C. J., Lewis, C. P., Frye, M. A., & Veldic, M. (2017). Metabotropic glutamate receptors as emerging research targets in bipolar disorder. *Psychiatry Research*. <http://doi.org/10.1016/j.psychres.2017.07.059>
- Bliss, T. V. P., & Lømo, T. (1973). Long-lasting potentiation of synaptic transmission in the dentate area of the anaesthetized rabbit following stimulation of the perforant path. *The Journal of Physiology*, *232*(2), 331–356. <http://doi.org/10.1113/jphysiol.1973.sp010273>
- Bloodgood, B. L., Giessel, A. J., & Sabatini, B. L. (2009). Biphasic synaptic Ca influx arising from compartmentalized electrical signals in dendritic spines. *PLoS Biology*, *7*(9). <http://doi.org/10.1371/journal.pbio.1000190>
- Bloodgood, B. L., & Sabatini, B. L. (2005). Neuronal Activity Regulates Diffusion Across the Neck of Dendritic Spines. *Science*, *310*(5749), 866–869. <http://doi.org/10.1126/science.1114816>
- Bloodgood, B. L., & Sabatini, B. L. (2007). Nonlinear Regulation of Unitary Synaptic Signals

by CaV2.3 Voltage-Sensitive Calcium Channels Located in Dendritic Spines. *Neuron*, 53(2), 249–260. <http://doi.org/10.1016/j.neuron.2006.12.017>

Bloodgood, B. L., & Sabatini, B. L. (2009). *NMDA Receptor-Mediated Calcium Transients in Dendritic Spines*. *Biology of the NMDA Receptor*. Retrieved from <http://www.ncbi.nlm.nih.gov/pubmed/21204410>

Bowie, D., & Mayer, M. L. (1995). Inward rectification of both AMPA and kainate subtype glutamate receptors generated by polyamine-mediated ion channel block. *Neuron*, 15(2), 453–462. [http://doi.org/10.1016/0896-6273\(95\)90049-7](http://doi.org/10.1016/0896-6273(95)90049-7)

Branco, T., & Häusser, M. (2011). Synaptic Integration Gradients in Single Cortical Pyramidal Cell Dendrites. *Neuron*, 69(5), 885–892. <http://doi.org/10.1016/j.neuron.2011.02.006>

Burnashev, N., Zhou, Z., Neher, E., & Sakmann, B. (1995). Fractional calcium currents through recombinant GluR channels of the NMDA, AMPA and kainate receptor subtypes. *The Journal of Physiology*, 485(2), 403–418. <http://doi.org/10.1113/jphysiol.1995.sp020738>

Camiré, O., & Topolnik, L. (2014). Dendritic calcium nonlinearities switch the direction of synaptic plasticity in fast-spiking interneurons. *The Journal of Neuroscience : The Official Journal of the Society for Neuroscience*, 34(11), 3864–77. <http://doi.org/10.1523/JNEUROSCI.2253-13.2014>

Cardin, J. a, Carlén, M., Meletis, K., Knoblich, U., Zhang, F., Deisseroth, K., ... Moore, C. I. (2009). Driving fast-spiking cells induces gamma rhythm and controls sensory responses. *Nature*, 459(7247), 663–667. <http://doi.org/10.1038/nature08002>

Carlé N, M., Meletis, K., Siegle, J., Cardin, J., Futai, K., Vierling-Claassen, D., ... Tsai, L.-H. (2011). A critical role for NMDA receptors in parvalbumin interneurons for gamma rhythm induction and behavior. *Molecular Psychiatry*, 17, 537–548. <http://doi.org/10.1038/mp.2011.31>

Carter, A. G., & Sabatini, B. L. (2004). State-dependent calcium signaling in dendritic spines of striatal medium spiny neurons. *Neuron*, 44(3), 483–493. <http://doi.org/10.1016/j.neuron.2004.10.013>

Clem, R. L., & Huganir, R. L. (2010). Calcium-permeable AMPA receptor dynamics mediate fear memory erasure. *Science (New York, N. Y.)*, 330(6007), 1108–12. <http://doi.org/10.1126/science.1195298>

Cull-Candy, S., Brickley, S., & Farrant, M. (2001). NMDA receptor subunits: diversity, development and disease. *Current Opinion in Neurobiology*, 11(3), 327–335. [http://doi.org/10.1016/S0959-4388\(00\)00215-4](http://doi.org/10.1016/S0959-4388(00)00215-4)

Curthoys, N. P. (1995). Regulation of Glutaminase Activity and Glutamine Metabolism. *Annual Review of Nutrition*, 15(1), 133–159. <http://doi.org/10.1146/annurev.nutr.15.1.133>

Dani, V. S., Chang, Q., Maffei, A., Turrigiano, G. G., Jaenisch, R., & Nelson, S. B. (2005). Reduced cortical activity due to a shift in the balance between excitation and inhibition in a mouse model of Rett Syndrome. *Proceedings of the National Academy of*

- Sciences*, 102(35), 12560–12565. <http://doi.org/10.1073/pnas.0506071102>
- del Castillo, J., & Katz, B. (1954). Quantal components of the end-plate potential. *The Journal of Physiology*, 124(3), 560–573. <http://doi.org/10.1113/jphysiol.1954.sp005129>
- Dingledine, R., Borges, K., Bowie, D., & Traynelis, S. F. (1999). The glutamate receptor ion channels. *Pharmacological Reviews*, 51(1), 7–61. <http://doi.org/10.10049997>
- Evans, R. C., Morera-Herreras, T., Cui, Y., Du, K., Sheehan, T., Koteleski, J. H., ... Blackwell, K. T. (2012). The effects of NMDA subunit composition on calcium influx and spike timing-dependent plasticity in striatal medium spiny neurons. *PLoS Comput Biol*, 8(4), e1002493. <http://doi.org/10.1371/journal.pcbi.1002493> rPCOMPBIOL-D-11-01191 [pii]
- Faber, E. S. L., Delaney, A. J., & Sah, P. (2005). SK channels regulate excitatory synaptic transmission and plasticity in the lateral amygdala. *Nature Neuroscience*, 8(5), 635–641. <http://doi.org/10.1038/nn1450>
- Fatt, P., & Katz, B. (1951). An analysis of the end-plate potential recorded with an intracellular electrode. *The Journal of Physiology*, 115(3), 320–370. <http://doi.org/10.1113/jphysiol.1951.sp004675>
- Fatt, P., & Katz, B. (1952). Spontaneous subthreshold activity at motor nerve endings. *The Journal of Physiology*, 117(1), 109–128. <http://doi.org/10.1113/jphysiol.1952.sp004735>
- Fortin, D. A., Davare, M. A., Srivastava, T., Brady, J. D., Nygaard, S., Derkach, V. A., & Soderling, T. R. (2010). Long-Term Potentiation-Dependent Spine Enlargement Requires Synaptic Ca²⁺-Permeable AMPA Receptors Recruited by CaM-Kinase I. *Journal of Neuroscience*, 30(35), 11565–11575. <http://doi.org/10.1523/JNEUROSCI.1746-10.2010>
- Freund, T. F., & Buzsáki, G. (1998). Interneurons of the hippocampus. *Hippocampus*, 6(4), 347–470. [http://doi.org/10.1002/\(SICI\)1098-1063\(1996\)6:4<347::AID-HIPO1>3.0.CO;2-I](http://doi.org/10.1002/(SICI)1098-1063(1996)6:4<347::AID-HIPO1>3.0.CO;2-I)
- Galarreta, M., & Hestrin, S. (1999). A network of fast-spiking cells in the neocortex connected by electrical synapses. *Nature*, 402(6757), 72–75. <http://doi.org/10.1038/47029>
- Gambino, F., Pagès, S., Kehayas, V., Baptista, D., Tatti, R., Carleton, A., & Holtmaat, A. (2014). Sensory-evoked LTP driven by dendritic plateau potentials in vivo. *Nature*, 515(7525), 116–119. <http://doi.org/10.1038/nature13664>
- Geiger, J. R. P., Lübke, J., Roth, A., Frotscher, M., & Jonas, P. (1997). Submillisecond AMPA receptor-mediated signaling at a principal neuron- interneuron synapse. *Neuron*, 18(6), 1009–1023. [http://doi.org/10.1016/S0896-6273\(00\)80339-6](http://doi.org/10.1016/S0896-6273(00)80339-6)
- Geiger, J. R. P., Melcher, T., Koh, D. S., Sakmann, B., Seeburg, P. H., Jonas, P., & Monyer, H. (1995). Relative abundance of subunit mRNAs determines gating and Ca²⁺ permeability of AMPA receptors in principal neurons and interneurons in rat CNS. *Neuron*, 15(1), 193–204. [http://doi.org/10.1016/0896-6273\(95\)90076-4](http://doi.org/10.1016/0896-6273(95)90076-4)
- Ghosh, a, & Greenberg, M. E. (1995). Calcium signaling in neurons: molecular

mechanisms and cellular consequences. *Science (New York, N.Y.)*, 268(5208), 239–247. <http://doi.org/10.1126/science.7716515>

Giese, K. P., Fedorov, N. B., Filipkowski, R. K., & Silva, A. J. (1998). Autophosphorylation at Thr286 of the α calcium-calmodulin kinase II in LTP and learning. *Science*, 279(5352), 870–873. <http://doi.org/10.1126/science.279.5352.870>

Gilbert-Juan, J., Castillo-Gomez, E., Pérez-Rando, M., Moltó, M. D., & Nacher, J. (2011). Chronic stress induces changes in the structure of interneurons and in the expression of molecules related to neuronal structural plasticity and inhibitory neurotransmission in the amygdala of adult mice. *Experimental Neurology*, 232(1), 33–40. <http://doi.org/10.1016/j.expneurol.2011.07.009>

Goldberg, J. H., Tamas, G., Aronov, D., & Yuste, R. (2003). Calcium microdomains in aspiny dendrites. *Neuron*, 40(4), 807–821. [http://doi.org/10.1016/S0896-6273\(03\)00714-1](http://doi.org/10.1016/S0896-6273(03)00714-1)

Goldberg, J. H., Yuste, R., & Tamas, G. (2003). Ca²⁺ imaging of mouse neocortical interneurone dendrites: Contribution of Ca²⁺-permeable AMPA and NMDA receptors to subthreshold Ca²⁺-dynamics. *The Journal of Physiology*, 551(1), 67–78. <http://doi.org/10.1113/jphysiol.2003.042598>

Greger, I. H., Ziff, E. B., & Penn, A. C. (2007). Molecular determinants of AMPA receptor subunit assembly. *Trends in Neurosciences*. <http://doi.org/10.1016/j.tins.2007.06.005>

Griffith, L. C., & Budnik, V. (2006). Plasticity and Second Messengers During Synapse Development. *International Review of Neurobiology*. [http://doi.org/10.1016/S0074-7742\(06\)75011-5](http://doi.org/10.1016/S0074-7742(06)75011-5)

Griffith, T., Tsaneva-Atanasova, K., & Mellor, J. R. (2016). Control of Ca²⁺Influx and Calmodulin Activation by SK-Channels in Dendritic Spines. *PLoS Computational Biology*, 12(5). <http://doi.org/10.1371/journal.pcbi.1004949>

Guirado, R., Perez-Rando, M., Sanchez-Matarredona, D., Castillo-Gómez, E., Liberia, T., Rovira-Esteban, L., ... Nacher, J. (2014). The dendritic spines of interneurons are dynamic structures influenced by PSA-NCAM expression. *Cerebral Cortex*, 24(11), 3014–3024. <http://doi.org/10.1093/cercor/bht156>

Gulledge, A. T., Carnevale, N. T., & Stuart, G. J. (2012). Electrical advantages of dendritic spines. *PLoS ONE*, 7(4). <http://doi.org/10.1371/journal.pone.0036007>

Gulyá, A. I., Megías, M., Emri, Z., & Freund, T. F. (1999). Total Number and Ratio of Excitatory and Inhibitory Synapses Converging onto Single Interneurons of Different Types in the CA1 Area of the Rat Hippocampus. *The Journal of Neuroscience*, 19(22), 10082–10097. <http://doi.org/10.1002/cne.902960202>

Haider, B. (2006). Neocortical Network Activity In Vivo Is Generated through a Dynamic Balance of Excitation and Inhibition. *Journal of Neuroscience*, 26(17), 4535–4545. <http://doi.org/10.1523/JNEUROSCI.5297-05.2006>

Harnett, M. T., Makara, J. K., Spruston, N., Kath, W. L., & Magee, J. C. (2012). Synaptic amplification by dendritic spines enhances input cooperativity. *Nature*, 491(7425), 599–602. <http://doi.org/10.1038/nature11554>

- Harris, K. M., & Weinberg, R. J. (2012). Ultrastructure of synapses in the mammalian brain. *Cold Spring Harbor Perspectives in Biology*. <http://doi.org/10.1101/cshperspect.a005587>
- Hong, I., Kim, J., Kim, J., Lee, S., Ko, H., Nader, K., ... Choi, S. (2013). AMPA receptor exchange underlies transient memory destabilization on retrieval. *Proc Natl Acad Sci*, *45110(2)*, 18279–18284. <http://doi.org/10.1073/pnas.1322627111>
- Howes, O., McCutcheon, R., & Stone, J. (2015). Glutamate and dopamine in schizophrenia: An update for the 21st century. *Journal of Psychopharmacology*. <http://doi.org/10.1177/0269881114563634>
- Hull, C., Isaacson, J. S., & Scanziani, M. (2009). Postsynaptic Mechanisms Govern the Differential Excitation of Cortical Neurons by Thalamic Inputs. *Journal of Neuroscience*, *29(28)*, 9127–9136. <http://doi.org/10.1523/JNEUROSCI.5971-08.2009>
- Jahr, C. E., & Stevens, C. F. (1990). Voltage dependence of NMDA-activated macroscopic conductances predicted by single-channel kinetics. *The Journal of Neuroscience*, *10(9)*, 3178–3182. <http://doi.org/1990/09/01 00:01>
- Jayant, K., Hirtz, J. J., Plante, I. J. La, Tsai, D. M., De Boer, W. D. A. M., Semonche, A., ... Yuste, R. (2017). Targeted intracellular voltage recordings from dendritic spines using quantum-dot-coated nanopipettes. *Nature Nanotechnology*, *12(4)*, 335–342. <http://doi.org/10.1038/nnano.2016.268>
- Juge, N., Yoshida, Y., Yatsushiro, S., Omote, H., & Moriyama, Y. (2006). Vesicular glutamate transporter contains two independent transport machineries. *Journal of Biological Chemistry*, *281(51)*, 39499–39506. <http://doi.org/10.1074/jbc.M607670200>
- Kawaguchi, Y. (1993). Groupings of nonpyramidal and pyramidal cells with specific physiological and morphological characteristics in rat frontal cortex. *Journal of Neurophysiology*, *69(2)*, 416–431.
- Kawaguchi, Y., Karube, F., & Kubota, Y. (2006). Dendritic branch typing and spine expression patterns in cortical nonpyramidal cells. *Cerebral Cortex*, *16(5)*, 696–711. <http://doi.org/10.1093/cercor/bhj015>
- Kawato, M., & Tsukahara, N. (1984). Electrical properties of dendritic spines with bulbous end terminals. *Biophysical Journal*, *46(2)*, 155–166. [http://doi.org/10.1016/S0006-3495\(84\)84008-4](http://doi.org/10.1016/S0006-3495(84)84008-4)
- Keck, T., Scheuss, V., Jacobsen, R. I., Wierenga, C. J., Eysel, U. T., Bonhoeffer, T., & Hübener, M. (2011). Loss of sensory input causes rapid structural changes of inhibitory neurons in adult mouse visual cortex. *Neuron*, *71(5)*, 869–882. <http://doi.org/10.1016/j.neuron.2011.06.034>
- Kim, K., Lee, S. G., Kegelman, T. P., Su, Z. Z., Das, S. K., Dash, R., ... Fisher, P. B. (2011). Role of Excitatory Amino Acid Transporter-2 (EAAT2) and glutamate in neurodegeneration: Opportunities for developing novel therapeutics. *Journal of Cellular Physiology*. <http://doi.org/10.1002/jcp.22609>
- Kirschuk, S., Héja, L., Kardos, J., & Billups, B. (2016). Astrocyte sodium signaling and the regulation of neurotransmission. *GLIA*. <http://doi.org/10.1002/glia.22943>

- Kloc, M., & Maffei, a. (2014). Target-Specific Properties of Thalamocortical Synapses onto Layer 4 of Mouse Primary Visual Cortex. *Journal of Neuroscience*, 34(46), 15455–15465. <http://doi.org/10.1523/JNEUROSCI.2595-14.2014>
- Korotkova, T., Fuchs, E. C., Ponomarenko, A., von Engelhardt, J., & Monyer, H. (2010). NMDA Receptor Ablation on Parvalbumin-Positive Interneurons Impairs Hippocampal Synchrony, Spatial Representations, and Working Memory. *Neuron*, 68(3), 557–569. <http://doi.org/10.1016/j.neuron.2010.09.017>
- Kubota, Y., Karube, F., Nomura, M., Gullledge, A. T., Mochizuki, A., Schertel, A., & Kawaguchi, Y. (2011). Conserved properties of dendritic trees in four cortical interneuron subtypes. *Scientific Reports*, 1. <http://doi.org/10.1038/srep00089>
- Kwon, T., Sakamoto, M., Peterka, D. S., & Yuste, R. (2017). Attenuation of Synaptic Potentials in Dendritic Spines. *Cell Reports*, 20(5), 1100–1110. <http://doi.org/10.1016/j.celrep.2017.07.012>
- Lamsa, K. P., Heeroma, J. H., Somogyi, P., Rusakov, D. a, & Kullmann, D. M. (2007). Anti-Hebbian long-term potentiation in the hippocampal feedback inhibitory circuit. *Science (New York, N. Y.)*, 315(5816), 1262–1266. <http://doi.org/10.1126/science.1137450>
- Le Roux, N., Cabezas, C., Böhm, U. L., & Poncer, J. C. (2013). Input-specific learning rules at excitatory synapses onto hippocampal parvalbumin-expressing interneurons. *The Journal of Physiology*, 591(Pt 7), 1809–22. <http://doi.org/10.1113/jphysiol.2012.245852>
- Lee, S. J. R., Escobedo-Lozoya, Y., Szatmari, E. M., & Yasuda, R. (2009). Activation of CaMKII in single dendritic spines during long-term potentiation. *Nature*, 458(7236), 299–304. <http://doi.org/10.1038/nature07842>
- Lisman, J., Schulman, H., & Cline, H. (2002). THE MOLECULAR BASIS OF CaMKII FUNCTION IN SYNAPTIC AND BEHAVIOURAL MEMORY. *Nature Reviews Neuroscience*, 3(3), 175–190. <http://doi.org/10.1038/nrn753>
- Lisman, J., Yasuda, R., & Raghavachari, S. (2012). Mechanisms of CaMKII action in long-term potentiation. *Nature Reviews Neuroscience*. <http://doi.org/10.1038/nrn3192>
- Losonczy, A., Makara, J. K., & Magee, J. C. (2008). Compartmentalized dendritic plasticity and input feature storage in neurons. *Nature*, 452(7186), 436–441. <http://doi.org/10.1038/nature06725>
- Lüscher, C., & Malenka, R. C. (2012). NMDA receptor-dependent long-term potentiation and long-term depression (LTP/LTD). *Cold Spring Harbor Perspectives in Biology*, 4(6), 1–15. <http://doi.org/10.1101/cshperspect.a005710>
- Matta, J. a, Pelkey, K. a, Craig, M. T., Chittajallu, R., Jeffries, B. W., & McBain, C. J. (2013). Developmental origin dictates interneuron AMPA and NMDA receptor subunit composition and plasticity. *Nature Neuroscience*, 16(8), 1032–41. <http://doi.org/10.1038/nn.3459>
- McCormick, D. a, Connors, B. W., Lighthall, J. W., & Prince, D. a. (1985). Comparative electrophysiology of pyramidal and sparsely spiny stellate neurons of the neocortex. *Journal of Neurophysiology*, 54(4), 782–806. <http://doi.org/10.1152/jn.00728.2004>

- Meldrum, B. S. (2000). Glutamate as a neurotransmitter in the brain: review of physiology and pathology. *The Journal of Nutrition*, 130(4S Suppl), 1007S–15S. <http://doi.org/10736372>
- Meng, Y., Zhang, Y., Tregoubov, V., Janus, C., Cruz, L., Jackson, M., ... Jia, Z. (2002). Abnormal spine morphology and enhanced LTP in LIMK-1 knockout mice. *Neuron*, 35(1), 121–133. [http://doi.org/10.1016/S0896-6273\(02\)00758-4](http://doi.org/10.1016/S0896-6273(02)00758-4)
- Moriyoshi, K., Masu, M., Ishii, T., Shigemoto, R., Mizuno, N., & Nakanishi, S. (1991). Molecular cloning and characterization of the rat NMDA receptor. *Nature*, 354(6348), 31–37. <http://doi.org/10.1038/354031a0>
- Murakoshi, H., Wang, H., & Yasuda, R. (2011). Local, persistent activation of Rho GTPases during plasticity of single dendritic spines. *Nature*, 472(7341), 100–106. <http://doi.org/10.1038/nature09823>
- Nevian, T., & Sakmann, B. (2006). Spine Ca²⁺ Signaling in Spike-Timing-Dependent Plasticity. *Journal of Neuroscience*, 26(43), 11001–11013. <http://doi.org/10.1523/JNEUROSCI.1749-06.2006>
- Ngo-Anh, T. J., Bloodgood, B. L., Lin, M., Sabatini, B. L., Maylie, J., & Adelman, J. P. (2005). SK channels and NMDA receptors form a Ca²⁺-mediated feedback loop in dendritic spines. *Nature Neuroscience*, 8(5), 642–649. <http://doi.org/10.1038/nn1449>
- Nimchinsky, E. A., Sabatini, B. L., & Svoboda, K. (2002). Structure and Function of Dendritic Spines. *Annual Review of Physiology*, 64(1), 313–353. <http://doi.org/10.1146/annurev.physiol.64.081501.160008>
- Nissen, W., Szabo, A., Somogyi, J., Somogyi, P., & Lamsa, K. P. (2010). Cell Type-Specific Long-Term Plasticity at Glutamatergic Synapses onto Hippocampal Interneurons Expressing either Parvalbumin or CB1 Cannabinoid Receptor. *Journal of Neuroscience*, 30(4), 1337–1347. <http://doi.org/10.1523/JNEUROSCI.3481-09.2010>
- Nowak, L., Bregestovski, P., Ascher, P., Herbet, A., & Prochiantz, A. (1984). Magnesium gates glutamate-activated channels in mouse central neurones. *Nature*, 307(February), 462–465. <http://doi.org/10.1017/CBO9781107415324.004>
- O’Kane, E. M., Stone, T. W., & Morris, B. J. (2003). Activation of Rho GTPases by synaptic transmission in the hippocampus. *Journal of Neurochemistry*, 87(5), 1309–1312. <http://doi.org/10.1046/j.1471-4159.2003.02102.x>
- Opazo, P., Labrecque, S., Tigaret, C. M., Frouin, A., Wiseman, P. W., De Koninck, P., & Choquet, D. (2010). CaMKII triggers the diffusional trapping of surface AMPARs through phosphorylation of stargazin. *Neuron*. <http://doi.org/10.1016/j.neuron.2010.06.007>
- Oren, I., Nissen, W., Kullmann, D. M., Somogyi, P., & Lamsa, K. P. (2009). Role of Ionotropic Glutamate Receptors in Long-Term Potentiation in Rat Hippocampal CA1 Oriens-Lacunosum Moleculare Interneurons. *Journal of Neuroscience*, 29(4), 939–950. <http://doi.org/10.1523/JNEUROSCI.3251-08.2009>
- Pchitskaya, E., Popugaeva, E., & Bezprozvanny, I. (2017). Calcium signaling and molecular mechanisms underlying neurodegenerative diseases. *Cell Calcium*.

<http://doi.org/10.1016/j.ceca.2017.06.008>

- Pérez-Rando, M., Castillo-Gómez, E., Bellés, M., Carceller, H., & Nácher, J. (2017). The activation of NMDA receptors alters the structural dynamics of the spines of hippocampal interneurons. *Neuroscience Letters*, 658, 79–84. <http://doi.org/10.1016/j.neulet.2017.08.042>
- Perez-Rando, M., Castillo-Gómez, E., Guirado, R., Blasco-Ibañez, J. M., Crespo, C., Varea, E., & Nacher, J. (2017). NMDA Receptors Regulate the Structural Plasticity of Spines and Axonal Boutons in Hippocampal Interneurons. *Frontiers in Cellular Neuroscience*, 11. <http://doi.org/10.3389/fncel.2017.00166>
- Peters, A., & Regidor, J. (1981). A reassessment of the forms of nonpyramidal neurons in area 17 of cat visual cortex. *Journal of Comparative Neurology*, 203(4), 685–716. <http://doi.org/10.1002/cne.902030408>
- Pin, J.-P., & Duvoisin, R. (1995). The metabotropic glutamate receptors: Structure and functions. *Neuropharmacology*. [http://doi.org/10.1016/0028-3908\(94\)00129-G](http://doi.org/10.1016/0028-3908(94)00129-G)
- Ridding, M. C., Sheean, G., Rothwell, J. C., Inzelberg, R., & Kujirai, T. (1995). Changes in the balance between motor cortical excitation and inhibition in focal, task specific dystonia. *Journal of Neurology, Neurosurgery and Psychiatry*, 59(5), 493–498. <http://doi.org/10.1136/jnnp.59.5.493>
- Royer, S., Zemelman, B. V., Losonczy, A., Kim, J., Chance, F., Magee, J. C., & Buzsáki, G. (2012). Control of timing, rate and bursts of hippocampal place cells by dendritic and somatic inhibition. *Nature Neuroscience*, 15(5), 769–775. <http://doi.org/10.1038/nn.3077>
- Segal, M. (2005). Dendritic spines and long-term plasticity. *Nature Reviews Neuroscience*. <http://doi.org/10.1038/nrn1649>
- Sheng, M., & Hoogenraad, C. C. (2007). The Postsynaptic Architecture of Excitatory Synapses: A More Quantitative View. *Annual Review of Biochemistry*, 76(1), 823–847. <http://doi.org/10.1146/annurev.biochem.76.060805.160029>
- Silva, A. J., Kogan, J. H., Frankland, P. W., & Kida, S. (1998). CREB AND MEMORY. *Annual Review of Neuroscience*. <http://doi.org/10.1146/annurev.neuro.21.1.127>
- Sin, W. C., Haas, K., Ruthazer, E. S., & Cline, H. T. (2002). Dendrite growth increased by visual activity requires NMDA receptor and Rho GTPases. *Nature*, 419(6906), 475–480. <http://doi.org/10.1038/nature00987>
- Sobczyk, A., Scheuss, V., & Svoboda, K. (2005). NMDA receptor subunit-dependent [Ca²⁺] signaling in individual hippocampal dendritic spines. *Journal of Neuroscience*, 25(26), 6037–6046.
- Sohal, V. S. (2012). Insights into cortical oscillations arising from optogenetic studies. *Biological Psychiatry*. <http://doi.org/10.1016/j.biopsych.2012.01.024>
- Sugihara, H., Moriyoshi, K., Ishii, T., Masu, M., & Nakanishi, S. (1992). Structures and properties of seven isoforms of the NMDA receptor generated by alternative splicing. *Biochemical and Biophysical Research Communications*, 185(3), 826–832.

[http://doi.org/10.1016/0006-291X\(92\)91701-Q](http://doi.org/10.1016/0006-291X(92)91701-Q)

- Sutula, T. P., & Dudek, F. E. (2007). Unmasking recurrent excitation generated by mossy fiber sprouting in the epileptic dentate gyrus: an emergent property of a complex system. *Progress in Brain Research*. [http://doi.org/10.1016/S0079-6123\(07\)63029-5](http://doi.org/10.1016/S0079-6123(07)63029-5)
- Svoboda, K., & Sabatini, B. L. (2000). Analysis of calcium channels in single spines using optical fluctuation analysis. *Nature*, *408*(6812), 589–593. <http://doi.org/10.1038/35046076>
- Szabo, A., Somogyi, J., Cauli, B., Lambolez, B., Somogyi, P., & Lamsa, K. P. (2012). Calcium-permeable AMPA receptors provide a common mechanism for LTP in glutamatergic synapses of distinct hippocampal interneuron types. *The Journal of Neuroscience : The Official Journal of the Society for Neuroscience*, *32*(19), 6511–6. <http://doi.org/10.1523/JNEUROSCI.0206-12.2012>
- Tada, T., & Sheng, M. (2006). Molecular mechanisms of dendritic spine morphogenesis. *Current Opinion in Neurobiology*. <http://doi.org/10.1016/j.conb.2005.12.001>
- Tian, X., & Feig, L. A. (2006). Age-dependent participation of Ras-GRF proteins in coupling calcium-permeable AMPA glutamate receptors to Ras/Erk signaling in cortical neurons. *Journal of Biological Chemistry*, *281*(11), 7578–7582. <http://doi.org/10.1074/jbc.M512060200>
- Ting, J. T., Kelley, B. G., Lambert, T. J., Cook, D. G., & Sullivan, J. M. (2007). Amyloid precursor protein overexpression depresses excitatory transmission through both presynaptic and postsynaptic mechanisms. *Proc Natl Acad Sci U S A*, *104*(1), 353–358. <http://doi.org/10.1073/pnas.0608807104> [pii]10.1073/pnas.0608807104
- Tomita, S., Stein, V., Stocker, T. J., Nicoll, R. A., & Brecht, D. S. (2005). Bidirectional synaptic plasticity regulated by phosphorylation of stargazin-like TARPs. *Neuron*, *45*(2), 269–277. <http://doi.org/10.1016/j.neuron.2005.01.009>
- Vicini, S., Wang, J. F., Li, J. H., Zhu, W. J., Wang, Y. H., Luo, J. H., ... Grayson, D. R. (1998). Functional and pharmacological differences between recombinant N-methyl-D-aspartate receptors. *Journal of Neurophysiology*, *79*(2), 555–66. [http://doi.org/10.1016/0014-5793\(92\)80648-Z](http://doi.org/10.1016/0014-5793(92)80648-Z)
- Vogels, T. P., Sprekeler, H., Zenke, F., Clopath, C., & Gerstner, W. (2011). Inhibitory plasticity balances excitation and inhibition in sensory pathways and memory networks. *Science*, *334*(6062), 1569–1573. <http://doi.org/10.1126/science.1211095>
- Wang, H., Ardiles, A. O., Yang, S., Tran, T., Posada-Duque, R., Valdivia, G., ... Kirkwood, A. (2016). Metabotropic Glutamate Receptors Induce a Form of LTP Controlled by Translation and Arc Signaling in the Hippocampus. *Journal of Neuroscience*. <http://doi.org/10.1523/JNEUROSCI.0878-15.2016>
- Wang, K., Lin, M. T., Adelman, J. P., & Maylie, J. (2014). Distinct Ca²⁺ sources in dendritic spines of hippocampal CA1 Neurons Couple to SK and Kv4 Channels. *Neuron*, *81*(2), 379–387. <http://doi.org/10.1016/j.neuron.2013.11.004>
- Washburn, M. S., Numberger, M., Zhang, S., & Dingledine, R. (1997). Differential dependence on GluR2 expression of three characteristic features of AMPA receptors.

The Journal of Neuroscience : The Official Journal of the Society for Neuroscience, 17(24), 9393–9406.

Weber, J. P., Andrásfalvy, B. K., Polito, M., Magó, Á., Ujfalussy, B. B., & Makara, J. K. (2016). Location-dependent synaptic plasticity rules by dendritic spine cooperativity. *Nature Communications*, 7. <http://doi.org/10.1038/ncomms11380>

Yizhar, O., Fenno, L. E., Prigge, M., Schneider, F., Davidson, T. J., Ogshea, D. J., ... Deisseroth, K. (2011). Neocortical excitation/inhibition balance in information processing and social dysfunction. *Nature*, 477(7363), 171–178. <http://doi.org/10.1038/nature10360>

Yuste, R. (2013). Electrical Compartmentalization in Dendritic Spines. *Annual Review of Neuroscience*, 36(1), 429–449. <http://doi.org/10.1146/annurev-neuro-062111-150455>

Yuste, R., & Denk, W. (1995). Dendritic spines as basic functional units of neuronal integration. *Nature*. <http://doi.org/10.1038/375682a0>

Zhou, Y., Takahashi, E., Li, W., Halt, A., Wiltgen, B., Ehninger, D., ... Silva, A. J. (2007). Interactions between the NR2B Receptor and CaMKII Modulate Synaptic Plasticity and Spatial Learning. *Journal of Neuroscience*, 27(50), 13843–13853. <http://doi.org/10.1523/JNEUROSCI.4486-07.2007>

Zhu, J. J., Qin, Y., Zhao, M., Van Aelst, L., & Malinow, R. (2002). Ras and Rap control AMPA receptor trafficking during synaptic plasticity. *Cell*. [http://doi.org/10.1016/S0092-8674\(02\)00897-8](http://doi.org/10.1016/S0092-8674(02)00897-8)

Zhu, S., & Gouaux, E. (2017). Structure and symmetry inform gating principles of ionotropic glutamate receptors. *Neuropharmacology*. <http://doi.org/10.1016/j.neuropharm.2016.08.034>

Chapter 2. Functional distinctions between dendritic and spines synapses made onto parvalbumin-positive interneurons in mouse visual cortex

PV INs in layer II/III of V1 are sparsely spiny

We quantified spine density in PV INs of juvenile *Pvalb-cre* x *tdtomato^{fl/fl}* mice (**Figure 2.1A** and **B**). Whole-cell patch clamp recordings were obtained from tdTomato-expressing neurons in layer II/III of primary visual cortex (V1, **Figure 2.1C**). AP kinetics (**Figure 2.1D**) and intrinsic membrane properties were consistent with fast-spiking, PV-positive INs from juvenile mice (full-width at half maximum: 1.0 ± 0.04 ms; input resistance: 113.1 ± 9.3 M Ω ; membrane capacitance: 36.4 ± 2.0 pF; spike rate: 83.9 ± 6.2 Hz; Okaty et al. 2009; Azouz et al. 1997). Neurons were filled with the red fluorescent dye Alexa Fluor-594 (100 μ M; **Figure 2.1C** and **E**) and dendrites were imaged by two-photon microscopy. This allowed for rapid filling of the dendrites with dye that could be imaged independently of tdTomato protein present in the dense axonal arbor and other nearby neurons. We detected approximately one spine per 10 μ m and spine densities were similar in tissue from mice before and during the critical period (**Figure 2.1F**; P15-19: 1.2 ± 0.1 spines/10 μ m; P20-30: 0.85 ± 0.1 spines/10 μ m; P45-56: 0.69 ± 0.054 spines/10 μ m). For young mice, spine density was comparable along the length of the dendrite; in P46-56 mice, spine density was higher in distal relative to proximal dendrites (**Figure 2.1G**; P15-19, <50 μ m from the soma: 1.4 ± 0.2 , >50 μ m: 1.2 ± 0.3 ; P20-30, <50 μ m: 0.7 ± 0.1 , >50 μ m: 1.4 ± 0.5 ; P46-56, <50 μ m: 0.52 ± 0.083 , >50 μ m: 0.83 ± 0.085 , $p = 0.016$). However, there was a small, but significant, decrease in the spine density on the proximal dendrites in P20-30 and P46-56 mice as compared to the younger mice (**Figure 2.1G**), suggesting that spines are a consistent, yet dynamic, anatomical feature of PV INs in the juvenile visual cortex.

Spines on PV INs enclose functional glutamatergic synapses

Spine-like membrane protrusions have been previously described in PV INs (Gulyás et al. 1999; Peters & Regidor 1981). It is less clear, however, if these spines enclose functional excitatory synapses. To determine if synapses are made onto dendritic spines, whole-cell voltage clamp recordings were obtained from PV INs and local axons were stimulated with an extracellular (EC) electrode placed near a PV IN dendrite (**Figure 2.2A**). The neurons were filled with Alexa Fluor-594 (15 μ M) and the green Ca-sensitive fluorophore Fluo-5F (300 μ M) through the patch pipette. Initially, EC stimulus intensity was set to evoke a large current at the soma but no Ca signal at the dendritic shaft or spine head imaged (“no calcium transient”; **Figure 2.2C** and **G**; see **Methods**). While the presence or lack of a Ca transient is used as a proxy for synaptic transmission, it is important to note that the lack of Ca transients could be due to failure of transmission or failure to evoke a presynaptic AP. The EC stimulus strength was gradually increased until all-or-nothing Ca signals were accompanied by large currents, consistent with transmission from many axons synapsing throughout the dendrites including the imaged location (**Figure 2.2D, E, and H**; see **Methods**). Moreover, in a fraction of trials for both dendritic and spine events, the stimulus failed to produce a Ca transient, evocative of a failure of synaptic transmission. The stimulus-evoked Ca transients were observed as green fluorescence hot-spots in dendrites or as increases in fluorescence in the spine head and were similar in amplitude and kinetics at both locations (**Figure 2.2I**). Ca transients measured in spines had rapid rise times (20-80%: 4.6 ± 0.6 ms), suggesting that they originated within the spine head and were not due to Ca-bound Fluo-5F diffusing in from the adjacent dendrite. In 12 out of 19 spines, the evoked Ca transient was restricted to the spine head as

previously reported for synaptically-evoked Ca signals (Bloodgood, Giessel, & Sabatini, 2009; Bernardo L. Sabatini, Oertner, & Svoboda, 2002).

To exclude the possibility that the Ca transients were due to direct depolarization of the dendrites, NMDAR and AMPAR antagonists were sequentially applied to the bath (10 μ M CPP and NBQX, respectively) and the evoked Ca transients were compared to control conditions. Blocking NMDARs significantly reduced the peak Ca transients in the dendrites and in the spine head (**Figure 2.2J-L**). Subsequent antagonism of AMPARs eliminated the remaining Ca transients (**Figure 2.2J-L**). Thus, spines on PV INs contain functional glutamatergic synapses. Moreover, we find that NMDAR activation accounts for a significant fraction of the synaptic Ca response for both spine and dendrite synapses.

Since PV INs express high levels of CP-AMPA receptors, we sought to determine if these receptors contribute to the synaptically-evoked Ca signal in spines, as has been previously reported for dendrites (Goldberg et al. 2003a; Goldberg et al. 2003c). Wash-in of philanthotoxin-433 (PhTx, 10 μ M) to selectively block CP-AMPA receptors led to a significant reduction in the peak dendritic and spine Ca transient (**Figure 2.2M-O**). Importantly, since PhTx is a use-dependent blocker, the first 10-15 trials after wash-in were excluded from our analysis. In both regions, the evoked response was further reduced, but not eliminated, by the subsequent application of NBQX (**Figure 2.2M-O**). The residual Ca transient, attributable to NMDARs, was significantly smaller than the CPP-sensitive component, consistent with AMPAR-mediated depolarization leading to the enhancement of NMDAR-mediated currents.

While evoked Ca transients measured at both dendrite and spine synapses are sensitive to NMDAR and CP-AMPA blockers, the synapse-to-synapse variability was high, particularly for spine synapses (**Figure 2.3**). One synaptically-evoked Ca transient

produced in a dendrite was unaffected by CPP and several of the Ca transients measured in spines were unaffected by either CPP or PhTx, indicating the absence of the respective receptor type at that location. Thus, dendritic and spine synapses can contain both CP-AMPARs and NMDARs, but the glutamate receptor composition of individual synapses is variable, most notably for spines where synapses may lack either CP-AMPARs or NMDARs.

Two-photon glutamate uncaging and Ca imaging reveals NMDARs are enriched at spine synapses

Since extracellular stimulation activates many synapses that are distributed throughout the neuron's dendrites, this prevents concomitant analysis of synaptic potentials and Ca transients. Additionally, while we performed the above experiments in voltage clamp to limit the effects of currents generated elsewhere in the neuron on the receptors at the synapses being examined, recent work has shown that spine depolarizations, in contrast to dendritic depolarizations, cannot be adequately voltage-clamped (Beaulieu-Laroche & Harnett, 2017). Thus, in order to dissect the contributions of the two Ca-permeable glutamate receptor subtypes to the electrical and Ca signals produced by individual dendritic and spine synapses, we performed simultaneous two-photon MNI-glutamate uncaging and Ca imaging, in combination with electrophysiology and pharmacology, in both voltage and current clamp (**Figure 2.4A**; Bloodgood & Sabatini 2007; Bloodgood & Sabatini 2005).

Whole-cell recordings from PV INs were obtained and the neurons were filled with Alexa Fluor-594 and Fluo-5F through the pipette as above. MNI-glutamate was bath-applied and brief pulses of light (0.5 ms, 720 nm) were delivered focally to uncage

glutamate at putative dendritic synapses, defined as local current hot-spots (**Figure 2.4B** and **D**), or at spine heads (**Figure 2.4F**, **Figure 2.5A-C**, see **Methods**). Twenty-two of the 31 imaged spines displayed both an uncaging-evoked EPSC (uEPSC) and Ca signal; analyses were restricted to that sub-group. Of the spines omitted from the data set, 6 generated a Ca transient and no measureable uEPSC, suggesting the presence of “silent” synapses (Isaac et al. 1995; Liao et al. 1995), and 3 generated a uEPSC but no Ca transient, suggesting the presence of a synapse without Ca-permeable glutamate receptors.

Uncaging glutamate at dendritic hot-spots resulted in Ca transients that were similar to those produced in response to EC stimulation (**Figure 2.4C**) indicating uncaging at dendritic sites is comparable to synaptic transmission. Moreover, dendritic sites produced small uEPSCs and uEPSPs (**Figure 2.4E**) comparable in amplitude and rise time to the average miniature events recorded from PV INs (**Figure 2.5D** and **E**; Dehorter et al. 2015). Analogous experiments conducted in the presence of CPP resulted in uEPSCs and uEPSPs that were similar to control conditions. However, the peak of the uEPSP-associated Ca transient was 26% than in control conditions (**Figure 2.4E, H-K**). Thus, NMDARs are activated by glutamate presented at discrete dendritic sites and contribute significantly to the resulting Ca signal, but not the uEPSP.

Activation of synapses enclosed by spines also produced uEPSCs with rise times similar to miniature events (**Figure 2.5D** and **E**), although with slightly smaller amplitudes than those observed at dendritic sites (**Figure 2.4F** and **G**). Repeating these experiments with NMDARs antagonized resulted in uEPSCs, uEPSPs, and uEPSP-evoked Ca transients that were nearly 50% smaller than in control conditions. Additionally, there was a notable reduction in the late phase of the uEPSC. The difference of the uEPSC recorded in CPP from control conditions revealed a slow, small current consistent with the slower

kinetics of NMDAR-mediated currents (**Figure 2.4G** and **H-K**; Lester et al. 1990). In stark contrast to dendrites, NMDARs at individual spines contribute significantly to both the depolarization and the associated Ca signal.

Is the larger contribution of NMDARs to signals originating from spines simply due to the biophysical properties of spines enhancing synaptic depolarization or are there a greater number of NMDARs in spines as compared to dendrites? To distinguish between these possibilities, NMDARs were pharmacologically isolated (10 μ M NBQX) and magnesium (Mg) was excluded from the extracellular solution to eliminate the voltage dependence of the receptors. Glutamate was uncaged at the spine head and then at multiple locations over the adjacent dendrite, and the dendritic signals were averaged and compared to the spine signal (**Figure 2.4L**). With AMPARs blocked, it was not possible to identify putative dendritic synapses by uEPSC amplitude hot-spots, but in the absence of Mg, we were able to probe receptor density. Considering all nine spine-dendritic cluster comparisons, the uncaging-evoked Ca transient was, on average, 40% larger in the spine head than the parent dendrite (**Figure 2.4M**). Moreover, of the 31 individual dendritic sites probed, 29 produced a smaller Ca transient than the corresponding spine (**Figure 2.4N**). Therefore, while the biophysical properties of the spine likely enhance NMDAR activation, these data also suggest spines have more NMDARs or NMDARs that flux more Ca (Monyer et al. 1992; Bloodgood & Sabatini 2009), as compared to the neighboring dendrite.

CP-AMPA- mediated Ca influx and depolarization are similar in dendrites and spines

As PV INs express CP-AMPARs and these receptors may act as a Ca source that is orthogonal to NMDARs, we sought to determine if CP-AMPARs were also unevenly

distributed between dendritic and spine locations. MNI-glutamate was uncaged at putative dendritic synapses or over spines in the presence of PhTx and responses were compared to control experiments, as above. The first 10 uncaging trials were excluded to contend with the use-dependence of PhTx. Blockade of CP-AMPARs resulted in uEPSPs and associated Ca transients that were significantly smaller than those in control conditions, similarly in both dendritic sites and spines (**Figure 2.6A** and **C-E**). This suggests that, in contrast to NMDARs, CP-AMPARs have relatively similar distributions between dendrites and spines.

The rectification of CP-AMPARs is similar in dendrites and spines

Depolarization drives intracellular polyamines into the pore of CP-AMPARs (Geiger et al., 1995; Kamboj et al. 1995), resulting in a marked inward rectification of CP-AMPAR-mediated currents. As the biophysical properties of spines allow small currents to produce relatively large local depolarizations, we sought to determine if CP-AMPARs at spine synapses could be partially blocked by polyamines during uEPSPs, leading us to underestimate the contribution of CP-AMPARs to synaptic signals in this compartment. To test this, whole-cell recordings were made from PV INs with an internal solution lacking spermine and intracellular polyamines were dialyzed out of the cell. In the absence of polyamines, uEPSPs and Ca signals were similar to those measured in control experiments for both dendrites and spines (**Figure 2.6B** and **C-E**). Thus, it is unlikely that depolarization originating from individual spine or dendritic synapses is sufficient to engage the polyamine block of CP-AMPARs.

In addition to depolarization, the affinity of polyamines for CP-AMPARs can be influenced by the receptor subunit composition (Washburn et al., 1997) and association

with specific TARPs (transmembrane AMPAR regulatory proteins), such as stargazin (Soto et al. 2007), which is expressed in PV INs (Pelkey et al., 2015). If CP-AMPARs at dendritic and spine synapses have systematic differences in subunit composition or stargazin interactions, this would be apparent in comparisons of the rectification of AMPA currents measured from these two locations. Glutamate was uncaged at dendritic sites or over spines in the presence of CPP, and AMPAR currents were measured while holding the neurons at membrane potentials from -70 mV to +40 mV (**Figure 2.6F**). Experiments were also performed in the absence of intracellular spermine for dendritic sites to confirm that polyamines are in fact responsible for any non-linear current-voltage relationship. Current amplitudes were normalized to the peak current recorded at -70 mV (**Figure 2.6G**) and the rectification index (RI) was calculated by dividing the slope of the linear fit of the data at positive voltages by the slope of the fit of the data at negative voltages (**Figure 2.6H**; see **Methods** for details; Soto et al. 2007); RIs below one indicate inward rectification. The RIs measured at dendrites and spines in the presence of intracellular polyamines were not significantly different (**Figure 2.6I**), indicating that AMPARs at dendritic sites and spines have similar affinities for polyamines and are unlikely to be systematically different in composition or TARP interaction. However, excluding spermine resulted in linear current-voltage relationship for dendritic sites; RIs in dendrites with and without spermine were significantly different ($p = 0.025$), confirming the relevance of intracellular polyamines.

Ca signaling through glutamate receptors on dendrites, but not spines, is bi-directionally modulated by back-propagating action potentials

In pyramidal neurons, NMDAR-mediated Ca signals are enhanced when an EPSP is paired with back-propagating action potentials (bAPs) (Yuste & Denk 1995; Wu et al.

2012; Magee & Johnston 1997) and the precise timing of the bAPs can lead to synaptic potentiation or depression (Markram et al. 1997; Froemke & Dan 2002; Nevian & Sakmann 2006). While the dendrites of PV INs do not support the active back-propagation of APs (Hu et al. 2010; Goldberg et al. 2003b), the proximal dendrites do depolarize tens of millivolts as the AP invades (Hu et al. 2010) and small bAP-triggered Ca transients can be measured in proximal dendrites and spines (**Figure 2.7A-D**; Goldberg et al. 2003b). Thus, we hypothesized that glutamate receptor mediated Ca signals originating from synapses made onto the proximal dendrites or spines may be modulated by the coincident firing of the neuron. However, since excitatory synapses made on PV INs contain both CP-AMPA receptors and NMDARs, which are inwardly and outwardly rectifying, respectively, it is unclear if the bAPs would reduce or enhance synaptic Ca signals. Additionally, since spine synapses produce larger NMDAR-mediated Ca transients and are more variable in their receptor composition than the adjacent dendrite, we hypothesized that Ca signals produced at spine synapses may demonstrate a heightened sensitivity to the spiking of the neuron.

To examine the effects of pairing synaptic activation with bAPs in PV INs, we uncaged glutamate at proximal ($\leq 50 \mu\text{m}$ from soma) dendritic sites or spines in conjunction with a burst of five somatically-evoked bAPs delivered either 10 ms before (“pre”) or 10 ms after (“post”) uncaging (**Figure 2.8A**; see **Methods**), timing intervals that are optimal for spike-timing dependent plasticity in pyramidal neurons (Froemke & Dan, 2002). Interactions between the depolarization from the bAPs and the local glutamate receptors were assessed by comparing the sum of the Ca transients measured from the bAPs and the uEPSPs alone to the values measured from the paired stimuli and were reported as the percent difference relative to the calculated sum, referred to as the non-linearity index (NI, **Figure 2.8A**).

Uncaging at dendritic sites resulted in Ca transients that were sub-linear when preceded by a burst of bAPs and supra-linear when the uEPSP was followed by bAPs (**Figure 2.8B and C**; $NI_{pre} = -8.8 \pm 1.8\%$; $NI_{post} = 24.0 \pm 4.0\%$). The impact of the bAPs on the amplitude of the Ca transient was more pronounced when following the uEPSP; nonetheless, nearly all of the dendritic sites showed consistent bi-directional modulation of the uncaging-evoked Ca transient (**Figure 2.8D**). Importantly, the NI was not correlated with the amplitude of the Ca transient, indicating that sub-linearities were not due to saturation of the indicator (**Figure 2.9A**). Finally, reducing the latency between the dendritic uEPSP and bAPs to 2 ms eliminated the sub-linearity observed when spikes preceded the dendritic uEPSP, but still produced a significant supra-linearity when spikes followed the uEPSP (**Figure 2.8D**; $NI_{pre} = 0.7 \pm 2.7\%$; $NI_{post} = 30.2 \pm 10.6\%$), suggesting that the sub-linearity is particularly timing-dependent. Thus, proximal dendritic sites are sensitive to the relative timing of the PV IN's firing as reflected by the difference of the amplitude of the Ca transient produced by the uEPSP.

Modulation of the uncaging- evoked Ca transient by the somatic activity of the PV IN could be due to NMDARs, CP-AMPARs, or both. To distinguish among these possibilities, we repeated the above experiments in the presence of CPP or PhTx. Antagonizing NMDARs did not affect the sub-linearity but eliminated the supra-linearity observed when bAPs followed the uEPSP (**Figure 2.8E**; $NI_{pre} = -9.0 \pm 2.8\%$; $NI_{post} = -2.4 \pm 4.7\%$). Complementing the role of NMDARs, blocking CP-AMPARs abolished the sub-linearity observed when the bAPs preceded the uEPSP, but the post pairing paradigm continued to produce a significant supra-linearity (**Figure 2.8F**; $NI_{pre} = -1.7 \pm 1.7\%$; $NI_{post} = 18.4 \pm 2.6\%$). Moreover, this sub-linearity was due to the direct modulation of CP-AMPARs by intracellular polyamines, as when we repeated these experiments in the absence of spermine in the internal solution, we abolished the significant sub-linearity in the pre

paradigm, but not the supra-linearity in the post paradigm (**Figure 2.8G**; $NI_{pre} = -2.6 \pm 2.9\%$; $NI_{post} = 13.7 \pm 3.6\%$). We also evaluated the NI as a function of the amplitude of the after-hyperpolarization, the membrane potential at the onset of the uEPSP, and the uEPSP amplitude and found that none were correlated (**Figure 2.9B**). This suggests that while the sub-linearity is CP-AMPA-dependent, it is unlikely to be related to the effects of membrane potential on the driving force or intracellular block of the receptors. These data indicate that subtypes of glutamate receptors on the proximal dendrites of PV INs are sensitive to the neuron's firing such that when spikes precede a uEPSP, synaptic Ca influx is reduced via a CP-AMPA-dependent mechanism and when spikes follow a uEPSP, NMDAR-mediated Ca transients are enhanced.

Since NMDARs contribute more to synaptic potentials and Ca transients originating in spines than dendrites, we hypothesized that glutamate receptors localized to spines may be more sensitive to bAPs. Unexpectedly, when bAPs were paired with spine uEPSPs, neither the pre nor the post pairing paradigms resulted in a significant non-linearity (**Figure 2.10A-C**; $NI_{pre} = -7.9 \pm 6.1\%$; $NI_{post} = 4.3 \pm 6.6\%$). Moreover, while the difference between pre and post temporal pairings was significant, it was substantially smaller than that observed when uncaging at dendritic sites (dendrite: 31%, spine: 12%). Reducing the latency to 2 ms did not reveal any significant supra- or sub-linearities (**Figure 2.10C**). Additionally, antagonizing NMDARs or CP-AMPA receptors did not produce any significant non-linearities or changes that were significantly different than control conditions (**Figure 2.10D and E**; CPP: $NI_{pre} = -1.5 \pm 7.3\%$, $NI_{post} = -12.4 \pm 7.5\%$; PhTx: $NI_{pre} = -2.4 \pm 5.1\%$, $NI_{post} = 11.0 \pm 6.7\%$). In all conditions, the NI was uncorrelated with the amplitude of the Ca signal, suggesting our measurements are not confounded by saturation of the indicator (**Figure 2.11A**). These data demonstrate that proximal spine synapses, unlike their dendritic counterparts, are largely insensitive to somatic activity, despite being invaded by bAPs.

Spine synapses are sensitive to the co-activation of neighboring dendritic synapses

If spine synapses are insensitive to bAPs, are they sensitive to EPSPs originating in the adjacent dendrite (Losonczy & Magee 2006; Harnett et al. 2012; Polsky et al. 2004; Gasparini et al. 2004)? Glutamate was uncaged at an individual spine alone or in combination with five uncaging pulses delivered at a nearby dendritic site, mimicking the depolarization that would be produced by a barrage of synaptic inputs (**Figure 2.12A**; see **Methods** for details). Dendritic uncaging occurred either 2 ms before (pre) or after (post) spine stimulation, timing intervals that are efficacious in principle neurons (Branco & Häusser, 2011; Losonczy & Magee, 2006), and non-linearities in the spine Ca signal were calculated and quantified as above (**Figure 2.12B**, see **Methods** for details). Spines were excluded from the analysis if dendritic uncaging alone produced a significant Ca transient in the spine, indicative of the diffusion of Ca-bound indicator into the spine head. We observed that spine Ca signals were boosted by dendritic uEPSPs, regardless of whether the dendritic uEPSP preceded or followed the spine uEPSP, as reflected by positive NI values for both the pre and post pairing paradigms (**Figure 2.12C-E**; $NI_{pre} = 26.0 \pm 11.6\%$, $NI_{post} = 34.2 \pm 11.4\%$). Moreover, the distribution of NI values was similar for both pre and post pairings, suggesting a common mechanism, and was not correlated with the amplitude of the Ca signal (**Figure 2.13A-C**). While the Ca signals were significantly supra-linear, the uEPSPs summated linearly in both pairing paradigms (**Figure 2.13D**) and comparing the magnitude of the paired uEPSP with the NI of the Ca signal revealed a strong positive correlation (**Figure 2.12F**; pre: slope= 12.8 ± 6.2 , $r^2 = 0.262$; post: slope= 12.3 ± 7.9 , $r^2 = 0.167$). This suggests that a process with a graded voltage dependence, rather than a strict voltage threshold, underlies the enhanced Ca signal.

Modulation of NMDARs at spine synapses is the most parsimonious mechanism for the supra-linearity observed in control conditions. To test this, we repeated the above experiment with the addition of CPP to the bath. Indeed, with NMDARs antagonized, the spine Ca transients were no longer boosted by the dendritic uEPSP, but instead had negative NIs (**Figure 2.12G and H**; $NI_{pre} = -9.4 \pm 3.2\%$, $NI_{post} = -21.0 \pm 4.5\%$). In contrast to control conditions, the NI was negatively correlated with uEPSP amplitude, possibly due to larger uEPSPs reducing the driving force through AMPARs leading to a larger Ca sub-linearity (**Figure 2.12I**; pre: slope = -4.8 ± 2.4 , $r^2 = -0.309$; post: slope = -5.4 ± 3.1 , $r^2 = -0.255$). This reveals the presence of an additional graded voltage-dependent Ca source, likely CP-AMPA, that is typically masked by the large NMDAR-mediated Ca influx. Reinforcing this idea, the uEPSPs summated sub-linearly with NMDARs blocked in both timing paradigms (**Figure 2.13E**). Additionally, to further demonstrate that the dendritic depolarization was boosting Ca influx through spine NMDARs, we repeated these experiments in voltage-clamp and saw no significant non-linearities (**Figure 2.12J-L**; $NI_{pre} = -9.4 \pm 3.2\%$, $NI_{post} = -21.0 \pm 4.5\%$; pre: slope = 0.038 ± 0.23 , $r^2 = 0.0022$; post: slope = -0.096 ± 0.11 , $r^2 = 0.057$). Thus, NMDARs at spine synapses are insensitive to bAPs yet are highly modulated by depolarization that arises from the neighboring dendrite.

DISCUSSION

Spines on PV INs enclose functional glutamatergic synapses enriched with NMDARs

Little is known about how spines expand the information gathering capabilities of synapses on sparsely spiny interneurons. Our findings demonstrate that the dendrites of PV INs, while often described as smooth, have ~ 1 spine per $10 \mu\text{m}$ and that these spines enclose functional glutamatergic synapses. The synapses formed onto the relatively large

spines evaluated in this study contain both NMDARs and CP-AMPARs, like their dendritic counterparts. However, at spine synapses, the receptor composition is more varied, with a small but significant proportion of synapses lacking one receptor type or the other. Using two-photon glutamate uncaging to probe individual sites, we find that on average NMDARs play a more prominent role at spines, contributing to both the synaptic depolarization and concomitant Ca signal. Indeed, in comparison to the dendrites, NMDARs are enriched in spines. This is in contrast to CP-AMPARs, which are equivalent in their distribution and modulation by intracellular polyamines at either location. These findings demonstrate that synapses made onto spines and dendrites of PV INs share many basic properties, yet are distinguishable based on the NMDAR receptor content.

Our observation that spines on PV INs contain functional synapses establishes a new cellular model in which to examine fundamental questions in spine synapse biology. The similarities and distinctions between spine and dendrite synapses indicate fine regulation of receptor trafficking that discriminates between these two compartments. Specifically, our data allude to mechanisms that enrich NMDARs in spines over dendrites – perhaps through the trafficking of receptors with a particular subunit composition, the selective sequestration or stabilization of NMDARs at spine synapses, or the removal and degradation of NMDARs in the dendrites.

Differences in the modulation of synaptic Ca by bAPs

With two types of Ca-permeable voltage-sensitive glutamate receptors present at spine and dendrite synapses, we examined how Ca influx at the two locations is modulated by coincident spiking of the neuron. The difference between spines and dendrites was unexpected and striking. Ca signals originating from dendritic sites are uniformly, bi-

directionally modulated by bAPs. We found that NMDARs mediate the boosting of Ca signals when somatic activity follows receptor activation, while CP-AMPARs mediate the suppression of the Ca signals when somatic activity precedes receptor activation. This indicates that individual, proximal dendritic synapses are highly sensitive to the neuron's integrated activity. The relative timing of spikes may allow individual dendritic synapses to modulate NMDAR- and CP-AMPAR-mediated signaling pathways, providing a platform for engaging different mechanisms for plasticity.

Boosting of synaptic Ca influx through NMDARs by bAPs has been previously described in principal neurons and relies on the straightforward relief of the Mg block. We have now also demonstrated that bAPs significantly suppress uEPSP-associated Ca signals through CP-AMPARs and their intracellular polyamine block. We also did not observe any relationship between various features of the membrane potential and the measured sub-linearity, which suggests that the reduction in Ca influx is not simply due to a reduction in the driving force through CP-AMPARs. Additionally, while CP-AMPARs and NMDARs seemed to account for the majority of the Ca signal measured at both spine and dendritic synapses, it is important to note that PV INs express several types of voltage-gated Ca channels (VGCCs), including low-threshold T-types (Chiovini et al. 2014; Jiang & Swann 2005; Goldberg et al. 2003b), which may be part of the interplay between bAPs and uEPSPs.

We were surprised to see that bAPs had minimal impact on Ca influx at spine synapses, since APs readily propagate into spines and the biophysical properties of spines boost synaptic depolarization and engage voltage-dependent features of receptors and channels. Spines may be enriched for voltage-gated potassium (K) channels that counteract or truncate non-linearities or depolarizations in the spine head, akin to their role in reducing bAPs in general (Hu et al., 2010). Irrespective of the specific mechanism, spine

synapses are insensitive to bAPs; thus, it is unlikely that they are capable of undergoing plasticity that is coordinated with the output of the neuron.

Spines are sensors of local activity

While spine synapses may be relatively insensitive to bAPs, they are highly sensitive to depolarization that originates in the parent dendrite. We observed that NMDARs play a more prominent role in uEPSPs and Ca transients in spines as compared to neighboring dendritic shafts. Functionally, this asymmetry is exploited when the parent dendrite is co-active and Ca influx through spine NMDARs is enhanced. As a natural consequence of NMDAR channel function, the magnitude of this NMDAR-mediated Ca supra-linearity scales with the amplitude of the depolarization. This suggests spine synapses may engage specific downstream Ca-dependent signaling pathways as synaptic activity in the adjacent dendrite crosses various thresholds. It is also interesting to consider the distance between spines on PV IN dendrites, as this may reflect the spatial extent over which spine synapses can effectively sample dendritic activity (Lee, Soares, Thivierge, & Béïque, 2016) or the distance over which signaling molecules originating from spines can effectively exert their influence (Murakoshi et al. 2011; Nishiyama & Yasuda 2015; Colgan & Yasuda 2014). Moreover, this distance may be dynamically regulated by active conductances in the dendrites, such as Kv3.1 channels, which have been shown to modulate the spatial and temporal window of EPSP summation in PV dendrites (Hu et al., 2010).

Synapse plasticity in PV INs

We find that the location of a synapse, the specific receptor composition, and the timing and type of coincident activity all contribute to the repertoire of Ca signals produced by a synapse on a PV IN. Contextualizing these results, previous work has shown that both NMDARs and CP-AMPARs can induce long-term synaptic plasticity (Le Roux et al. 2013; Lamsa et al. 2007), albeit with different induction protocols. Additionally, Ca non-linearities, measured in the dendrites and produced by the activation of many synapses, can switch the direction of plasticity (Camiré & Topolnik 2014). Furthermore, synaptic Ca signals are highly compartmentalized, either by the spine as we show, or by the precise localization of Ca pumps in the dendrites (Goldberg et al. 2003a), creating boundaries that can impose synapse-specific plasticity. It will be interesting to determine if spine synapses may readily express NMDAR-mediated plasticity while those formed on the dendrites may be subject to ongoing and competing regulation by spatially constrained CP-AMPAR and NMDAR-initiated signaling pathways.

Presynaptic partners

Previous work has shown that in cortex thalamic inputs either do or do not produce NMDAR-mediated currents (Kloc & Maffei 2014; Bagnall et al. 2011). These studies highlight functional differences in excitatory synapses on the basis of presynaptic afferent identity and cortical area. Here, we have described functional differences based on subcellular location of excitatory synapses. The identification of the presynaptic neurons that synapse on spines or avoid them will be likewise illuminating for our understanding of PV IN function and the specific operations performed by spine and dendritic synapses.

The role of NMDARs in regulating PV IN function

We have demonstrated that NMDARs are biased towards spine synapses where they serve to integrate local dendritic activity to produce supra-linear Ca signals. NMDARs are expressed at low levels in PV INs in comparison to pyramidal neurons and other INs (Matta et al., 2013), yet are essential for PV IN function within a circuit. Selective deletion of the obligatory NR1 subunit in PV INs leads to the dysregulation of gamma oscillations in the cortex, reduction of the spatial coherence of place cells in the hippocampus, and a host of behavioral abnormalities (Carlén et al. 2011; Cardin et al. 2009; Korotkova et al. 2010). Indeed, NMDAR hypofunction is a leading hypothesis for the etiology of schizophrenia. We have now demonstrated a divergent role for NMDARs at spine versus dendritic synapses. Despite the low expression levels of NMDARs in PV INs, these receptors are critical for dynamic synaptic responses to different kinds of cellular activity. Deeper understanding of NMDAR function in spines on PV INs will provide new insight into PV IN function in healthy states and dysfunction in psychiatric disorders.

Figure 2.1. PV INs are sparsely spiny

(A) Confocal image of primary visual cortex (V1) from a *Pvalb-cre x tdTomato^{fl/fl}* mouse. Scale bar: 100 μm . **(B)** High magnification image of layer II/III in V1. Scale bar: 20 μm . **(C)** Two-photon image of a tdTomato-expressing PV IN filled with Alexa Fluor-594 through the patch pipette. Scale bar: 20 μm . **(D)** Representative trace recorded from a tdTomato-expressing PV IN in response to a somatic current injection (1 s, 400 pA, left). Scale bars: 10 mV and 100 ms. Action potential full width at half maximum is shown (FWHM, $n = 24$ neurons, 16 mice right). **(E)** Example two-photon images of PV IN dendrites (P15, top; P22, middle; P52, bottom). Scale bars: 10 μm . **(F)** Quantification of PV IN spine density from P15-19 ($n = 17$ branches, 11 neurons, 6 mice), P20-30 ($n = 13$ branches, 10 neurons, 4 mice), and P46-56 ($n = 13$ branches, 6 neurons, 3 mice) mice. $p = 0.077$, Kruskal-Wallis Test. **(G)** Quantification of spine density from proximal (first 50 μm) and distal (remaining length) dendrites. Proximal vs. distal – P15-19: $p = 0.62$; P20-30: $p = 0.15$; P46-56: $p = 0.016$ (Wilcoxon Signed Ranks Test). Proximal vs. proximal: $p = 0.0040$; P15-19 vs P20-30: $p = 0.030$, P15-19 vs P46-46: $p = 0.0070$. Distal vs. distal: $p = 0.97$. Kruskal-Wallis Test for three-way comparisons, pairwise comparisons adjusted by Bonferroni correction. Red circles indicate individual branches. Data are shown as mean \pm SEM.

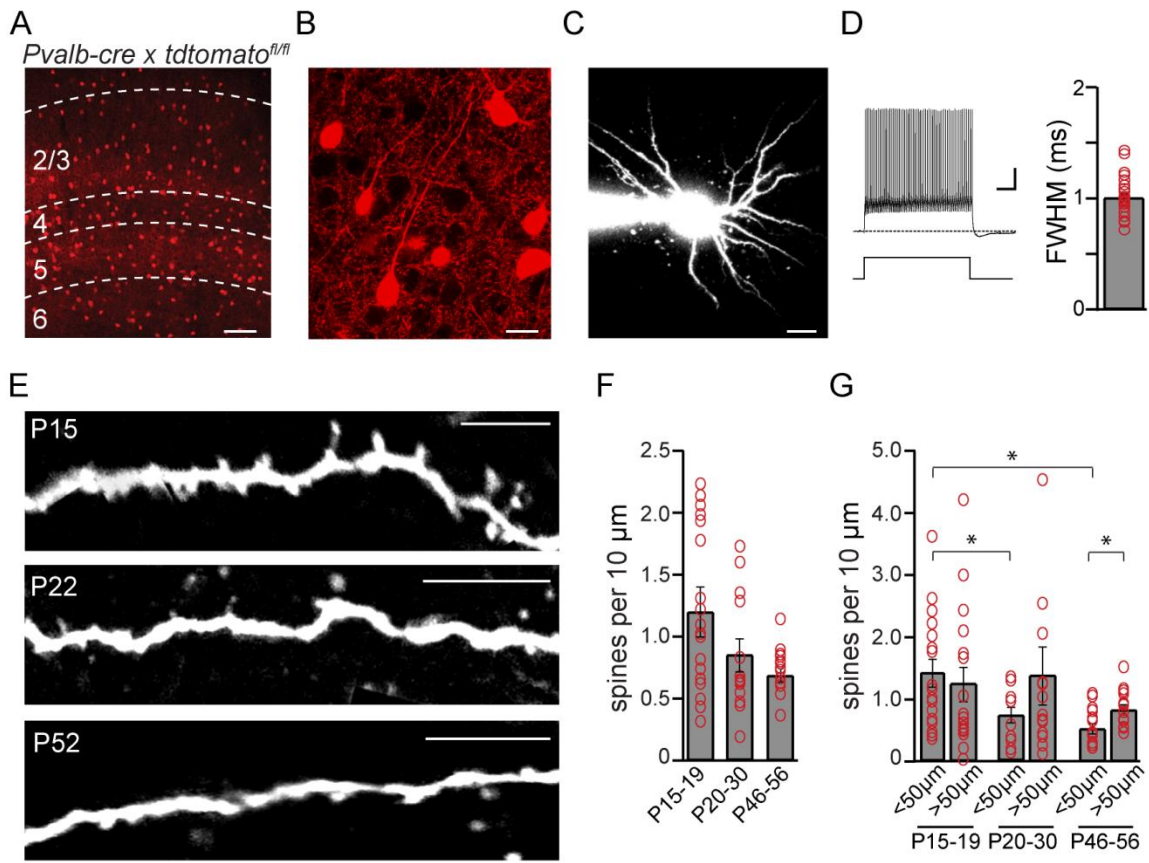


Figure 2.2 Spines on PV INs enclose functional glutamatergic synapses

(A) Schematic depicting a recording from a PV IN, the stimulating electrode, and two-photon Ca imaging. **(B)** Example of a dendritic segment, dashed yellow line indicates orientation and position of line scans. The neuron is filled with Alexa Fluor-594 (red) and Fluo-5F (green). Stimulating electrode is schematized in white. Scale bar: 1 μm . **(C)** Stimulation intensity evoking an EPSC but no Ca transient in the region of interest (ROI). Line scans through the dendrite in (B) (left) and accompanying Ca transients ($n = 15$ trials; right, top) and average EPSC (right, bottom). Ca transients: individual trials (gray) and mean (black). Scale bars: 25 ms (left), 5% $\Delta\text{G}/\text{G}_{\text{sat}}$ and 50 pA (right). **(D)** Stimulation intensity evoking both an EPSC and a Ca transient in the ROI. Line scans (left) and accompanying Ca transients ($n = 25$ trials; right, top) and average EPSC (right, bottom). Ca transients: individual trials (gray), mean of the successes (black), and mean of the failures (dashed) are indicated (top). Scale bars: 25 ms (left), 5% $\Delta\text{G}/\text{G}_{\text{sat}}$ and 50 pA (right). **(E)** Peak $\Delta\text{G}/\text{G}_{\text{sat}}$ in Ca transient condition plotted against no Ca transient condition. Dendrites (Den): open gray circles; spines (Sp): open black circles. **(F)** Example of spine, dashed yellow line indicates region imaged in line scans. Scale bar: 1 μm . **(G)** Stimulation intensity evoking an EPSC but no Ca transient in the ROI. Line scans through the spine head in (E) (left) and accompanying Ca transients ($n = 8$ trials; right, top) and average EPSC (right, bottom). Ca transients: individual trials (gray) and mean (black). Scale bars: 25 ms (left), 10% $\Delta\text{G}/\text{G}_{\text{sat}}$ and 50 pA (right). **(H)** Stimulation intensity evoking both an EPSC and a Ca transient in the ROI. Line scans (left) and accompanying Ca transients ($n = 23$ trials; right, top) and average EPSC (right, bottom). Ca transients: individual trials (gray), mean of the successes (black), and mean of the failures (dashed) are indicated (top). Scale bars: 25 ms (left), 10% $\Delta\text{G}/\text{G}_{\text{sat}}$ and 50 pA (right). **(I)** Population average in Ca transient condition. Dendrites (Den): gray; spines (Sp): black. Average Ca transient including failures (top; average number of trials: dendrites = 18 ± 2 , spines = 23 ± 2 ; average number of successes: dendrites = 13 ± 2 , spines = 15 ± 1). Scale bars: 5% $\Delta\text{G}/\text{G}_{\text{sat}}$ and 25 ms. Ca peak including failures (% $\Delta\text{G}/\text{G}_{\text{sat}}$; bottom); individual cells: open black circles. Dendrites = 8.8 ± 1.7 ($n = 17$, 9 mice), spines = 7.1 ± 9.3 ($n = 19$, 9 mice); $p = 0.79$. Average for successes only (not shown): dendrites = 10.9 ± 1.9 , spines = 10.5 ± 1.9 . **(J)** Evoked Ca transients (% $\Delta\text{G}/\text{G}_{\text{sat}}$) measured at dendritic hot-spots in control conditions (black; 10.8 ± 3.0) followed by wash-in of CPP (red; 3.5 ± 1.2) and NBQX (blue; 0.2 ± 0.1 ; $n = 8$ dendrites, 9 neurons, 6 mice). **(K)** As described in (J) but measured in spines. Control = 8.0 ± 1.4 ; CPP = 3.1 ± 0.8 ; CPP + NBQX = 0.5 ± 0.2 ($n = 10$ spines, 10 neurons, 7 mice). Scale bars: 5% $\Delta\text{G}/\text{G}_{\text{sat}}$ and 25 ms. **(L)** Ca peak as a percent of control with sequential wash-in of CPP and NBQX. Dendrite (Den): gray, spine (Sp): black. Individual sites and population average are indicated by the thin and thick lines, respectively. P-values are shown for the dendrite/spine. Control vs. CPP: $p = 0.012/p = 0.0093$. Control vs. CPP + NBQX: $p = 0.012/p = 0.0051$. **(M)** Evoked Ca transients (% $\Delta\text{G}/\text{G}_{\text{sat}}$) measured at dendritic hot-spots in control conditions (black; 7.0 ± 1.4) followed by wash-in of philanthotoxin (PhTx, red; 4.2 ± 1.0) and NBQX (blue; 1.4 ± 0.5 ; $n = 9$ dendrites, 9 neurons, 3 mice). **(N)** As described in (M) but measured in spines. Scale bars: 5% $\Delta\text{G}/\text{G}_{\text{sat}}$ and 25 ms. Control = 6.5 ± 1.2 ; PhTx = 2.2 ± 0.4 ; PhTx + NBQX = 1.2 ± 0.4 ($n = 9$ spines, 9 neurons, 2 mice). **(O)** As described in (L) but with sequential wash-in of PhTx and NBQX. P-values are shown for the dendrite/spine. Control vs. PhTx: $p = 0.0077/p = 0.0077$. Control vs. PhTx + NBQX: $p = 0.0077/p = 0.0077$. Data are shown as mean \pm SEM unless otherwise indicated. Mann-Whitney U-Test for unpaired data, Wilcoxon Signed Ranks Test for paired data.

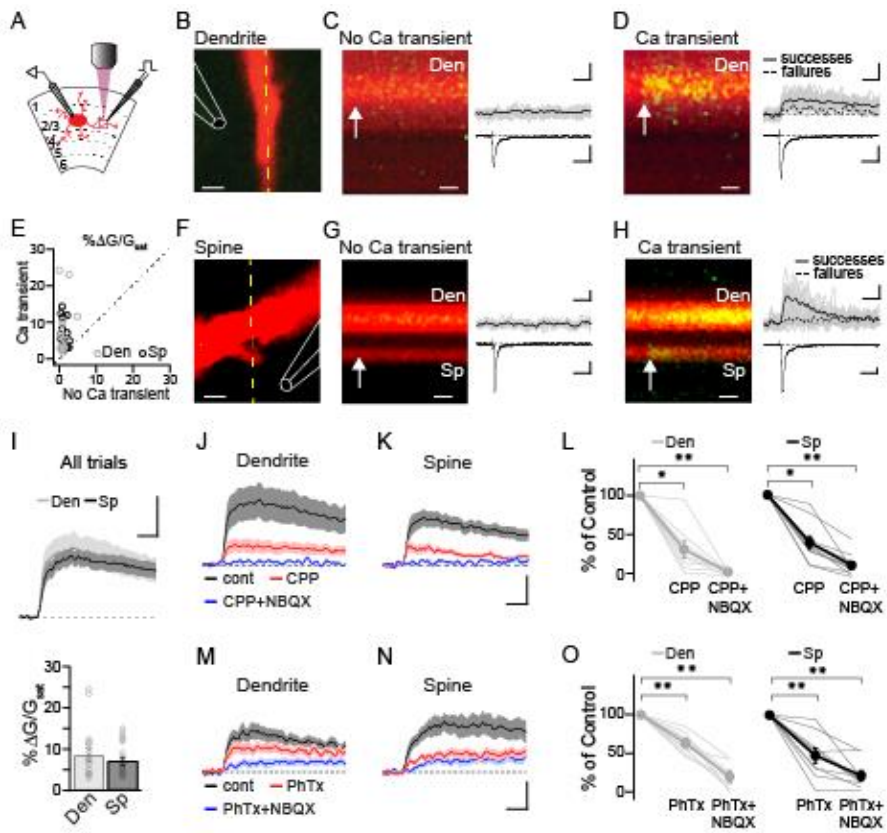


Figure 2.3. Variability in receptor composition.

(A) Coefficient of variation (CV) of the percent reduction (%) with each drug wash-in. Dendrite (Den): light gray, spine (Sp): dark gray.

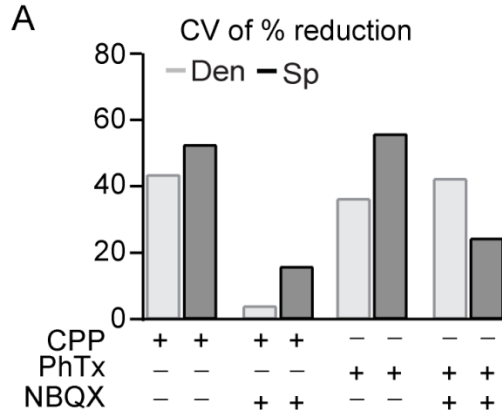


Figure 2.4. Spines are enriched for NMDARs

(A) Schematic depicting a recording from a PV IN, two-photon glutamate uncaging, and Ca imaging. The neuron is filled with Alexa Fluor-594 and Fluo-5F through the patch pipette. **(B)** Hot-spot localization in dendritic shafts. 1) uncaging power set at spine head. 2-5) uncaging at several dendritic sites (left). Uncaging-evoked EPSCs (uEPSCs) recorded at the soma in response to uncaging on the corresponding sites (right). Spine: black, dendrites: gray. Scale bars: 1 μm (left), 10 pA and 25 ms (right). **(C)** Dendritic Ca transient in voltage clamp in response to uEPSCs and to EC stimulation. Scale bars: 5% $\Delta\text{G}/\text{G}_{\text{sat}}$ and 25 ms. **(D)** Uncaging-elicited dendritic responses. Example of a dendritic segment (left) and line scan image through the dendrite (right) from the region indicated by the dashed yellow line. The yellow arrow head indicates the location (left) or time (right) of the uncaging pulse; white inset (right) is an example uEPSP. Scale bars: 1 μm (left) and 25 ms (right). **(E)** Dendritic site population average: uEPSC (top), uEPSP (middle), and Ca transient (bottom) recorded in control conditions (black, $n = 17$ sites, 11 neurons, 9 mice) or in the presence of CPP (red, $n = 20$ sites, 10 neurons, 8 mice). Inset in the top panel is the uEPSC difference (CPP subtracted from control). Scale bars: 10 pA (top), 0.5 mV (middle), 5% $\Delta\text{G}/\text{G}_{\text{sat}}$ (bottom), and 25 ms. **(F)** As described in (D) but with uncaging at a spine head. **(G)** As described in (E) but for spine population averages. Control conditions ($n = 22$ spines, 17 neurons, 16 mice) and CPP ($n = 18$ spines, 13 neurons, 9 mice). **(H-K)** Responses to uncaging over dendrites and spines in control conditions and with CPP in the bath. Dendrite (Den): light gray, spine (Sp): dark gray. Open gray circles denote individual dendrites and spines. **(H)** Average uEPSC_{peak} (pA). Dendrites: cont = -29.4 ± 3.0 , CPP = -25.3 ± 4.5 ; $p = 0.18$. Spines: cont = -23.6 ± 3.2 , CPP = -14.4 ± 2.1 ; $p = 0.035$. **(I)** uEPSC_{late} (pA; 12-16 ms after uncaging). Dendrites: cont = -2.4 ± 0.4 , CPP = -3.3 ± 0.7 ; $p = 0.43$. Spines: cont = -5.4 ± 1.1 , CPP = -1.6 ± 0.4 ; $p = 0.012$. **(J)** uEPSP_{peak} (mV). Dendrites: cont = 1.6 ± 0.2 , CPP = 1.3 ± 0.3 ; $p = 0.13$. Spines: cont = 1.0 ± 0.1 , CPP = 0.6 ± 0.07 ; $p = 0.022$. **(K)** Ca_{peak} (% $\Delta\text{G}/\text{G}_{\text{sat}}$). Dendrites: cont = 8.8 ± 1.1 , CPP = 5.6 ± 1.1 ; $p = 0.014$. Spines: cont = 13.9 ± 1.9 , CPP = 7.3 ± 1.7 ; $p = 0.010$. **(L)** Isolation of NMDARs. Example of image of a spine and dendrite (left). Yellow arrow heads indicate uncaging sites. Recordings were performed in aCSF containing NBQX and 0 mM Mg. Ca transients and uEPSCs were recorded from spine synapses and adjacent dendritic sites. Ca transients measured in response to uncaging over the spine (Sp, black) or each of three dendritic sites (Den 1-3, gray) are shown (right). Scale bars: 1 μm (left), 10% $\Delta\text{G}/\text{G}_{\text{sat}}$ and 25 ms (right). **(M)** Comparison of Ca_{peak} measured in the spine head (Sp) and average of the adjacent dendrite (Den, average of 2-4 sites) when NMDARs are isolated. Population average and individual spine/den comparisons are indicated by the thick and thin lines ($n = 9$ clusters, 6 neurons, 5 mice), respectively. Spine: $16.8 \pm 2.5\%$ $\Delta\text{G}/\text{G}_{\text{sat}}$, dendrite: $10.0 \pm 2.5\%$ $\Delta\text{G}/\text{G}_{\text{sat}}$; $p = 0.0051$. **(N)** Comparison of spine (filled black circle) and dendritic Ca normalized to the spine Ca_{peak} (average for the cluster: filled gray circle; individual site: open gray circle). Data are shown as mean \pm SEM unless otherwise indicated. Mann-Whitney U-test for unpaired data, Wilcoxon Signed Ranks Test for paired data.

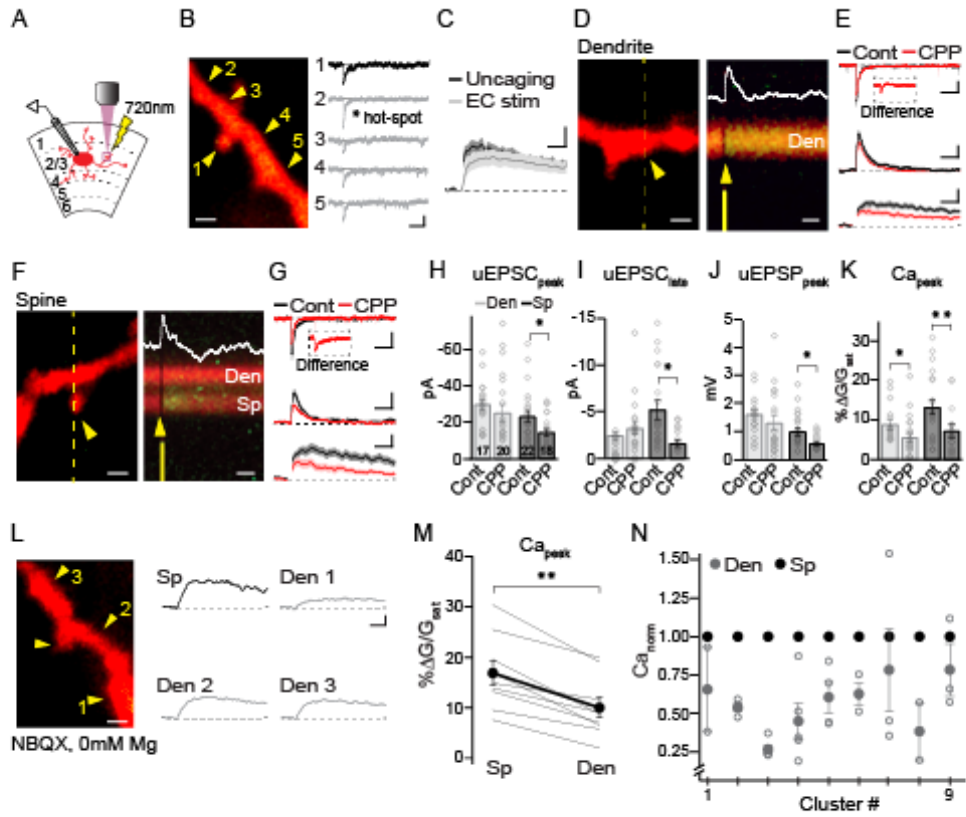


Figure 2.5. Standardization of uncaging power.

(A) Laser power calibration at spine heads. Representative spine. Scale bar: 1 μm . Yellow arrows denote location (A) or time of uncaging (B and C). Yellow dashed line: line scans through spine head. **(B)** Top, line scans over the spine head in (A). Red channel only is shown. White trace illustrates the photobleaching of the red fluorophore. Scale bar: 25 ms. Middle, population average of the red fluorescence after uncaging. Scale bar: 10% $\Delta F/F$ and 25 ms. Bottom, average uEPSC. Scale bar: 10 pA and 25 ms. **(C)** Top, line scans of the spine in (A). Red and green fluorescence are shown; uEPSP inset in white. Scale bar: 25 ms. Middle, population average uEPSP. Scale bar: 0.5 mV and 25 ms. Bottom, population average Ca transient, black, and neighboring dendrite, gray. Note the Ca transient is restricted to the spine head. Scale bar: 5% $\Delta G/G_{\text{sat}}$ and 25 ms. **(D)** 20-80% rise times of uEPSCs measured from spines (Sp) and dendrites (Den). **(E)** Histograms of mEPSC characteristics recorded from three PV INs (Cell 1: black, Cell 2: blue, Cell 3: green). Peak amplitude, top; rise rate, middle; decay tau, bottom. Average uEPSC peak amplitudes, rise rates, and decay taus displayed in dark gray (spine) and light gray (dendrite) for comparison. **(F)** Average % photo-bleaching at spine heads for all appropriate experiments. Open black circles denote individual spine heads. $P = 0.38$, Kruskal-Wallis Test.

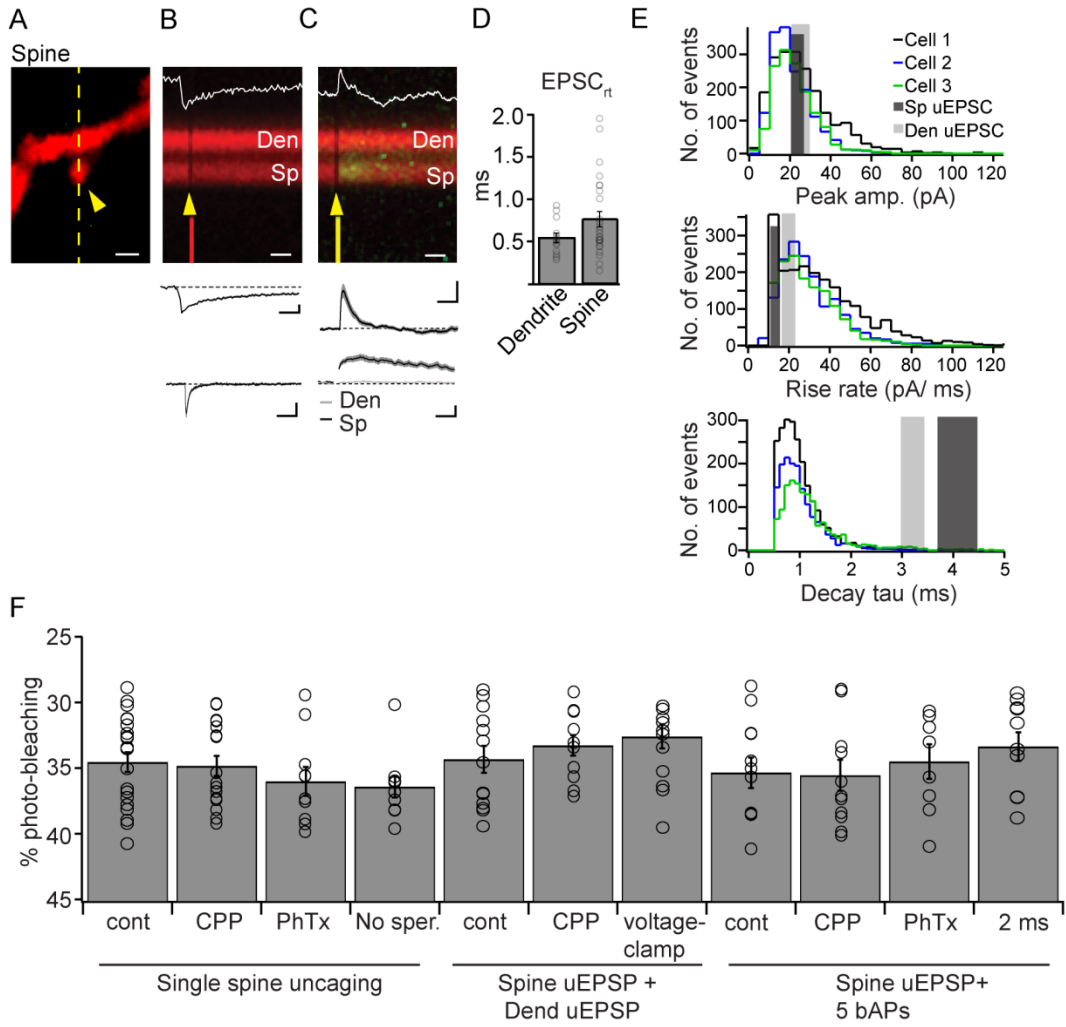


Figure 2.6. CP-AMPA- mediated Ca influx and depolarization are similar in dendrites and spines

(A) Population average uEPSC (top), uEPSP (middle), and Ca (bottom) measured in response to uncaging at dendritic sites (left) or spines (right) in control conditions (black, replotted from Figure 3) or in the presence of PhTx (red, dendrite: n = 11 sites, 8 neurons, 5 mice; spine: n = 19 spines, 11 neurons, 8 mice). Inset in the top panel is the uEPSC difference. Top, scale bars: 10 pA and 25 ms. Middle, scale bars: 0.5 mV and 25 ms. Bottom, scale bars: 5% $\Delta G/G_{\text{sat}}$ and 25 ms. **(B)** As described in (A) but with no spermine (red) in the patch pipette (dendrite: n = 10 sites, 5 neurons, 4 mice; spine: n = 10 spines, 5 neurons, 2 mice). Top, scale bars: 10 pA and 25 ms. Middle, scale bars: 0.5 mV and 25 ms. Bottom, scale bars: 5% $\Delta G/G_{\text{sat}}$ and 25 ms. **(C-E)** Responses to uncaging over dendrites and spines with PhTx in the bath or spermine excluded from the pipette (no sper.). Dendrite (Den): light gray, spine (Sp): dark gray. Open circles denote individual dendrites and spines. Horizontal shaded area indicates SEM range from control conditions. Comparisons done against control conditions in **Figure 2.4**. **(C)** Average uEPSC_{peak} (pA). Dendrites: PhTx = -21.0 ± 2.6 , p = 0.057; no sper. = -33.5 ± 5.0 , p = 0.29. Spines: PhTx = -15.3 ± 2.1 , p = 0.029; no sper. = -25.4 ± 5.8 , p = 0.89. **(D)** uEPSP_{peak} (mV). Dendrites: PhTx = 1.0 ± 0.2 , p = 0.020; no sper. = 1.3 ± 0.2 , p = 0.55. Spines: PhTx = 0.6 ± 0.07 , p = 0.018; no sper. = 1.1 ± 0.3 , p = 1.0. **(E)** Ca_{peak} (% $\Delta G/G_{\text{sat}}$). Dendrites: PhTx = 5.7 ± 1.0 , p = 0.046; no sper. = 8.0 ± 1.2 , p = 0.62. Spines: PhTx = 8.3 ± 1.4 , p = 0.025; no sper. = 10.6 ± 2.5 , p = 0.33. **(F)** Current-voltage plot for AMPA-mediated uEPSCs measured in response to uncaging over dendrites (gray circle) or spines (black circles). CPP is included in the bath. **(G)** I-V plot from (F) normalized to the uEPSC_{peak} measured at -70mV. **(H)** Schematic of rectification index (RI) calculation. **(I)** Average RIs for dendritic and spine uEPSCs. Dendrite (Den): light gray, spine (Sp): dark gray, Dendrite, no spermine (Den, no sper.): open or dashed light gray. Dendrites: RI = 0.63 ± 0.23 , spines: RI = 0.78 ± 0.17 ; p = 0.44. Dendrite, no spermine: RI = 1.2 ± 0.21 , p = 0.025 (vs. Dendrites). Data are shown as mean \pm SEM unless otherwise indicated. Mann-Whitney U-tests.

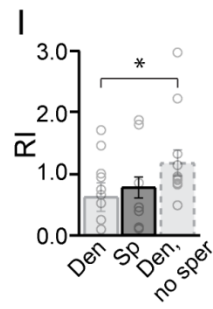
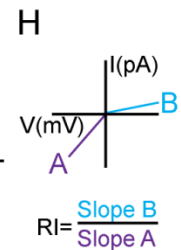
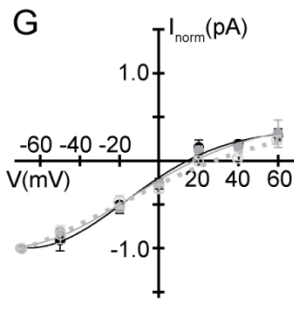
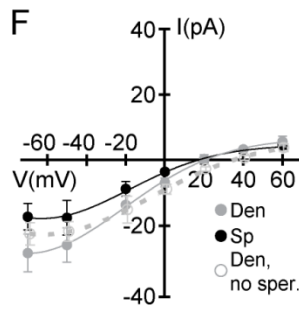
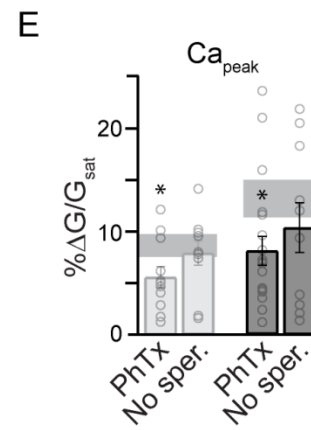
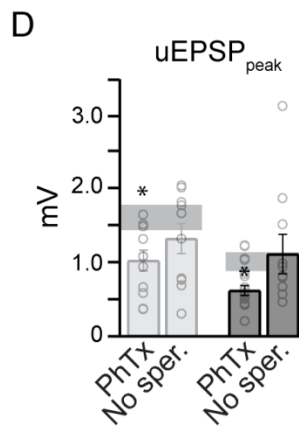
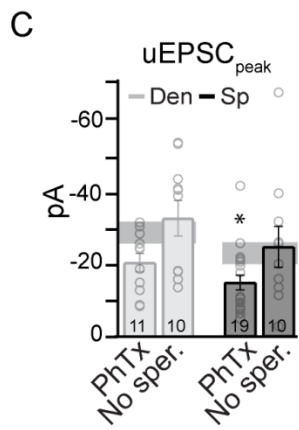
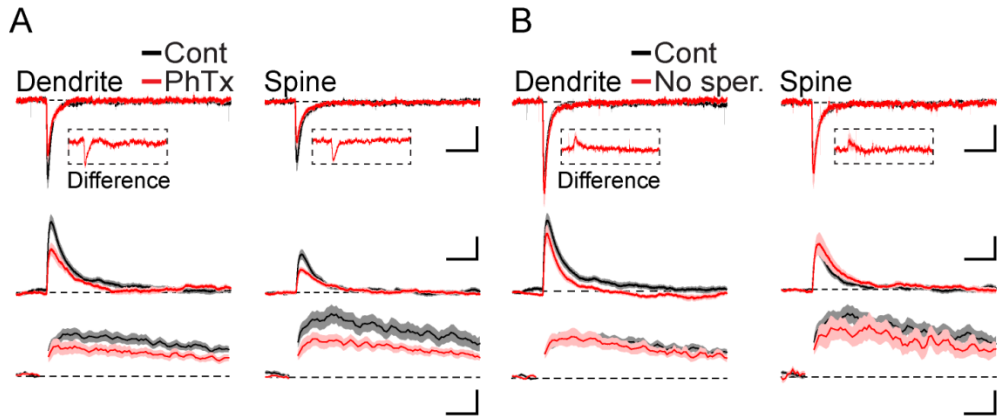


Figure 2.7. bAP-mediated Ca influx

(A) Schematic showing a single bAP or a train of 5 bAPs being elicited by current injection at the soma of a PV IN and a Ca signal being imaged in a dendritic region (left). Two-photon image showing a z-stack of a PV IN dendrite (right). Yellow lines (1-4) indicate approximate regions (spine and adjacent dendritic shaft) imaged in line scan mode. Scale bar: 10 μm . **(B)** Ca transient measured at spine and adjacent dendritic sites indicated in (A) in response to 1 (gray) or 5 bAPs (black). Scale bars: 5% $\Delta G/G_{\text{sat}}$ and 50 ms. **(C)** bAP(s) evoked Ca transients plotted against distance from soma for dendrites (left) and spines (right). 1 bAP: light gray; 5 bAPs: black (n = 40 sites, 14 neurons, 11 mice). **(D)** Ca peak measured for 1 bAPs (left; spine vs. dendrite, p = 0.98) or 5 bAPs (right; p = 0.70) in the spine compared to the adjacent dendrite.

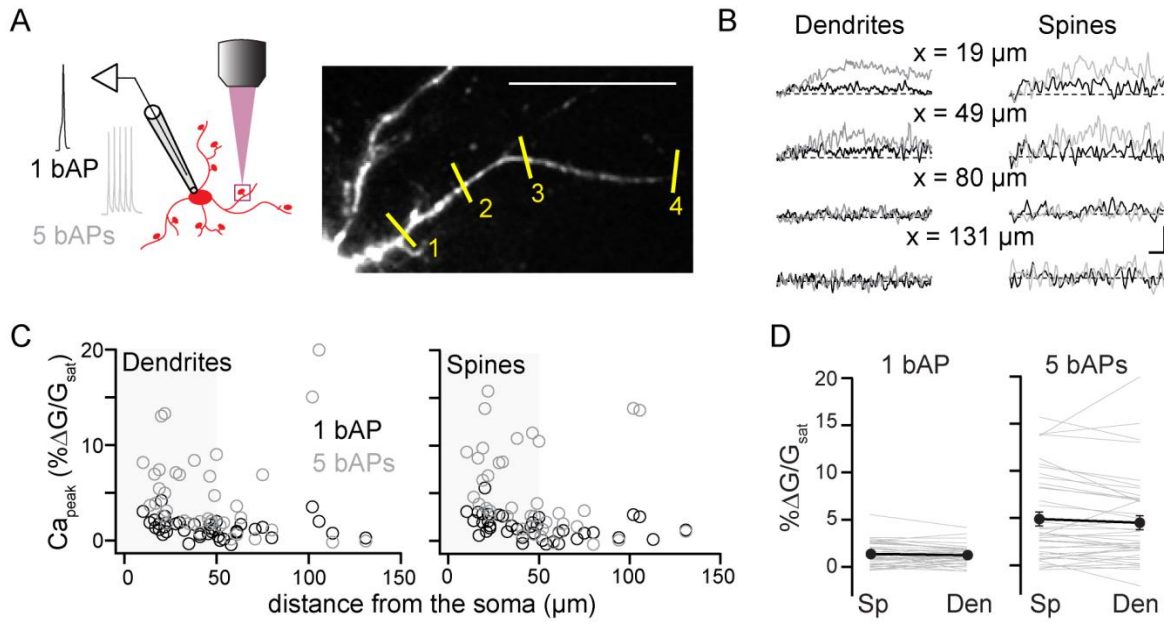


Figure 2.8. Ca signaling through glutamate receptors on dendrites is bi-directionally modulated by back-propagating action potentials

(A) Schematic depicting the experimental set-up (left). Current injection at the soma is paired with two-photon glutamate uncaging at the dendrite and Ca imaging (left). Five bAPs (100 Hz) were evoked either 10 ms before (“pre”, blue) or after (“post”, green) uncaging over the dendrite. (middle). Schematic of example non-linearity indexes (NI) is shown (right). **(B)** Average Ca transients measured from the dendrite in response to 5 bAPs ($3.0 \pm 0.8\% \Delta G/G_{\text{sat}}$) or uncaging at the dendrite alone (left; $7.0 \pm 1.2\% \Delta G/G_{\text{sat}}$), and in pre/post (blue/green; pre = $10.6 \pm 1.4\% \Delta G/G_{\text{sat}}$, post = $12.1 \pm 1.6\% \Delta G/G_{\text{sat}}$) pairing configurations (right). The sum and measured Ca transient are indicated by pale and dark lines, respectively. Scale bars: $5\% \Delta G/G_{\text{sat}}$ and 50 ms. **(C)** Measured Ca transients in the pre (blue) and post (green) pairing paradigms plotted against the sum of the Ca transients produced by bAPs and uEPSP alone ($n = 13, 9$ neurons, 4 mice). **(D)** Control, 10 ms (black or darker) and 2 ms (gray or lighter). For each dendritic site (10 ms: $n = 13, 9$ neurons, 4 mice; 2 ms: $n = 10, 6$ neurons, 3 mice), the NIs calculated for the pre and post paradigms are plotted (left). 10 ms, $NI_{\text{pre}} = -8.8 \pm 1.8\%$ ($p = 8.6E-04$), $NI_{\text{post}} = 24.0 \pm 4.0\%$ ($p = 0.00014$); 2 ms, $NI_{\text{pre}} = 0.7 \pm 2.7\%$ ($p = 0.80$); $NI_{\text{post}} = 30.2 \pm 10.6$ ($p = 0.013$; Wilcoxon Signed Ranks Test, measured vs. sum). Cumulative probability distributions of the NI calculated from pre (blue) and post (green) pairing (right). 10 ms: NI_{pre} vs. NI_{post} , $p = 4.5E-07$; 2 ms: NI_{pre} vs. NI_{post} , $p = 0.0096$. 10 ms vs 2 ms: NI_{pre} , $p = 0.010$; NI_{post} , $p = 0.59$. **(E-G)** Within- condition comparisons done as in (C). Between- condition comparisons done against control, 10 ms data (dotted lines for reference). **(E)** CPP, 10 ms ($n = 12, 8$ neurons, 4 mice). Left, $NI_{\text{pre}} = -9.0 \pm 2.8\%$, $p = 0.023$; $NI_{\text{post}} = -2.4 \pm 4.7\%$, $p = 0.31$ (Wilcoxon Signed Ranks Test). Right, NI_{pre} vs. NI_{post} , $p = 0.17$. NI_{pre} , $p = 0.0094$; NI_{post} , $p = 0.25$. **(F)** PhTx, 10 ms ($n = 11, 6$ neurons, 3 mice). Left, $NI_{\text{pre}} = -1.7 \pm 1.7\%$, $p = 0.91$; $NI_{\text{post}} = 18.4 \pm 2.6\%$, $p = 0.0021$. Right, NI_{pre} vs. NI_{post} , $p = 0.000059$. NI_{pre} , $p = 0.0094$; NI_{post} , $p = 0.25$. **(G)** No spermine, 10 ms ($n = 14, 9$ neurons, 4 mice). Left, $NI_{\text{pre}} = -2.6 \pm 2.9\%$, $p = 0.16$; $NI_{\text{post}} = 13.7 \pm 3.7\%$, $p = 0.047$. Right, NI_{pre} vs. NI_{post} , $p = 0.0012$. NI_{pre} , $p = 0.031$; NI_{post} , $p = 0.19$. Data were tested for normality; parametric tests were run unless otherwise specified.

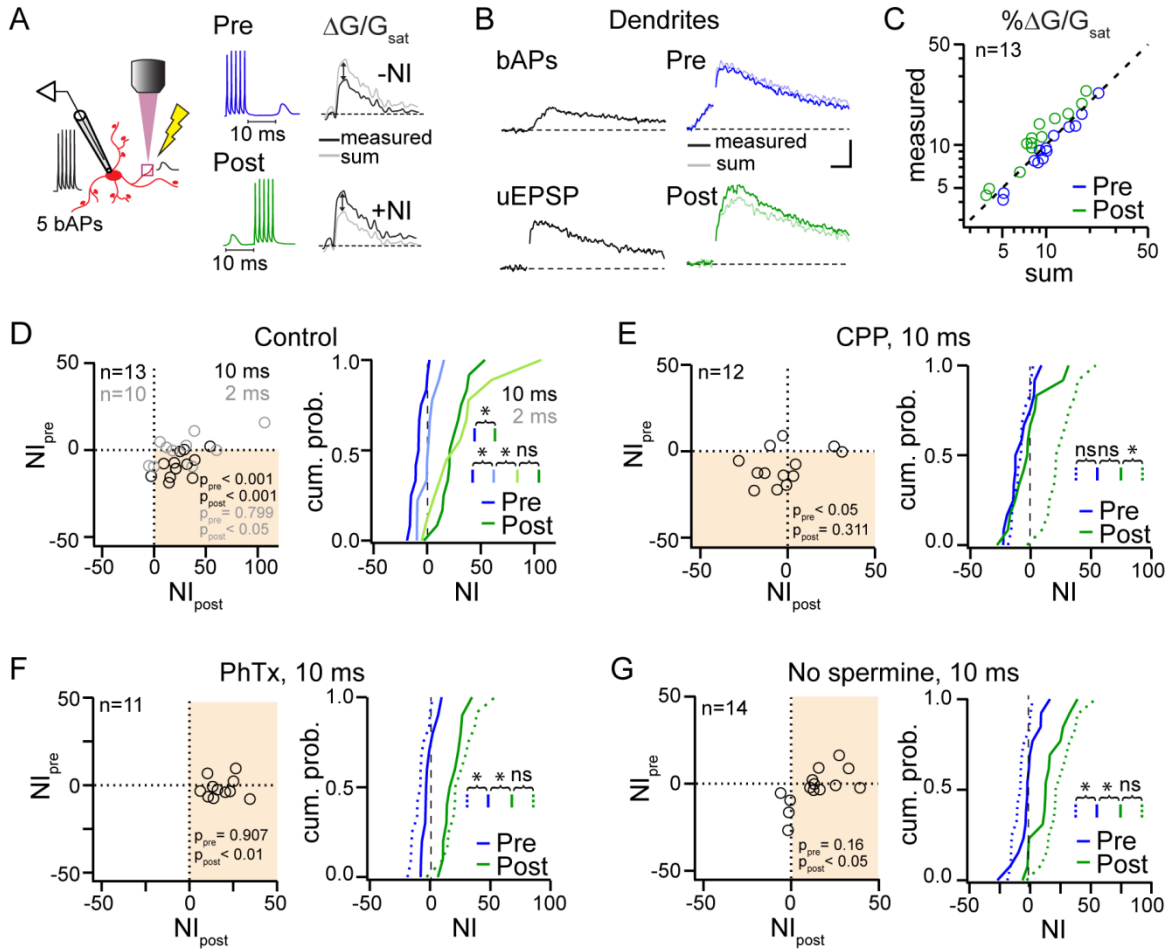


Figure 2.9. Modulation of dendritic Ca signals by bAPs.

(A) 5 bAPs-uEPSP pairing experiment, dendrites. Ca_{peak} in pre (blue) and post (green) pairing paradigms plotted against non-linearity index (NI). Control, 10 ms; control, 2 ms ISI; CPP (10 μ M); PhTx (10 μ M); no spermine conditions. **(B)** Membrane potential (mV) plotted against non-linearity in the pre pairing paradigm (NI_{pre}). From left, minimum membrane potential (V_{min}) after train of APs but before the uEPSP, membrane potential at $t = 0$ for uEPSP ($V_{preEPSP}$), peak of the uEPSP in the uEPSP only condition.

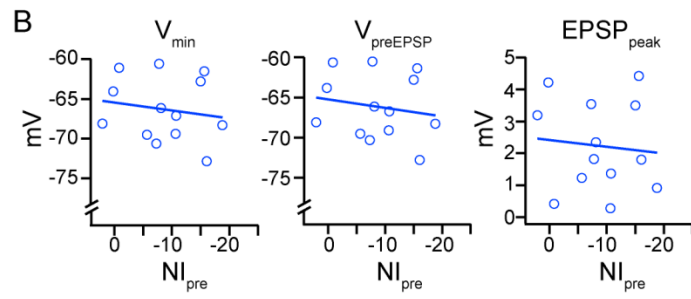
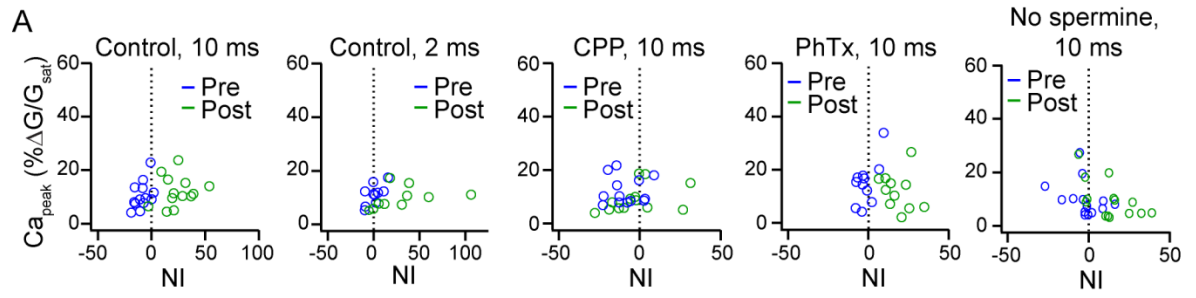


Figure 2.10. Spine CP-AMPARs and NMDARs do not exhibit modulation by somatic activity

(A) Average Ca transients measured from the dendrite in response to 5 bAPs ($3.8 \pm 1.4\% \Delta G/G_{\text{sat}}$) or glutamate uncaging alone (left; $18.4 \pm 2.4\% \Delta G/G_{\text{sat}}$), and in the pre (blue; $21.6 \pm 3.5\% \Delta G/G_{\text{sat}}$) and post (green; $21.3 \pm 3.2\% \Delta G/G_{\text{sat}}$) pairing configurations (right). The sum and measured paired Ca transient are indicated by pale and dark lines, respectively. Scale bars: $5\% \Delta G/G_{\text{sat}}$ and 50 ms. **(B)** Measured Ca transients in the pre (blue) and post (green) pairing paradigms plotted against the sum of the Ca transients produced by bAPs and uEPSP alone ($n = 12$, 10 neurons, 6 mice). **(C)** Control, 10 ms (black or darker) and 2 ms (gray or lighter). For each spine (10 ms: $n = 12$, 10 neurons, 6 mice; 2 ms: $n = 10$, 7 neurons, 4 mice), the NIs calculated for the pre and post paradigms are plotted (left). 10 ms: $NI_{\text{pre}} = -7.9 \pm 6.1\%$ ($p = 0.11$), $NI_{\text{post}} = 4.3 \pm 6.6\%$ ($p = 0.85$); 2 ms: $NI_{\text{pre}} = -1.3 \pm 2.8\%$ ($p = 0.51$), $NI_{\text{post}} = 5.1 \pm 3.6\%$ ($p = 0.11$; measured vs. sum). Cumulative probability distributions of the NI calculated from pre (blue) and post (green) pairing (right). 10 ms: NI_{pre} vs. NI_{post} , $p = 0.032$; 2 ms: $p = 0.24$. 10 ms vs 2 ms: NI_{pre} , $p = 0.065$. NI_{post} , $p = 0.90$. **(D)** Cumulative probability distributions of the NI_{pre} and NI_{post} as in (C), but in CPP ($n = 11$, 7 neurons, 4 mice). $NI_{\text{pre}} = -1.5 \pm 7.3\%$, $p = 0.51$. $NI_{\text{post}} = -12.4 \pm 7.5\%$, $p = 0.11$. **(E)** Cumulative probability distributions of the NI_{pre} and NI_{post} as in (C), but in PhTx ($n = 8$, 6 neurons, 2 mice). $NI_{\text{pre}} = -2.4 \pm 5.1\%$, $p = 0.49$. $NI_{\text{post}} = 11.0 \pm 6.7\%$, $p = 0.48$. Data were tested for normality and T-tests (paired or unpaired) were run. For (D), (E) and (F), comparisons were against Control, 10 ms dataset in (C).

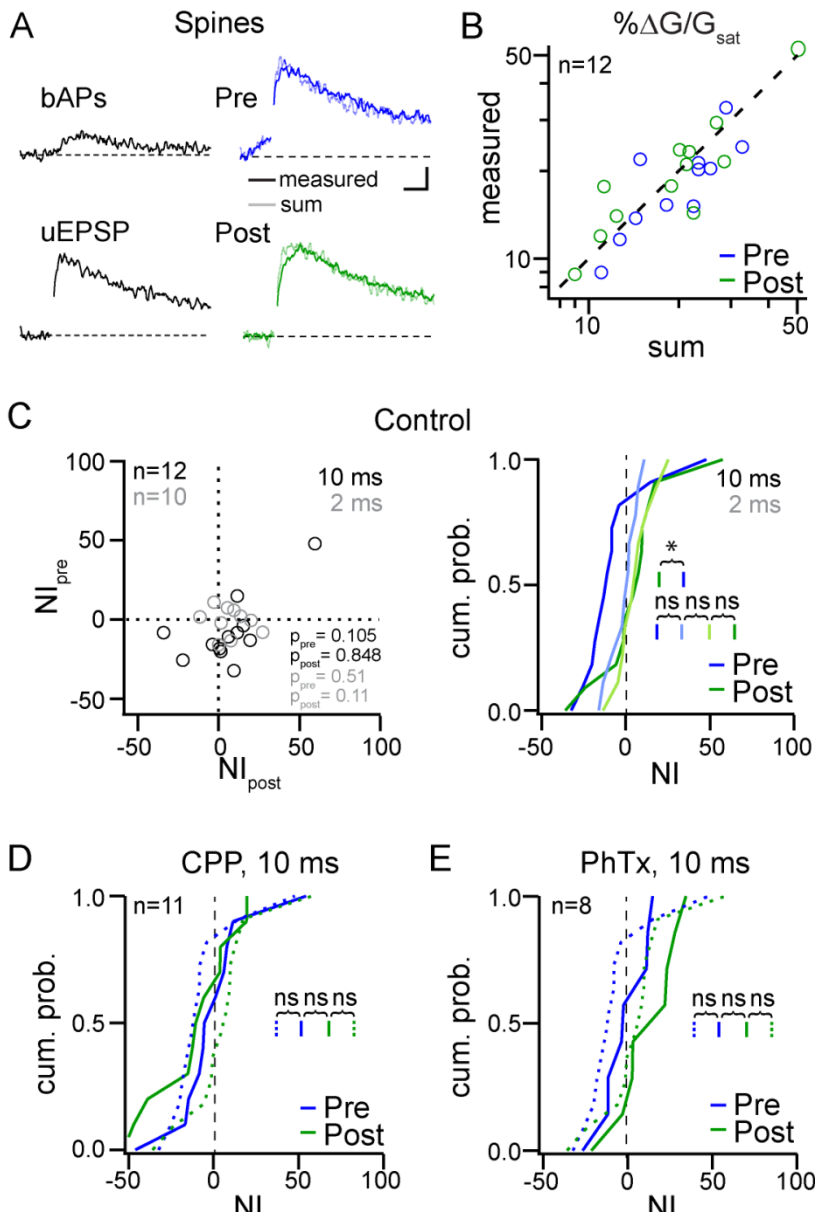


Figure 2.11. bAPs do not modulate spine Ca signals.

(A) 5 bAPs-uEPSP pairing experiment, spines. Ca_{peak} in pre (blue) and post (green) pairing paradigms plotted against non-linearity index (NI). Control, 10 ms; control, 2 ms ISI; CPP (10 μ M); PhTx (10 μ M).

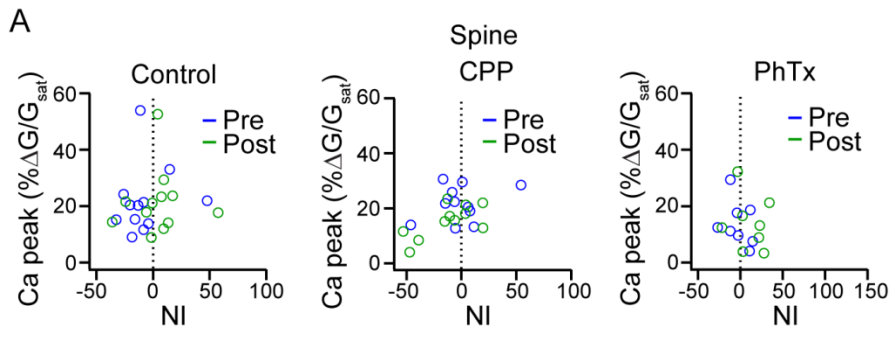


Figure 2.12. Spines on PV INs produce NMDAR-dependent supra-linear Ca signals in response to local dendritic activity

(A) Schematic depicting experimental set-up for the spine uEPSP-dendritic uEPSPs pairing. Top, 5 dendritic uEPSPs (at 100 Hz; 10-15 μm away) either preceded (bottom, pre: blue) or followed (bottom, post: green) a spine uEPSP by 2 ms. Scale bar: 1 μm . **(B)** Average Ca transients from different conditions: spine uEPSPs only (“Sp uEPSP”; $13.5 \pm 1.6\% \Delta\text{G}/\text{G}_{\text{sat}}$), dendritic uEPSPs only (“Den uEPSP”; $3.8 \pm 0.6\% \Delta\text{G}/\text{G}_{\text{sat}}$), pre ($20.7 \pm 2.6\% \Delta\text{G}/\text{G}_{\text{sat}}$), and post ($22.9 \pm 3.2\% \Delta\text{G}/\text{G}_{\text{sat}}$) paradigms. The sum and measured Ca transient are indicated by pale and dark lines, respectively. Scale bars: $5\% \Delta\text{G}/\text{G}_{\text{sat}}$ and 25 ms. **(C)** Measured Ca transients in the pre (blue) and post (green) pairing paradigms plotted against the sum of the Ca transients produced by bAPs and uEPSP alone ($n = 14$, 10 neurons, 6 mice). **(D)** For each spine ($n = 14$, 10 neurons, 6 mice), the NIs calculated for the pre and post paradigms are plotted. $\text{NI}_{\text{pre}} = 27.3 \pm 9.0\%$, $p = 0.022$; $\text{NI}_{\text{post}} = 37.7 \pm 10.7\%$, $p = 0.0033$ (measured vs. sum). **(E)** Control, cumulative probability distributions of the NI calculated from the pre (blue) and post (green) paradigms. NI_{pre} vs. NI_{post} , $p = 0.14$. **(F)** NI plotted against peak amplitude of the uEPSP in the pre and post paradigms. Best line of fit: pre, $r^2 = 0.262$; post, $r^2 = 0.167$. **(G)** As in (D) but for CPP. NI_{pre} plotted against NI_{post} ($n = 11$, 6 neurons, 4 mice). $\text{NI}_{\text{pre}} = -9.4 \pm 3.2\%$, $p = 0.012$; $\text{NI}_{\text{post}} = -21.0 \pm 1.6\%$, $p = 0.0080$. **(H)** Cumulative probability distributions of the NI_{pre} and NI_{post} as in (E), but in CPP. Dotted line denotes control as in (E). NI_{pre} , $p = 0.014$; NI_{post} , $p = 0.00086$ (CPP vs. control). **(I)** NI plotted against peak amplitude of the uEPSP in the pre and post paradigms. Best line of fit: pre, $r^2 = -0.309$; post, $r^2 = -0.255$. **(J)** V-clamp condition. For each spine ($n = 14$, 8 neurons, 5 mice), the NIs calculated for the pre and post paradigms are plotted. $\text{NI}_{\text{pre}} = 0.18 \pm 6.0\%$, $p = 0.47$; $\text{NI}_{\text{post}} = 1.2 \pm 3.4\%$, $p = 0.82$ (measured vs. sum). **(K)** Cumulative probability distributions of the NI calculated from the pre (blue) and post (green) paradigms. NI_{pre} vs. NI_{post} , $p = 0.88$. NI_{pre} , $p = 0.015$; NI_{post} , $p = 0.0050$ (V-clamp vs. I-clamp). **(L)** NI plotted against peak amplitude of the uEPSC in the pre and post paradigms. Best line of fit: pre, $r^2 = 0.0022$; post, $r^2 = -0.057$. Data were tested for normality, T-tests were run.

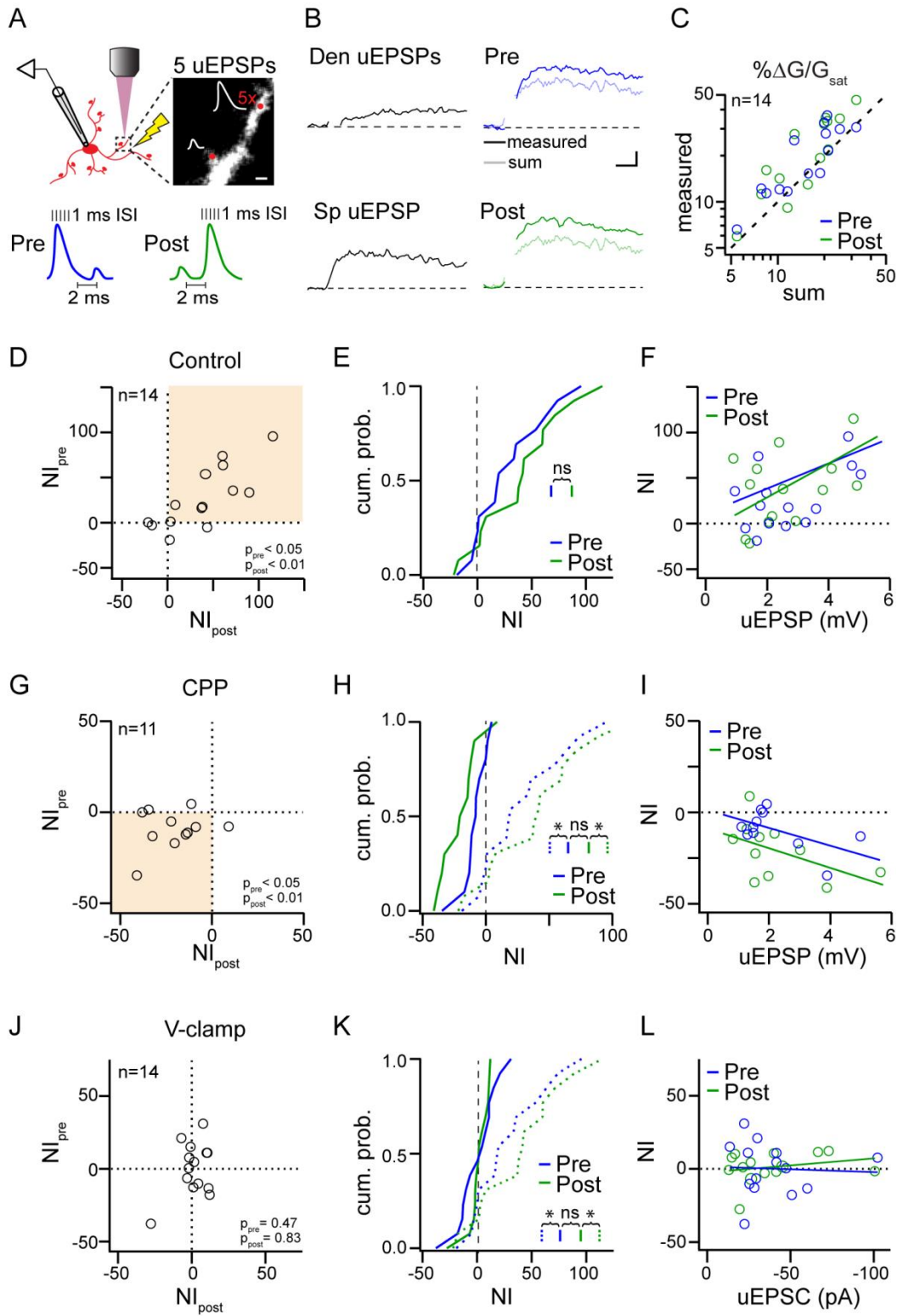
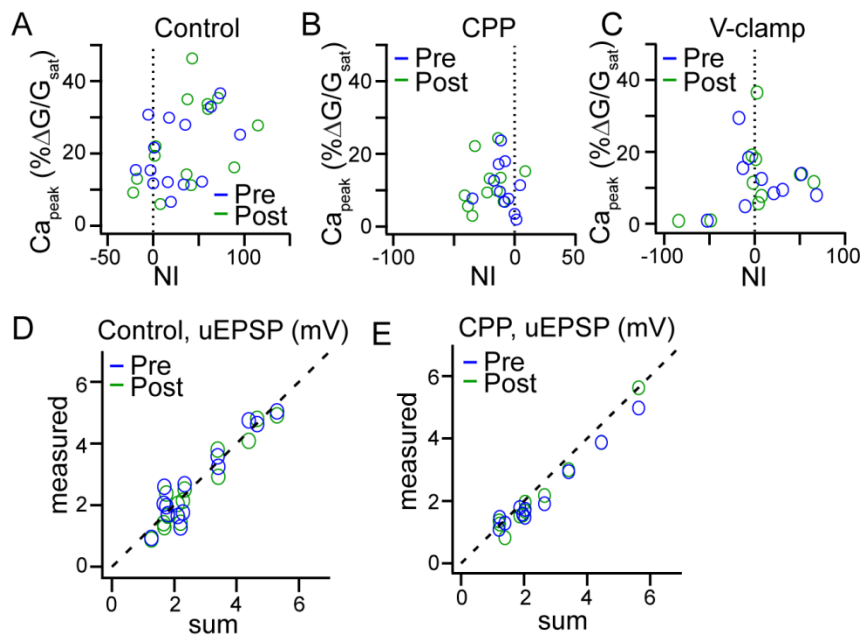


Figure 2.13. Spine Ca signals are modulated by local dendritic activity.

(A-C) Spine uEPSP- dendritic uEPSPs pairing experiment. Ca_{peak} plotted against non-linearity index (NI) in pre (blue) and post (green) pairing paradigms for control conditions (A) with CPP (10 μ M) (B) in the bath, and in V-clamp (C). **(D)** Measured peak uEPSP in pre and post paradigms plotted against the theoretical sum of the uEPSPs, control conditions. **(E)** Same as (D) but in CPP.



METHODS:

Immunostaining and confocal imaging

Pvalb-cre x tdTomato^{fl/fl} mice (P15-30) were perfused using cold 1x PBS for 5 minutes followed by cold 4% PFA for 10-15 minutes. The brain was removed and post-fixed in 4% PFA overnight at 4°C. The brain was then washed in 1x PBS and sectioned on a Leica VT1000s vibratome (100 µm coronal sections). Sections were immuno-stained with rabbit anti-RFP (Abcam, ab62341). The immuno-staining protocol was as follows: two nights of overnight incubation and permeabilization in blocking solution (5% NGS and 0.05% Triton X-100), two nights of overnight incubation in primary antibody solution (1:500 in blocking solution), and one night of overnight incubation in secondary antibody solution (goat anti-rabbit Alexa Fluor-568, 1:1000 in blocking solution). Slices were then mounted onto slides and coverslipped with Aquamount and coverglass.

Acute slice preparation

Sagittal slices of primary visual cortex (V1) were prepared from *Pvalb-cre x tdTomato^{fl/fl}* or WT mice (P15-30 or P20-30 and P46-56 for spine density quantification experiments) similar to Kuhlman et al., 2010 and Xue, Atallah and Scanziani, 2014. Animals were deeply anesthetized by inhalation of isoflurane and immediately decapitated. The brain was removed, hemi-sectioned, and cut into 300 µm sagittal sections using a Leica VT1000s vibratome (Leica Instruments, Nussloch, Germany). For older mice (P46-56), the mice were anesthetized with ketamine and xylazine (100 mg/kg and 10 mg/kg, respectively) and quickly perfused prior to decapitation with cold sucrose dissection media consisting of (in mM): 83 NaCl, 2.5 KCl, 3.3 MgSO₄, 1 Na₂HPO₄, 22 glucose, 72 sucrose, 0.5 CaCl₂, and 26.2 NaHCO₃. The brain dissection was performed in cold, choline-based

dissection solution consisting of (in mM): 110 choline-Cl, 25 NaHCO₃, 1.25 Na₂HPO₄, 2.5 KCl, 7 MgCl₂, 25 glucose, 0.5 CaCl₂, 11.6 ascorbic acid, 3.1 pyruvic acid and equilibrated with carbogen (95% O₂/ 5% CO₂). Slices were then placed in a recovery chamber containing artificial cerebrospinal fluid (aCSF) consisting of (in mM): 127 NaCl, 25 NaHCO₃, 1.25 Na₂HPO₄, 2.5 KCl, 2 CaCl₂, 1 MgCl₂, 25 glucose, saturated with carbogen. Slices recovered for 30 min at 31°C and were then maintained at room temperature until recordings were performed (4-6 hours).

Morphological Analysis

To quantify spine density, whole-cell recordings were made from PV INs and filled with a high concentration of Alexa Fluor-594 (100µM) in the pipette to allow for rapid filling of the dendrites. On average, two dendritic branches per cell were imaged under two-photon microscopy at 800 nm using the Alexa Fluor-594 signal. Images were taken at 256 x 256 pixels (1 pixel = 0.058 µm) and were stitched together using an ImageJ pairwise Stitching plugin (Preibisch, Saalfeld, & Tomancak, 2009). Dendrites were straightened using a Straightening plugin (Kocsis et al. 1991) and spines were manually counted on unprocessed images. Brightness and contrast were enhanced for representative images only.

Electrophysiology

Slices were placed in a recording chamber and perfused with a recirculating bath of carbogen-saturated aCSF maintained at 31-33°C. Whole-cell patch clamp recordings were obtained from tdTomato-expressing interneurons in layer II/III of V1 that were visualized

using epifluorescence under IR-DIC on an Olympus BX52 microscope. Open pipette resistances were 2-5 M Ω (borosilicate glass pipette; BF150-86-10, Sutter Instruments). Recordings were performed using a Multiclamp 700B amplifier (Molecular Devices, Sunnyvale, CA). Data were sampled at 10 kHz, filtered at 6 kHz, and recordings were discarded if the series resistances were >30 M Ω . All cells were confirmed as fast-spiking with little-to-no spike-frequency adaptation by injecting a 1 s current step and recording the frequency and AP FWHM (**Figure 1D**). Additionally, neurons had a low input resistance and multipolar morphology.

In all experiments except those described in **Figure 4F-I**, a potassium (K)-gluconate internal consisting of (in mM) was used: 115.0 K-gluconate, 20.0 KCl, 10.0 phosphocreatine disodium salt, 10.0 HEPES acid, 2.0 Na-ATP, 0.3 Na-GTP, and 5.0 MgCl₂. For the rectification experiments (**Figure 4F-I**), a cesium methane-sulfonate internal (in mM) was used: 120.0 cesium methane-sulfonate, 10 HEPES acid, 4.0 MgCl₂, 0.4 Na-GTP, 4.0 Na-ATP, and 10.0 phosphocreatine disodium salt. In all Ca imaging experiments (**Figures 2-7**), Fluo-5F (300 μ M, ThermoFisher Scientific, F14221) was included as a Ca indicator and buffer and Alexa Fluor-594 (15 μ M, ThermoFisher Scientific, A12922) was used to visualize the morphology. In all experiments except those in described in **Figure 4B** and **F-I**, spermine (100 μ M) was included in the intracellular solution. Osmolarity and pH of the internal solutions were adjusted to 290-310 mOsm and 7.3-7.4 with double-distilled water and with KOH or CsOH, respectively.

Miniature excitatory postsynaptic currents (mEPSC) were recorded in voltage clamp at -70 mV with 0.2 μ M TTX and 50 μ M picrotoxin in the bath, the K-gluconate internal used in Ca imaging experiments (**Figure S3E**). mEPSCs were sampled at 10 kHz, filtered at 6 kHz, and recordings were discarded if the series resistances were >30 M Ω . 10 s acquisitions were taken.

Extracellular stimulation experiments

A theta-glass extracellular (EC) stimulating electrode with a diameter of ~5-10 μm was lowered into the slice and placed 10-15 μm away from the spine or dendritic shaft of interest (**Figure 2A, B, and E**). Current was injected for 0.5 ms at 0.1 Hz using a stimulus isolator (ISO-Flex, A.M.P.I.) to control intensity.

Spines: “No Ca transient” stimulation condition produced an EPSC recorded at the soma but failed to evoke a Ca transient in the spine head (**Figure 2F**). The stimulus intensity was slowly increased until an all-or-nothing Ca signal was observed in the spine (“Ca transient”) but generally not the neighboring dendrite (**Figure 2G**). For the pharmacology (**Figure 2J-O**; CPP, CPP + NBQX, PhTx, PhTx + NBQX), the first 10-15 trials after wash-in were discarded. On average, 10-20 trials were obtained for each condition with a 10 s inter-trial interval (ITI).

Dendrites: 2D images of dendrites were acquired while slowly increasing stimulus strength until a hot spot of Ca was observed. Line scans, imaged horizontally through the dendrites, were then acquired through the hot spots and Ca transients were analyzed (**Figure 2C and D**). Pharmacology was done as described above (**Figure 2J-O**).

Two-photon imaging and uncaging

Combined two-photon imaging and MNI-glutamate uncaging was performed using a custom-built two-photon laser-scanning microscope (Bloodgood & Sabatini, 2005; Carter & Sabatini, 2004). MNI-caged-L-glutamate (#1490, Tocris, Ellisville, MO) was bath applied to a final concentration of 2.5mM and uncaged using a 0.5 ms light pulse (720 nm, MaiTai

DeepSee, Spectra Physics). The Ca-insensitive dye Alexa Fluor-594 and the Ca-sensitive indicator Fluo-5F were excited with a second laser tuned to 800 nm.

Uncaging laser power was set to bleach 30-40% of the red fluorescence as described previously (Bloodgood & Sabatini 2007; **Figure S2A-C**). This results in a consistent amount of glutamate uncaged at each location (irrespective of depth, tissue inhomogeneities, or pharmacological manipulation), thus allowing for direct comparison of data-sets (**Figure S2F**). For uncaging at dendritic sites, laser power was set by photo-bleaching a neighboring spine located within the same z-plane (**Figure 3B**). Dendritic sites were selected by finding the locations where the uEPSCs had maximal amplitudes and sub-millisecond 20-80% rise-times (**Figure S2D**). Dendritic and spine uEPSCs had similar amplitudes and rise times to mEPSCs recorded from these cells. uEPSCs had longer decay taus (**Figure S2E**; Dehorter et al. 2015), likely due to activation of extrasynaptic receptors associated with this method. Stimulus-evoked changes in fluorescence (and the Ca signal) were reported as $\% \Delta G / G_{\text{sat}}$, reflecting measurements of $\Delta G / R$ normalized to G / R in saturating Ca as described previously (Bloodgood & Sabatini 2007; Sabatini & Svoboda 2000; Sabatini et al. 2002). This allows for quantification of evoked responses that are insensitive to small changes in the resting Ca, independent of spine or compartment volume, and comparable across multiple time-points, microscopes, or experimenters. Imaging and uncaging were performed using ScanImage software (Pologruto, Sabatini, & Svoboda, 2003). Line scans (500 Hz) were interleaved with a 2D image (spine or dendrite) and the focus was adjusted as necessary. Ten-20 pulses (10 s ITI) were delivered to each site and averaged. Experiments were done first in voltage clamp and then in current clamp for each site.

Twenty-two of the 31 imaged spines displayed both an uEPSC and Ca signal; analyses were restricted to that sub-group (**Figure 3F and G**). Of the spines omitted from

the data set, 6 generated a Ca transient and no measureable uEPSC, suggesting the presence of “silent” synapses (Isaac et al. 1995; Liao et al. 1995), and 3 generated a uEPSC but no Ca transient, suggesting the presence of a synapse without Ca-permeable glutamate receptors.

For rectification index experiments (**Figure 4XX**), PV INs were patched using the cesium methane-sulfonate internal and glutamate was uncaged at dendritic sites or over spines in the presence of CPP, and AMPAR currents were measured at membrane potentials from -70 mV to +40 mV. Experiments were repeated excluding spermine from the internal for dendritic sites.

Data analysis

Off-line data analyses were performed using custom software in Igor Pro (Wavemetrics) and MATLAB. Acquisitions were excluded that contained spontaneous activity or if the baseline Ca was above 0.05 Δ G/R. Trials were averaged, baselined to the period immediately preceding the stimulus. Ca transients were also smoothed using a 3 point box function.

EC stimulation and single synapse uncaging: The Ca_{peak} was measured over a 40 ms window starting 6 ms after stimulation. In experiments with CPP in the bath, the window was shortened to 20 ms due to the faster kinetics of the Ca transient. The Ca_{late} was measured over the last 40 ms of the imaging acquisition (116-156 ms after stimulation). The $uEPSC_{peak}$ was determined by averaging the amplitude from 0.25 ms before to 1.75 ms after the minimum uEPSC value. The $uEPSC_{late}$ was determined by averaging the current amplitude from 12 - 16 ms after stimulation. The $uEPSP_{peak}$ was determined by averaging the amplitude from 0.25 ms before to 1.75 ms after the maximum uEPSP value.

Rectification index (RI): The current-voltage (I-V) relationship was plotted and the RI was calculated as the slope of the linear fit for positive voltages divided by the slope of the linear fit for negative voltages (Soto et al., 2007)

Pairing experiments: The theoretical sum reflected the sum of the Ca transients measured in response to bAPs (or dendritic uEPSPs in the spine-dendrite co-activation experiment in Figure 7) and uEPSPs alone. The Ca signals were time-shifted to account for the distinct timings used in the pre and post paradigms. Non-linearity indexes (NIs) were calculated by dividing the difference between the theoretical sum and the experimental pairing by the experimental pairing and multiplying by 100. Analyses were restricted to sites that produced Ca transients in response to bAPs, as these synapses could be demonstrated to reliably experience the backpropagation of APs, and a Ca transient in response to uncaging. For the spine-dendrite co-activation experiments, analyses were restricted to spines and dendrites that produced uEPSPs and where dendritic uncaging did not result in a Ca transient in the spine head.

Statistics

Data sets were tested for normality using a Shapiro-Wilk test. For normally distributed data, parametric tests were conducted as noted; paired t-tests were done for paired data and independent t-tests for done for unpaired data. For comparison between non-normal data, non-parametric statistical tests were performed. Specifically, Wilcoxon Signed Ranks Tests were performed for paired data, and Mann Whitney U-Tests were done for unpaired data. For comparison between the cumulative probably distributions of non-parametric data, Kologorov Smirnov tests were conducted. For comparison between the three age groups in **Figure 1**, a 3-way Kruskal-Wallis Test was performed; if there were

significant differences, pairwise comparisons were done using a Mann Whitney U-test with a Bonferroni correction. Statistical tests were conducted using IBM SPSS. In all cases, significance was set at $p < 0.05$.

Chapter 2 is material currently in press for publication at *Cell Reports*. Sancho, L., & Bloodgood, B.L. (2018). Functional distinctions between spine and dendritic synapses in parvalbumin positive interneurons of mouse cortex. The dissertation author was the primary investigator and author of this material.

REFERENCES

- Azouz, R., Gray, C. M., Nowak, L. G., & McCormick, D. A. (1997). Physiological properties of inhibitory interneurons in cat striate cortex. *Cerebral Cortex*, *7*(6), 534–545. <http://doi.org/10.1093/cercor/7.6.534>
- Bagnall, M. W., Hull, C., Bushong, E. A., Ellisman, M. H., & Scanziani, M. (2011). Multiple Clusters of Release Sites Formed by Individual Thalamic Afferents onto Cortical Interneurons Ensure Reliable Transmission. *Neuron*, *71*(1), 180–194. <http://doi.org/10.1016/j.neuron.2011.05.032>
- Beaulieu-Laroche, & Harnett, M. T. (2017). Dendritic Spines Prevent Synaptic Voltage Clamp. *Neuron*, *97*, 75–82.
- Bloodgood, B. L., Giessel, A. J., & Sabatini, B. L. (2009). Biphasic synaptic Ca influx arising from compartmentalized electrical signals in dendritic spines. *PLoS Biology*, *7*(9). <http://doi.org/10.1371/journal.pbio.1000190>
- Bloodgood, B. L., & Sabatini, B. L. (2005). Neuronal Activity Regulates Diffusion Across the Neck of Dendritic Spines. *Science*, *310*(5749), 866–869. <http://doi.org/10.1126/science.1114816>
- Bloodgood, B. L., & Sabatini, B. L. (2007). Nonlinear Regulation of Unitary Synaptic Signals by CaV2.3 Voltage-Sensitive Calcium Channels Located in Dendritic Spines. *Neuron*, *53*(2), 249–260. <http://doi.org/10.1016/j.neuron.2006.12.017>
- Bloodgood, B. L., & Sabatini, B. L. (2009). *NMDA Receptor-Mediated Calcium Transients in Dendritic Spines. Biology of the NMDA Receptor*. Retrieved from <http://www.ncbi.nlm.nih.gov/pubmed/21204410>
- Bowie, D., & Mayer, M. L. (1995). Inward rectification of both AMPA and kainate subtype glutamate receptors generated by polyamine-mediated ion channel block. *Neuron*, *15*(2), 453–462. [http://doi.org/10.1016/0896-6273\(95\)90049-7](http://doi.org/10.1016/0896-6273(95)90049-7)
- Branco, T., & Häusser, M. (2011). Synaptic Integration Gradients in Single Cortical Pyramidal Cell Dendrites. *Neuron*, *69*(5), 885–892. <http://doi.org/10.1016/j.neuron.2011.02.006>
- Camiré, O., & Topolnik, L. (2014). Dendritic calcium nonlinearities switch the direction of synaptic plasticity in fast-spiking interneurons. *The Journal of Neuroscience : The Official Journal of the Society for Neuroscience*, *34*(11), 3864–77. <http://doi.org/10.1523/JNEUROSCI.2253-13.2014>
- Cardin, J. a, Carlén, M., Meletis, K., Knoblich, U., Zhang, F., Deisseroth, K., ... Moore, C. I. (2009). Driving fast-spiking cells induces gamma rhythm and controls sensory responses. *Nature*, *459*(7247), 663–667. <http://doi.org/10.1038/nature08002>
- Carlén, M., Meletis, K., Siegle, J., Cardin, J., Futai, K., Vierling-Claassen, D., ... Tsai, L.-H. (2011). A critical role for NMDA receptors in parvalbumin interneurons for gamma rhythm induction and behavior. *Molecular Psychiatry*, *17*, 537–548. <http://doi.org/10.1038/mp.2011.31>

- Carter, A. G., & Sabatini, B. L. (2004). State-dependent calcium signaling in dendritic spines of striatal medium spiny neurons. *Neuron*, *44*(3), 483–493. <http://doi.org/10.1016/j.neuron.2004.10.013>
- Chiovini, B., Turi, G. F., Katona, G., Kaszás, A., Pálfi, D., Maák, P., ... Rózsa, B. (2014). Dendritic Spikes Induce Ripples in Parvalbumin Interneurons during Hippocampal Sharp Waves. *Neuron*, *82*(4), 908–924. <http://doi.org/10.1016/j.neuron.2014.04.004>
- Colgan, L. A., & Yasuda, R. (2014). Plasticity of Dendritic Spines: Subcompartmentalization of Signaling. *Annual Review of Physiology*, *76*(1), 365–385. <http://doi.org/10.1146/annurev-physiol-021113-170400>
- Dehorter, N., Ciceri, G., Bartolini, G., Lim, L., del Pino, I., & Marin, O. (2015). Tuning of fast-spiking interneuron properties by an activity-dependent transcriptional switch. *Science*, *349*(6253), 1216–1220. <http://doi.org/10.1126/science.aab3415>
- Froemke, R. C., & Dan, Y. (2002). Spike-timing-dependent synaptic modification induced by natural spike trains. *Nature*, *416*(6879), 433–438. <http://doi.org/10.1038/416433a>
- Gasparini, S., Migliori, M., & Magee, J. C. (2004). On the Initiation and Propagation of Dendritic Spikes in CA1 Pyramidal Neurons. *Journal of Neuroscience*, *24*(49), 11046–11056. <http://doi.org/10.1523/JNEUROSCI.2520-04.2004>
- Goldberg, J. H., Tamas, G., Aronov, D., & Yuste, R. (2003). Calcium microdomains in aspiny dendrites. *Neuron*, *40*(4), 807–821. [http://doi.org/10.1016/S0896-6273\(03\)00714-1](http://doi.org/10.1016/S0896-6273(03)00714-1)
- Goldberg, J. H., Tamas, G., & Yuste, R. (2003). Ca²⁺ imaging of mouse neocortical interneurone dendrites: Ia-type K⁺ channels control action potential backpropagation. *Journal of Physiology*. <http://doi.org/10.1113/jphysiol.2003.042580>
- Goldberg, J. H., Yuste, R., & Tamas, G. (2003). Ca²⁺ imaging of mouse neocortical interneurone dendrites: Contribution of Ca²⁺-permeable AMPA and NMDA receptors to subthreshold Ca²⁺dynamics. *The Journal of Physiology*, *551*(1), 67–78. <http://doi.org/10.1113/jphysiol.2003.042598>
- Gulyá, A. I., Megías, M., Emri, Z., & Freund, T. F. (1999). Total Number and Ratio of Excitatory and Inhibitory Synapses Converging onto Single Interneurons of Different Types in the CA1 Area of the Rat Hippocampus. *The Journal of Neuroscience*, *19*(22), 10082–10097. <http://doi.org/10.1002/cne.902960202>
- Harnett, M. T., Makara, J. K., Spruston, N., Kath, W. L., & Magee, J. C. (2012). Synaptic amplification by dendritic spines enhances input cooperativity. *Nature*, *491*(7425), 599–602. <http://doi.org/10.1038/nature11554>
- Hu, H., Martina, M., & Jonas, P. (2010). Dendritic mechanisms underlying rapid synaptic activation of fast-spiking hippocampal interneurons. *Science (New York, N.Y.)*, *327*(5961), 52–58. <http://doi.org/10.1126/science.1177876>
- Isaac, J. T. R., Nicoll, R. A., & Malenka, R. C. (1995). Evidence for silent synapses: Implications for the expression of LTP. *Neuron*, *15*(2), 427–434. [http://doi.org/10.1016/0896-6273\(95\)90046-2](http://doi.org/10.1016/0896-6273(95)90046-2)

- Jiang, M., & Swann, J. W. (2005). A role for L-type calcium channels in the maturation of parvalbumin-containing hippocampal interneurons. *Neuroscience*, *135*(3), 839–850. <http://doi.org/10.1016/j.neuroscience.2005.06.073>
- Jonas, P., Racca, C., Sakmann, B., Seeburg, P. H., & Monyer, H. (1994). Differences in Ca²⁺ permeability of AMPA-type glutamate receptor channels in neocortical neurons caused by differential GluR-B subunit expression. *Neuron*, *12*(6), 1281–1289. [http://doi.org/10.1016/0896-6273\(94\)90444-8](http://doi.org/10.1016/0896-6273(94)90444-8)
- Kloc, M., & Maffei, a. (2014). Target-Specific Properties of Thalamocortical Synapses onto Layer 4 of Mouse Primary Visual Cortex. *Journal of Neuroscience*, *34*(46), 15455–15465. <http://doi.org/10.1523/JNEUROSCI.2595-14.2014>
- Kocsis, E., Trus, B. L., Steer, C. J., Bisher, M. E., & Steven, A. C. (1991). Image averaging of flexible fibrous macromolecules: The clathrin triskelion has an elastic proximal segment. *Journal of Structural Biology*, *107*(1), 6–14. [http://doi.org/10.1016/1047-8477\(91\)90025-R](http://doi.org/10.1016/1047-8477(91)90025-R)
- Korotkova, T., Fuchs, E. C., Ponomarenko, A., von Engelhardt, J., & Monyer, H. (2010). NMDA Receptor Ablation on Parvalbumin-Positive Interneurons Impairs Hippocampal Synchrony, Spatial Representations, and Working Memory. *Neuron*, *68*(3), 557–569. <http://doi.org/10.1016/j.neuron.2010.09.017>
- Kuhlman, S. J., Lu, J., Lazarus, M. S., & Huang, Z. J. (2010). Maturation of GABAergic inhibition promotes strengthening of temporally coherent inputs among convergent pathways. *PLoS Computational Biology*. <http://doi.org/10.1371/journal.pcbi.1000797>
- Lamsa, K. P., Heeroma, J. H., Somogyi, P., Rusakov, D. a, & Kullmann, D. M. (2007). Anti-Hebbian long-term potentiation in the hippocampal feedback inhibitory circuit. *Science (New York, N.Y.)*, *315*(5816), 1262–1266. <http://doi.org/10.1126/science.1137450>
- Le Roux, N., Cabezas, C., Böhm, U. L., & Poncer, J. C. (2013). Input-specific learning rules at excitatory synapses onto hippocampal parvalbumin-expressing interneurons. *The Journal of Physiology*, *591*(Pt 7), 1809–22. <http://doi.org/10.1113/jphysiol.2012.245852>
- Lee, K. F. H., Soares, C., Thivierge, J. P., & Béique, J. C. (2016). Correlated Synaptic Inputs Drive Dendritic Calcium Amplification and Cooperative Plasticity during Clustered Synapse Development. *Neuron*, *89*(4), 784–799. <http://doi.org/10.1016/j.neuron.2016.01.012>
- Lester, R. A. J., Clements, J. D., Westbrook, G. L., & Jahr, C. E. (1990). Channel kinetics determine the time course of NMDA receptor-mediated synaptic currents. *Nature*, *346*(6284), 565–567. <http://doi.org/10.1038/346565a0>
- Liao, D., Hessler, N. A., & Malinow, R. (1995). Activation of postsynaptically silent synapses during pairing-induced LTP in CA1 region of hippocampal slice. *Nature*. <http://doi.org/10.1038/375400a0>
- Losonczy, A., & Magee, J. C. (2006). Integrative Properties of Radial Oblique Dendrites in Hippocampal CA1 Pyramidal Neurons. *Neuron*, *50*(2), 291–307. <http://doi.org/10.1016/j.neuron.2006.03.016>

- Magee, J. C., & Johnston, D. (1997). A synaptically controlled, associative signal for Hebbian plasticity in hippocampal neurons. *Science*, 275(5297), 209–213. <http://doi.org/10.1126/science.275.5297.209>
- Markram, H., Lubke, J., Frotscher, M., & Sakmann, B. (1997). Regulation of synaptic efficacy by coincidence of postsynaptic APs and EPSPs. *Science*, 275(5297), 213–215. <http://doi.org/10.1126/science.275.5297.213>
- Monyer, H., Sprengel, R., Schoepfer, R., Herb, A., Higuchi, M., Lomeli, H., ... Seeburg, P. H. (1992). Heteromeric NMDA Receptors: Molecular and Functional Distinction of Subtypes. *Science*, 256(5060), 1217–1221. <http://doi.org/10.1126/science.256.5060.1217>
- Murakoshi, H., Wang, H., & Yasuda, R. (2011). Local, persistent activation of Rho GTPases during plasticity of single dendritic spines. *Nature*, 472(7341), 100–104. <http://doi.org/10.1038/nature09823>
- Nevian, T., & Sakmann, B. (2006). Spine Ca²⁺ Signaling in Spike-Timing-Dependent Plasticity. *Journal of Neuroscience*, 26(43), 11001–11013. <http://doi.org/10.1523/JNEUROSCI.1749-06.2006>
- Nishiyama, J., & Yasuda, R. (2015). Biochemical Computation for Spine Structural Plasticity. *Neuron*. <http://doi.org/10.1016/j.neuron.2015.05.043>
- Okaty, B. W., Miller, M. N., Sugino, K., Hempel, C. M., & Nelson, S. B. (2009). Transcriptional and Electrophysiological Maturation of Neocortical Fast-Spiking GABAergic Interneurons. *Journal of Neuroscience*, 29(21), 7040–7052. <http://doi.org/10.1523/JNEUROSCI.0105-09.2009>
- Pelkey, K. A., Barksdale, E., Craig, M. T., Yuan, X., Sukumaran, M., Vargish, G. A., ... McBain, C. J. (2015). Pentraxins coordinate excitatory synapse maturation and circuit integration of parvalbumin interneurons. *Neuron*, 85(6), 1257–1272. <http://doi.org/10.1016/j.neuron.2015.02.020>
- Peters, A., & Regidor, J. (1981). A reassessment of the forms of nonpyramidal neurons in area 17 of cat visual cortex. *Journal of Comparative Neurology*, 203(4), 685–716. <http://doi.org/10.1002/cne.902030408>
- Pologruto, T. A., Sabatini, B. L., & Svoboda, K. (2003). ScanImage: Flexible software for operating laser scanning microscopes. *BioMedical Engineering Online*, 2. <http://doi.org/10.1186/1475-925X-2-13>
- Polsky, A., Mel, B. W., & Schiller, J. (2004). Computational subunits in thin dendrites of pyramidal cells. *Nature Neuroscience*, 7(6), 621–627. <http://doi.org/10.1038/nn1253>
- Preibisch, S., Saalfeld, S., & Tomancak, P. (2009). Globally optimal stitching of tiled 3D microscopic image acquisitions. *Bioinformatics*, 25(11), 1463–1465. <http://doi.org/10.1093/bioinformatics/btp184>
- Sabatini, B. L., Oertner, T. G., & Svoboda, K. (2002). The life cycle of Ca²⁺ ions in dendritic spines. *Neuron*, 33(3), 439–452. [http://doi.org/10.1016/S0896-6273\(02\)00573-1](http://doi.org/10.1016/S0896-6273(02)00573-1)
- Sabatini, B. L., & Svoboda, K. (2000). Analysis of calcium channels in single spines using

optical fluctuation analysis.[In Process Citation]. *Nature*, 408(6812), 589–593.
Retrieved from pm:0011117746

Soto, D., Coombs, I. D., Kelly, L., Farrant, M., & Cull-Candy, S. G. (2007). Stargazin attenuates intracellular polyamine block of calcium-permeable AMPA receptors. *Nature Neuroscience*, 10(10), 1260–7. <http://doi.org/10.1038/nn1966>

Szabo, A., Somogyi, J., Cauli, B., Lambolez, B., Somogyi, P., & Lamsa, K. P. (2012). Calcium-permeable AMPA receptors provide a common mechanism for LTP in glutamatergic synapses of distinct hippocampal interneuron types. *The Journal of Neuroscience : The Official Journal of the Society for Neuroscience*, 32(19), 6511–6. <http://doi.org/10.1523/JNEUROSCI.0206-12.2012>

Washburn, M. S., Numberger, M., Zhang, S., & Dingledine, R. (1997). Differential dependence on GluR2 expression of three characteristic features of AMPA receptors. *The Journal of Neuroscience : The Official Journal of the Society for Neuroscience*, 17(24), 9393–9406.

Wu, Y. W., Grebenyuk, S., McHugh, T. J., Rusakov, D. A., & Semyanov, A. (2012). Backpropagating Action Potentials Enable Detection of Extrasynaptic Glutamate by NMDA Receptors. *Cell Reports*, 1(5), 495–505. <http://doi.org/10.1016/j.celrep.2012.03.007>

Xue, M., Atallah, B. V., & Scanziani, M. (2014). Equalizing excitation-inhibition ratios across visual cortical neurons. *Nature*. <http://doi.org/10.1038/nature13321>

Yuste, R., & Denk, W. (1995). Dendritic spines as basic functional units of neuronal integration. *Nature*. <http://doi.org/10.1038/375682a0>

Chapter 3. What is next?

Over the course of my doctoral studies, I have endeavored to provide an in-depth examination of the synaptic physiology of PV INs. While much was known about excitatory transmission onto PV INs, in that they are densely innervated (Gulyá *et al.*, 1999), are reliable integrators of synaptic input (Hu, Martina and Jonas, 2010), and contain both CP-AMPA and NMDARs (Goldberg *et al.*, 2003; Goldberg, Yuste and Tamas, 2003; Lamsa *et al.*, 2007; Szabo *et al.*, 2012; Le Roux *et al.*, 2013; Matta *et al.*, 2013), not much was known about the subcellular localization of these glutamate receptors and how they were modulated by the cell's on-going global or local activity. Using two-photon Ca imaging and glutamate uncaging in conjunction with electrophysiology and pharmacology, I investigated the heterogeneity of excitatory synapses onto PV INs. As a cell type, PV INs' roles in circuit function had been very well characterized, yet much remained to be understood about how these cells process their excitatory input and integrate it with their on-going activity to produce their output. With the work presented in this dissertation, I hope to contribute to the study of how PV INs actually produce their output, measured in their crucial roles in circuit regulation.

Bias of NMDARs towards spines

My work has shown that NMDARs are biased towards spine synapses, as compared to dendritic synapses. What mechanisms might allow for a distribution bias of NMDARs towards spines over dendrites? This could perhaps occur through the differential trafficking of receptors towards spines vs dendritic shafts or a difference in the internalization and degradation of these receptors at spines. NMDARs are assembled in the endoplasmic reticulum (ER) in a highly regulated and monitored process for eventual

transport to the plasma membrane (Horak *et al.*, 2014). NMDARs are further modified in the Golgi apparatus and are then transported to the *trans* Golgi network and endosomes, where they end up at the plasma membrane (Horak *et al.*, 2014). PDZ domain-containing proteins, such as the MAGUK proteins, PSD-95, SAP102, and SAP97, are the main scaffolding proteins that anchor NMDARs to synapses (Sheng, 1996; Sheng and Kim, 1996; Kornau *et al.*, 1995). As different NMDAR subunits seem to be associated with different MAGUKs or secretory pathways, it is plausible that the bias in the distribution of NMDARs towards spines that we see could arise from a subunit composition difference as well. Preliminary experiments done in the course of this dissertation suggest that this may in fact be the case. When we uncaged glutamate on the spine and then in several dendritic sites in the presence of NBQX to antagonize AMPARs and ifenprodil to block NR2B-containing receptors (while also recording in 0 mM Mg), we found that dendritic signals seemed to be more affected (**Figure 3.1A and B**). In fact, this experiment recapitulated the results shown in **Figure 2.4L-N**, yet revealed an exaggerated bias of NR2A-containing receptors to spines vs. dendrites. Thus, the apparent enrichment for NMDARs in spines may be predominantly NR2A-containing NMDARs, which may be mediated by different trafficking pathways. Further experiments inhibiting or disturbing specific elements of these transport mechanisms.

Furthermore, immunostaining experiments targeting NMDARs and AMPARs are needed to make assessments about the absolute densities of these receptors at different subcellular compartments. Along the course of this dissertation, I attempted to use expansion microscopy, normal confocal imaging, and array tomography. Using confocal imaging in conjunction with immunostaining proved a challenge (see **Figure 3.2**); I amplified the tdTomato signal expressed by the PV INs using an antibody against RFP (red fluorescent protein) while staining for NR1 (the obligatory NMDAR subunit). However, it

was still exceedingly difficult to distinguish between axonal boutons and dendritic spines given the density of the tdTomato signal. Another approach that was taken was to use array tomography, which gives high-resolution 3D immunofluorescence by virtue of ultrathin sections of tissue (Micheva and Smith, 2007; Micheva et al., 2010). However, the fixation process substantially quenched the fluorescence of the tdTomato signal, making this approach null. As a final attempt, expansion microscopy was performed on tdTomato and NR1-stained sections (Chen, Tillberg and Boyden, 2015; Chozinski et al., 2016). The resulting fluorescent signal was overall too dim to distinguish axonal boutons from dendritic spines. Further experiments are needed to optimize expansion microscopy for the purposes of imaging dense tdTomato signals.

Why are spines insensitive to bAPs?

The experiments in this dissertation showed that dendritic receptors were bi-directionally modulated by the bAPs; when bAPs preceded a uEPSP, Ca influx was sub-linear due to CP-AMPA-dependent mechanisms, and when bAPs followed a uEPSP, the Ca signal was supra-linear due to enhancement of Ca influx through NMDARs. Receptors on spines, however, were insensitive to bAPs. **Figure 2.7A-D** shows that bAPs generate similar Ca influx at spines equivalently to dendritic shafts. Furthermore, preliminary studies (**Figure 3.3A-C**) show that this Ca influx is in part mediated by L-type and T-type voltage-gated Ca channels (VGCCs), as has been previously reported for PV INs (Goldberg, Yuste and Tamas, 2003). These preliminary studies did not show whether there was a difference in the contribution of L- and T- type VGCCs to the Ca influx at spines vs. dendrites; moreover, we do not know whether different VGCCs are engaged differently by the pairing of somatic and glutamate receptor activation. We also do not know if there would be

differences in this engagement at spines vs. dendrites. Thus, repeating the somatic-synaptic activity pairing experiments in spines and dendrites would expand illuminate any potential role of VGCCs.

Additionally, it is possible that spines contain some type of active potassium (K)-conductance that could be truncating any depolarization arising from the bAPs. Preliminary experiments have shown that this may be the case. For example, comparing the Ca transient when uncaging glutamate in voltage- vs. current- clamp, spines show a smaller Ca transient in current-clamp, while dendrites do not show this difference (**Figure 3.4A**). This difference goes away when the cell is held at -95 mV (**Figure 3.4B**), the reversal potentials for K, indicating that some active K conductance could be engaged at spines by uncaging, in a manner that is not present at dendritic shaft sites. Examining the functional role of a K channel in mediating somatic- synaptic activity is difficult since pharmacological agents that block K channels will also deform the AP waveform.

Additionally, spines could contain another type of K conductance: SK or BK channels. SK (small conductance) channels are Ca-gated K channels that are present in pyramidal neurons spines (Faber, Delaney and Sah, 2005; Ngo-Anh et al., 2005; Bloodgood and Sabatini, 2007). These channels, in conjunction with L-type VGCCs, have been shown to form part of a negative feedback loop that reduces NMDAR-mediated Ca influx into spines (Bloodgood and Sabatini, 2007). Their presence on PV INs has not been established. Preliminary single spine uncaging experiments done in the presence of apamin, an SK channel antagonist, revealed no differences as compared to control conditions (**Figure 3.5A**). Analogous experiments in the presence of iberiotoxin to block BK (big conductance) K channels should be conducted; these channels are activated by Ca as well as voltage (Lee and Cui, 2010) and their presence on PV INs remains unknown. Furthermore, as the presence of mGluRs (metabotropic glutamate receptors) has been

established in PV INs (Camiré and Topolnik, 2014), we conducted preliminary single spine uncaging experiments in the presence of MPEP to antagonize mGluR5s. These experiments demonstrated no differences relative to control conditions (**Figure 3.5B**).

The functional consequences of dendritic bi-directional modulation: LTP/LTD

As receptors at proximal dendritic sites demonstrate bi-directional modulation depending on the relative timing of the somatic activity, this could underlie differential plasticity mechanism. The supra-linearity generated when bAPs follow synaptic activation that is mediated by NMDARs could provide the foundation for NMDAR-dependent LTP. On the other hand, the sub-linearity generated when bAPs precede synaptic activation that is mediated by CP-AMPA receptors could underlie CP-AMPA-dependent LTD. Perhaps the dual functional role of NMDARs and CP-AMPA receptors enables dendritic sites to integrate the relative timing of the cell's on-going activity. This dissertation has demonstrated these functional roles of CP-AMPA receptors and NMDARs, but has not established the presence of a long-term plasticity mechanism. It would be necessary to repeatedly pair uEPSP-bAPs at high frequencies ((Markram et al., 1997; Froemke and Dan, 2002; Nevian and Sakmann, 2006) to test whether LTP is induced or not, and whether it is dependent on NMDAR activation. Moreover, it remains unclear whether the CP-AMPA-mediated sub-linearity would underlie LTD. A similar pairing paradigm as for testing LTP would be necessary, but with the appropriate timing of somatic vs. synaptic activity.

It is also important to note that we did not elucidate any mechanisms underlying CP-AMPA-mediated LTP, which has been described before in PV INs. However, one of the limitations of these studies showing this LTP was that many held the postsynaptic cell at hyperpolarized potentials (Lamsa et al., 2007; Szabo et al., 2012; Le Roux et al., 2013);

this is problematic because neurons do not typically sit at hyperpolarized potentials. One plausible, physiological scenario under which CP-AMPA-mediated LTP could be induced could be if there is a local hyperpolarization in the dendrites due to inhibitory input. While pairing inhibition with MNI-glutamate remains experimentally intractable, presumably this could be done with presynaptic stimulation of axon terminals, though great care would have to be taken to restrict the number of stimulated axons. Optogenetic approaches would be useful as well.

Spines are integrators of local dendritic depolarization

As the data presented in this dissertation has demonstrated, Ca influx through NMDARs on spines is enhanced in the presence of a local dendritic depolarization. Dendritic depolarization was induced by uncaging 5 times onto a dendritic shaft to generate a large uEPSP 10- 15 μm away from the spine of interest; the precise distance dependence of this remains unclear. That distance was originally chosen to minimize diffusion of Ca-bound indicator into spines, which could contaminate the supra-linearity measurements. It would be interesting to uncage at increasing distances away from the target spine to map out the distance- supra-linearity relationship. In densely spiny pyramidal neurons, spines can integrate input over a distance of approximately 10 μm (Murakoshi, Wang and Yasuda, 2011; Colgan and Yasuda, 2014; Nishiyama and Yasuda, 2015; Lee et al., 2016). Does that same distance relationship hold for PV INs? Is it dependent on the magnitude of the depolarization?

This NMDAR-mediated enhancement could also not be related to the presence of a spine at all, and could also be present for dendritic-dendritic pairing. Thus, NMDARs on dendritic sites could also be sensitive to local dendritic activity; these experiments were not

performed, and could further elucidate the role of NMDARs in PV INs. This is particularly interesting, because while NMDARs are expressed at globally low levels (Matta et al., 2013), they are critical for PV IN circuit function (Carlén et al. 2011; Cardin et al. 2009; Korotkova et al. 2010). For example, NMDAR expression in PV INs is critical for their role in regulating gamma oscillations. Selective knock out of NMDARs in PV INs in mice results in enhanced baseline cortical gamma oscillations and impaired induced gamma oscillations; moreover, this results in specific cognitive deficits, such as impaired performance in habituation and fear conditioning tasks (Carlén et al., 2011).

However, little was known about how NMDARs actually contribute to the physiology and function of the synapses on these neurons. Thus, the results in this dissertation clearly demonstrate an important role for these receptors in integrating the on-going activity of neuron as well as local activity in the form of dendritic depolarization. Future experiments directly linking the role of NMDARs in Ca signaling in these cells to their network functions are needed. For example, NMDARs are required for supra-linear Ca summation and linear EPSP summation; thus, NMDARs are critical for ensuring the proper excitation of these neurons. However, the direct consequence of this remains unclear. Does this guarantee that PV INs will respond quickly to excitatory input, thus allowing them to maintain their proper network function? First off, it would be interesting to repeat some of the experiments done in this dissertation in PV-IN- specific NR1-knock out (KO) mice to determine the effects of knocking out NMDARs in PV INs. These experiments would enable us to examine any underlying disruptions in how synapses (both dendritic and spine) integrate the global and local activity of NR1-KO PV INs. Any dysfunctions in synaptic signaling could underlie abnormalities in the gamma oscillations produced by these neurons (Carlén et al., 2011). The importance of understanding how NMDARs contribute to PV IN function

cannot be overstated; in fact, one of the prevalent theories of schizophrenia in humans is the glutamate and NMDAR hypofunction theory.

The glutamate theory of schizophrenia was first proposed after the observation that ketamine, an NMDAR antagonist, induced symptoms in humans similar to those seen in schizophrenia (Luby et al., 1962). Additionally, postmortem studies looking at PV and GAD67 expression in brain tissue found deficits in schizophrenia patients (Reynolds et al., 2004; Torrey et al., 2005). Briefly, there is substantial evidence both in human patients and in animal models of schizophrenia highlighting the role of NMDARs and PV INs in schizophrenia phenotypes (Javitt, 2007). Moreover, cortical gamma oscillations, which are regulated by NMDAR function in PV INs, are abnormal in patients with schizophrenia (Williams and Boksa, 2010; Gonzalez-Burgos and Lewis, 2012). Consequently, it is important to understand how NMDARs function in PV INs to provide new insights into how dysfunction in psychiatric disorders can come about.

Development

Finally, the most intriguing questions raised by this dissertation relate to development. As the experiments presented in this dissertation were done in PV INs of the primary visual cortex (V1), they have important implications for critical period plasticity. Critical periods were first described by the biologist Konrad Lorenz, who found that the first hours after hatching are important to geese to form bonds with their mother (Lorenz, 1937). In brief, critical periods are periods in development during which neural connectivity is very dependent on experience or environmental influence. The visual critical period in mice takes place during P20- P30, a few days after eye opening (~P12; Levelt and Hübener, 2012) and is essential for the proper development and function of visual circuits. Proper

balance of excitation and inhibition in visual circuits is crucial for the critical period; for example, delaying the maturation of GABAergic transmission by deleting *Gad65* (which encodes the enzyme that synthesizing GABA; Hensch, 1998) also delays the opening of the critical period. Additionally, dark rearing animals delays both the onset of the critical period and the development of GABAergic circuits (Mower, 1991; Chen, Yang and Mower, 2001; Morales, Choi and Kirkwood, 2002).

PV INs have been shown to play a critical role in the opening of the visual critical period (van Versendaal and Levelt, 2016). In fact, the formation of PV IN inputs onto the perisomatic region of principal neurons of V1 is highly regulated by experience and activity during the critical period (Chattopadhyaya, 2004). Moreover, several studies have found an important role for the perineuronal nets (extracellular matrix or ECM) formed around these INs in development (Ye and Miao, 2013). Specifically, disruption of the ECM components of the perineuronal nets can reopen the visual critical period in adult mice (Pizzorusso et al., 2002). As the majority of the experiments done in this dissertation have been done in P15-19 mice (before the onset of the visual critical period), it is important to understand the results in the context of development. For example, the mechanisms underlying the pairing of somatic and synaptic activity and those underlying the pairing of local activity could have a critical role in establishing the critical period. These mechanisms, which underlie proper PV IN function and integration of somatic and local excitatory activity, could be instrumental in enabling PV IN to integrate themselves properly into the visual cortical network, thus maintaining the appropriate visual critical period.

Additionally, during the visual critical period, the tuning of these neurons in response to various features of visual stimuli such as orientation and direction of movement, becomes much broader (Kuhlman, Tring and Trachtenberg, 2011; Kuhlman et al., 2013; Runyan and Sur, 2013). This broadening of inhibition is also critical for the

refinement of the tuning curves of principal neurons (Li et al., 2012). The cellular mechanisms that underlie the broadening of the tuning curves of PV INs remains largely unknown. Thus, it is interesting to speculate on the role of the processes described in this dissertation in this broadening. To begin with, it is unknown whether the broadening of tuning is mediated by changes in the excitatory or inhibitory inputs made onto these cells; some studies suggest that it is the excitatory input (Runyan and Sur, 2013). However, these changes could be presynaptic or postsynaptic. Consequently, it would be interesting to repeat a subset of the experiments done in this dissertation in older, post-critical period mice to begin to understand what the cellular mechanisms are that underlie this shift in tuning during the critical period. Moreover, experiments looking at spine density in different age mice (**Figure 2.1**) clearly show a redistribution of spine density along the proximo-distal axis, with proximal spine density decreasing with age; this suggests that some postsynaptic change is occurring.

To briefly summarize, the research presented in this dissertation describe some key features of excitatory synapse function in PV INs, and move the field forward. They also raise very important questions and next steps. First, they raise questions about the subcellular trafficking mechanisms underlying the differential distribution of NMDARs towards spine and dendritic synapses. Then, the somatic pairing experiments raise the question of whether proximal spines, and not dendritic synapses, contain an active K conductance that renders them insensitive to bAPs. Moreover, while the mechanisms modulating Ca influx at spines and dendritic sites are now described in this dissertation, the resulting long-term plasticity remains unclear. Furthermore, these experiments clearly demonstrate a critical role of NMDARs in regulating Ca influx in response to different types of cellular activity; how this plays into the larger-scale function of these INs in cortical networks also remains unclear. And lastly, how the synapse properties and mechanisms

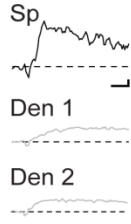
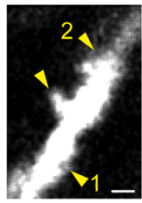
underlying the on-going modulation of synaptic Ca influx in response to different types of cellular activity changes across development is unknown. As these experiments were performed in the visual cortex, before the visual critical period, any changes associated with development would be instrumental for better understanding the role that PV INs play in critical period plasticity.

Chapter 3 contains experiments done during the course of this PhD, but not submitted for publication.

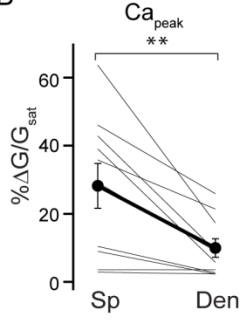
Figure 3.1. NR2A-containing NMDARs are biased towards spine synapses

(A) Isolation of NR2A- containing NMDARs. Example of image of a spine and dendrite (left). Yellow arrow heads indicate uncaging sites. Recordings were performed in aCSF containing NBQX (10 μ M), If (ifenprodil; 5 μ M), and 0 mM Mg. Ca transients and uEPSCs were recorded from spine synapses and adjacent dendritic sites. Ca transients measured in response to uncaging over the spine (Sp, black) or each of two dendritic sites (Den 1-2, gray) are shown (right). Scale bars: 1 μ m (left), 5% $\Delta G/G_{sat}$ and 25 ms (right). **(B)** Comparison of Ca_{peak} measured in the spine head (Sp) and average of the adjacent dendrite (Den, average of 2-4 sites) when NMDARs are isolated. Population average and individual spine/den comparisons are indicated by the thick and thin lines (n = 10 clusters), respectively. Spine: $28.2 \pm 6.6\%$ $\Delta G/G_{sat}$, dendrite: $9.9 \pm 2.7\%$ $\Delta G/G_{sat}$; p = 0.0051. **(C)** Ca peak in the spine vs. the average dendrite. NBQX data replotted from **Figure 2.4**.

A



B



C

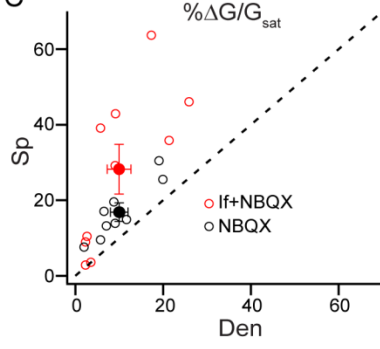


Figure 3.2. Confocal imaging of PV INs

(A) High-magnification confocal image. tdTomato (red) signaled is amplified by an anti-RFP antibody. NR1 (blue). Scale bar: 10 μ m.

A

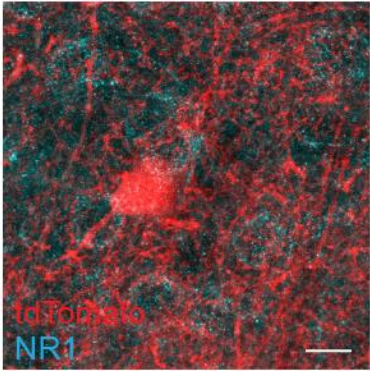


Figure 3.3. bAPs trigger Ca influx through VGCCs.

(A) Experimental set-up. Whole-cell recording, 1 bAP or 5 bAPs elicited at the soma. Line-scan through spine and adjacent dendrite for Ca imaging. **(B)**. Contribution of L-type Ca channels. 1 and 5 bAP- elicited Ca influx was measured at spines and dendrites. 20 μ M nimodipine (NIM) wash-in to block L-type VGCCs. Scale bars: 5% $\Delta G/G_{\text{sat}}$ and 25 ms. **(C)**. Same as (B), but looking at T-type Ca channels. Mibefradil (10 μ M) is washed in. Scale bars: 5% $\Delta G/G_{\text{sat}}$ and 25 ms.

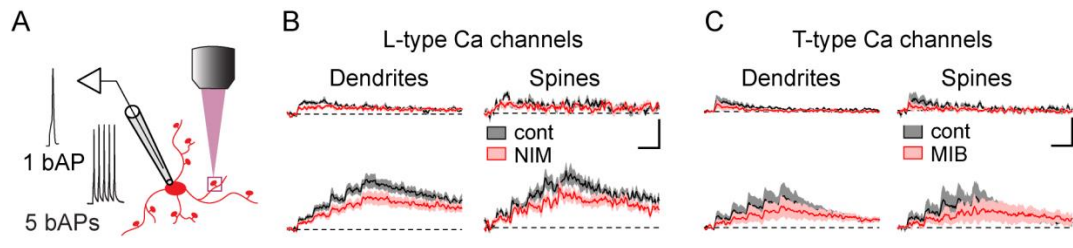
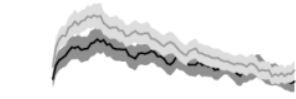


Figure 3.4. Comparing Ca influx in voltage-clamp vs. current-clamp.

(A) uEPSP-evoked Ca influx in spines (top) and dendrites (bottom). Measurements done in voltage- and current- clamp. **(B)** uEPSP-evoked Ca influx in spines, voltage- and current-clamp done at -95 mV.

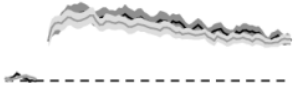
A

Spines



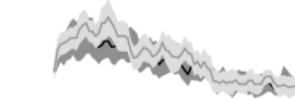
■ I-clamp
■ V-clamp

Dendrites



B

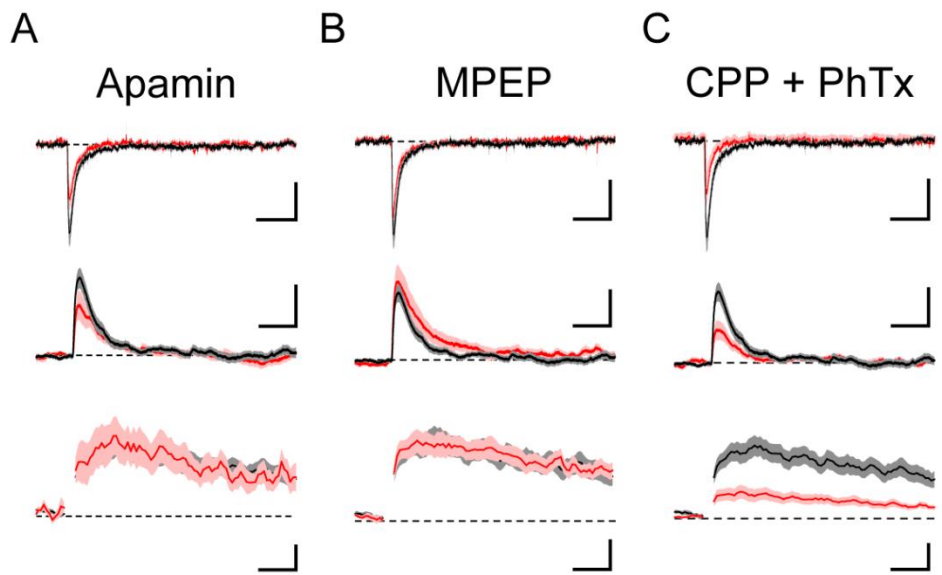
Spines at -95 mV



■ I-clamp
■ V-clamp

Figure 3.5. Other conductances in PV IN spines.

(A) Uncaging on spines in the presence of 10 μ M Apamin (red), to block SK channels. Control= black. Top, average uEPSC. Middle, average uEPSP. Bottom, average uEPSP-associated Ca transient. **(B)** Same as (A) but in 10 μ M MPEP to block mGluR5s. **(C)** Same as (A) but in 10 μ M CPP and 10 μ M PhTx. Scale bars: 10 pA (top), 0.5 mV (middle), 5% $\Delta G/G_{\text{sat}}$ (bottom), and 25 ms.



REFERENCES:

- Bloodgood, B. L. and Sabatini, B. L. (2007) 'Nonlinear Regulation of Unitary Synaptic Signals by CaV2.3 Voltage-Sensitive Calcium Channels Located in Dendritic Spines', *Neuron*, 53(2), pp. 249–260. doi: 10.1016/j.neuron.2006.12.017.
- Camiré, O. and Topolnik, L. (2014) 'Dendritic calcium nonlinearities switch the direction of synaptic plasticity in fast-spiking interneurons.', *The Journal of neuroscience : the official journal of the Society for Neuroscience*, 34(11), pp. 3864–77. doi: 10.1523/JNEUROSCI.2253-13.2014.
- Cardin, J. a, Carlén, M., Meletis, K., Knoblich, U., Zhang, F., Deisseroth, K., Tsai, L.-H. and Moore, C. I. (2009) 'Driving fast-spiking cells induces gamma rhythm and controls sensory responses.', *Nature*, 459(7247), pp. 663–667. doi: 10.1038/nature08002.
- Carlé N, M., Meletis, K., Siegle, J., Cardin, J., Futai, K., Vierling-Claassen, D., Rü Hlmann, C., Jones, S., Deisseroth, K., Sheng, M., Moore, C. and Tsai, L.-H. (2011) 'A critical role for NMDA receptors in parvalbumin interneurons for gamma rhythm induction and behavior', *Molecular Psychiatry*, 17, pp. 537–548. doi: 10.1038/mp.2011.31.
- Chattopadhyaya, B. (2004) 'Experience and Activity-Dependent Maturation of Perisomatic GABAergic Innervation in Primary Visual Cortex during a Postnatal Critical Period', *Journal of Neuroscience*. doi: 10.1523/JNEUROSCI.1851-04.2004.
- Chen, F., Tillberg, P. W. and Boyden, E. S. (2015) 'Expansion microscopy', *Science*. doi: 10.1126/science.1260088.
- Chen, L., Yang, C. and Mower, G. D. (2001) 'Developmental changes in the expression of GABA(A) receptor subunits (alpha(1), alpha(2), alpha(3)) in the cat visual cortex and the effects of dark rearing.', *Brain research. Molecular brain research*. doi: S0169328X01000420 [pii].
- Chozinski, T. J., Halpern, A. R., Okawa, H., Kim, H. J., Tremel, G. J., Wong, R. O. L. and Vaughan, J. C. (2016) 'Expansion microscopy with conventional antibodies and fluorescent proteins', *Nature Methods*. doi: 10.1038/nmeth.3833.
- Colgan, L. A. and Yasuda, R. (2014) 'Plasticity of Dendritic Spines: Subcompartmentalization of Signaling', *Annual Review of Physiology*, 76(1), pp. 365–385. doi: 10.1146/annurev-physiol-021113-170400.
- Faber, E. S. L., Delaney, A. J. and Sah, P. (2005) 'SK channels regulate excitatory synaptic transmission and plasticity in the lateral amygdala', *Nature Neuroscience*, 8(5), pp. 635–641. doi: 10.1038/nn1450.
- Froemke, R. C. and Dan, Y. (2002) 'Spike-timing-dependent synaptic modification induced by natural spike trains', *Nature*, 416(6879), pp. 433–438. doi: 10.1038/416433a.
- Goldberg, J. H., Tamas, G., Aronov, D. and Yuste, R. (2003) 'Calcium microdomains in aspiny dendrites', *Neuron*, 40(4), pp. 807–821. doi: 10.1016/S0896-6273(03)00714-1.
- Goldberg, J. H., Yuste, R. and Tamas, G. (2003) 'Ca²⁺ imaging of mouse neocortical interneurone dendrites: Contribution of Ca²⁺-permeable AMPA and NMDA receptors to

- subthreshold Ca²⁺dynamics', *The Journal of Physiology*, 551(1), pp. 67–78. doi: 10.1113/jphysiol.2003.042598.
- Gonzalez-Burgos, G. and Lewis, D. A. (2012) 'NMDA receptor hypofunction, parvalbumin-positive neurons, and cortical gamma oscillations in schizophrenia', *Schizophrenia Bulletin*. doi: 10.1093/schbul/sbs010.
- Gulyá, A. I., Megias, M., Emri, Z. and Freund, T. F. (1999) 'Total Number and Ratio of Excitatory and Inhibitory Synapses Converging onto Single Interneurons of Different Types in the CA1 Area of the Rat Hippocampus', *The Journal of Neuroscience*, 19(22), pp. 10082–10097. doi: 10.1002/cne.902960202.
- Hensch, T. K. (1998) 'Local GABA Circuit Control of Experience-Dependent Plasticity in Developing Visual Cortex', *Science*. doi: 10.1126/science.282.5393.1504.
- Horak, M., Petralia, R. S., Kaniakova, M. and Sans, N. (2014) 'ER to synapse trafficking of NMDA receptors', *Frontiers in Cellular Neuroscience*. doi: 10.3389/fncel.2014.00394.
- Hu, H., Martina, M. and Jonas, P. (2010) 'Dendritic mechanisms underlying rapid synaptic activation of fast-spiking hippocampal interneurons.', *Science (New York, N.Y.)*, 327(5961), pp. 52–58. doi: 10.1126/science.1177876.
- Javitt, D. C. (2007) 'Glutamate and Schizophrenia: Phencyclidine, N-Methyl-d-Aspartate Receptors, and Dopamine-Glutamate Interactions', *International Review of Neurobiology*. doi: 10.1016/S0074-7742(06)78003-5.
- Kornau, H., Schenker, L., Kennedy, M. and Seeburg, P. (1995) 'Domain interaction between NMDA receptor subunits and the postsynaptic density protein PSD-95', *Science*. doi: 10.1126/science.7569905.
- Korotkova, T., Fuchs, E. C., Ponomarenko, A., von Engelhardt, J. and Monyer, H. (2010) 'NMDA Receptor Ablation on Parvalbumin-Positive Interneurons Impairs Hippocampal Synchrony, Spatial Representations, and Working Memory', *Neuron*, 68(3), pp. 557–569. doi: 10.1016/j.neuron.2010.09.017.
- Kuhlman, S. J., Olivas, N. D., Tring, E., Ikrar, T., Xu, X. and Trachtenberg, J. T. (2013) 'A disinhibitory microcircuit initiates critical-period plasticity in the visual cortex.', *Nature*. Nature Publishing Group, 501(7468), pp. 543–6. doi: 10.1038/nature12485.
- Kuhlman, S. J., Tring, E. and Trachtenberg, J. T. (2011) 'Fast-spiking interneurons have an initial orientation bias that is lost with vision.', *Nature neuroscience*. Nature Publishing Group, 14(9), pp. 1121–1123. doi: 10.1038/nn.2890.
- Lamsa, K. P., Heeroma, J. H., Somogyi, P., Rusakov, D. a and Kullmann, D. M. (2007) 'Anti-Hebbian long-term potentiation in the hippocampal feedback inhibitory circuit.', *Science (New York, N.Y.)*, 315(5816), pp. 1262–1266. doi: 10.1126/science.1137450.
- Lee, K. F. H., Soares, C., Thivierge, J. P. and Béique, J. C. (2016) 'Correlated Synaptic Inputs Drive Dendritic Calcium Amplification and Cooperative Plasticity during Clustered Synapse Development', *Neuron*, 89(4), pp. 784–799. doi: 10.1016/j.neuron.2016.01.012.
- Lee, U. S. and Cui, J. (2010) 'BK channel activation: Structural and functional insights', *Trends in Neurosciences*. doi: 10.1016/j.tins.2010.06.004.

- Levelt, C. N. and Hübener, M. (2012) 'Critical-Period Plasticity in the Visual Cortex', *Annual Review of Neuroscience*. doi: 10.1146/annurev-neuro-061010-113813.
- Li, Y. -t., Ma, W. -p., Pan, C. -j., Zhang, L. I. and Tao, H. W. (2012) 'Broadening of Cortical Inhibition Mediates Developmental Sharpening of Orientation Selectivity', *Journal of Neuroscience*, 32(12), pp. 3981–3991. doi: 10.1523/JNEUROSCI.5514-11.2012.
- Lorenz, K. Z. (1937) 'The Companion in the Bird's World', *The Auk*. doi: 10.2307/4078077.
- LUBY, E. D., GOTTLIEB, J. S., COHEN, B. D., ROSENBAUM, G. and DOMINO, E. F. (1962) 'Model psychoses and schizophrenia', *The American journal of psychiatry*. doi: 10.1176/ajp.119.1.61.
- Markram, H., Lubke, J., Frotscher, M. and Sakmann, B. (1997) 'Regulation of synaptic efficacy by coincidence of postsynaptic APs and EPSPs', *Science*, 275(5297), pp. 213–215. doi: 10.1126/science.275.5297.213.
- Matta, J. a, Pelkey, K. a, Craig, M. T., Chittajallu, R., Jeffries, B. W. and McBain, C. J. (2013) 'Developmental origin dictates interneuron AMPA and NMDA receptor subunit composition and plasticity.', *Nature neuroscience*. Nature Publishing Group, 16(8), pp. 1032–41. doi: 10.1038/nn.3459.
- Micheva, K. D., O'Rourke, N., Busse, B. and Smith, S. J. (2010) 'Array tomography: High-resolution three-dimensional immunofluorescence', *Cold Spring Harbor Protocols*. doi: 10.1101/pdb.top89.
- Micheva, K. D. and Smith, S. J. (2007) 'Array Tomography: A New Tool for Imaging the Molecular Architecture and Ultrastructure of Neural Circuits', *Neuron*. doi: 10.1016/j.neuron.2007.06.014.
- Morales, B., Choi, S.-Y. and Kirkwood, A. (2002) 'Dark rearing alters the development of GABAergic transmission in visual cortex.', *The Journal of Neuroscience*. doi: 22/18/8084.
- Mower, G. D. (1991) 'The effect of dark rearing on the time course of the critical period in cat visual cortex', *Developmental Brain Research*. doi: 10.1016/0165-3806(91)90001-Y.
- Murakoshi, H., Wang, H. and Yasuda, R. (2011) 'Local, persistent activation of Rho GTPases during plasticity of single dendritic spines.', *Nature*. Nature Publishing Group, 472(7341), pp. 100–104. doi: 10.1038/nature09823.
- Nevian, T. and Sakmann, B. (2006) 'Spine Ca²⁺ Signaling in Spike-Timing-Dependent Plasticity', *Journal of Neuroscience*, 26(43), pp. 11001–11013. doi: 10.1523/JNEUROSCI.1749-06.2006.
- Ngo-Anh, T. J., Bloodgood, B. L., Lin, M., Sabatini, B. L., Maylie, J. and Adelman, J. P. (2005) 'SK channels and NMDA receptors form a Ca²⁺-mediated feedback loop in dendritic spines', *Nature Neuroscience*, 8(5), pp. 642–649. doi: 10.1038/nn1449.
- Nishiyama, J. and Yasuda, R. (2015) 'Biochemical Computation for Spine Structural Plasticity', *Neuron*, pp. 63–75. doi: 10.1016/j.neuron.2015.05.043.
- Pizzorusso, T., Medini, P., Berardi, N., Chierzi, S., Fawcett, J. W. and Maffei, L. (2002) 'Reactivation of ocular dominance plasticity in the adult visual cortex', *Science*. doi: 10.1126/science.1072699.

- Reynolds, G. P., Abdul-Monim, Z., Neill, J. C. and Zhang, Z.-J. (2004) 'Calcium binding protein markers of GABA deficits in schizophrenia--postmortem studies and animal models.', *Neurotoxicity research*.
- Le Roux, N., Cabezas, C., Böhm, U. L. and Poncer, J. C. (2013) 'Input-specific learning rules at excitatory synapses onto hippocampal parvalbumin-expressing interneurons.', *The Journal of physiology*, 591(Pt 7), pp. 1809–22. doi: 10.1113/jphysiol.2012.245852.
- Runyan, C. a and Sur, M. (2013) 'Response selectivity is correlated to dendritic structure in parvalbumin-expressing inhibitory neurons in visual cortex.', *The Journal of neuroscience : the official journal of the Society for Neuroscience*, 33(28), pp. 11724–33. doi: 10.1523/JNEUROSCI.2196-12.2013.
- Sheng, M. (1996) 'PDZs and receptor/channel clustering: Rounding up the latest suspects', *Neuron*. doi: 10.1016/S0896-6273(00)80190-7.
- Sheng, M. and Kim, E. (1996) 'Ion channel associated proteins.', *Current opinion in neurobiology*.
- Szabo, A., Somogyi, J., Cauli, B., Lambolez, B., Somogyi, P. and Lamsa, K. P. (2012) 'Calcium-permeable AMPA receptors provide a common mechanism for LTP in glutamatergic synapses of distinct hippocampal interneuron types.', *The Journal of neuroscience : the official journal of the Society for Neuroscience*, 32(19), pp. 6511–6. doi: 10.1523/JNEUROSCI.0206-12.2012.
- Torrey, E. F., Barci, B. M., Webster, M. J., Bartko, J. J., Meador-Woodruff, J. H. and Knable, M. B. (2005) 'Neurochemical markers for schizophrenia, bipolar disorder, and major depression in postmortem brains', *Biological Psychiatry*. doi: 10.1016/j.biopsych.2004.10.019.
- van Versendaal, D. and Levelt, C. N. (2016) 'Inhibitory interneurons in visual cortical plasticity.', *Cellular and molecular life sciences : CMLS*. doi: 10.1007/s00018-016-2264-4.
- Williams, S. and Boksa, P. (2010) 'Gamma oscillations and schizophrenia', *Journal of Psychiatry and Neuroscience*. doi: 10.1503/jpn.100021.
- Ye, Q. and Miao, Q. long (2013) 'Experience-dependent development of perineuronal nets and chondroitin sulfate proteoglycan receptors in mouse visual cortex', *Matrix Biology*. doi: 10.1016/j.matbio.2013.04.001.